Chair of Petroleum and Geothermal Energy Recovery

Master's Thesis

Delumping of Production Streams for Surface Facility Modeling

Markus Siegfried Frauwallner, BSc

May 2020

AFFIDAVIT

I declare on oath that I wrote this thesis independently, did not use other than the specified sources and aids, and did not otherwise use any unauthorized aids.

I declare that I have read, understood, and complied with the guidelines of the senate of the Montanuniversität Leoben for "Good Scientific Practice".

Furthermore, I declare that the electronic and printed version of the submitted thesis are identical, both, formally and with regard to content.

Date 18.05.2020

Signature Author
Markus Siegfried, Frauwallner

Master's Thesis

Delumping of Production Streams for Surface Facility Modeling

In collaboration with PM Lucas Enterprises

Written by:
Markus Frauwallner
01335111

Advisors, MUL:
Univ.-Prof. Dipl.-Ing. Dr.mont. Herbert Hofstätter
Dipl.-Ing. Fatemeh Fazeli Tehrani

Advisors, PML:
Dipl.-Ing. Dr.mont. Georg Mittermeir
MSc. Dr. Mehdi Assareh

Leoben, 20/05/2020

Acknowledgement

First of all, I want to deeply thank Dr. Georg Mittermeir and Dr. Mehdi Assareh, both PM Lucas Enterprises, for their active support in development of this thesis as well as the warm welcome into the company. Especially Dr. Assareh who taught me many things by giving me private lectures and was always available for consultation.

Special thanks to Dr. Pavle Matijevic, CEO of PM Lucas, for sponsoring this work via a scholarship and giving me the opportunity to visit and work at the branch office in Serbia, as well as involving me in the digital oilfield (DOF) project.

I am grateful to Dr. Snezana Sevic and Dr. Branko Grubac, for taking their time and providing us with valuable tutorial lessons for handling Aspen HYSYS®.

I want to thank my colleagues in Leoben, Dr. Christoph Steiner and Dipl.-Ing. Volker Pavalec, both PM Lucas, for the fruitful discussions.

I want to express my gratitude to PMT Technologie- und Forschungsimpulszentrum for providing office room and the necessary hardware.

Finally, I want to thank my parents for giving me the opportunity to be able to study unconditionally and always supporting me during my so far accomplishments. I love you.

Kurzfassung

Diese Masterarbeit untersucht die Machbarkeit und Auswirkung der Komponentenrückführung auf die in einer Prozessanlage erzeugten Produkte. Hierfür wurden zusammengeführte Sondenförderraten von Lagerstättensimulationen für ein Gaskondensat und ein flüchtiges Leichtrohöl wieder rückgeführt, um die erzeugten Produkte einer Prozesssimulation zu analysieren.

Aufgrund der Anzahl an Gleichungen, welche während einer Lagerstättensimulation gelöst werden müssen, ist es geläufig, die Zahl der Komponenten in einem Zustandsmodell zu verringern, indem man einige Komponenten zusammenfasst. Die Rückführung von zusammengefassten Zustandsmodellen von Lagerstättenflüssigkeiten ermöglicht es, detaillierte Informationen über das System zu erlangen und zeitgleich eine Reduktion der Simulationslaufzeit zu ermöglichen.

Zu Beginn wurden detailliert aufgeschlüsselte Zustandsmodelle von Lagerstättenflüssigkeiten analysiert. Diese wurden im weiteren Schritt mit Fuzzy-Clustering untersucht, um Zusammenführungsschemen zu erlangen, welche mit Hilfe der Fluidmodellierungssoftware PVTi® anhand dieser Schemen zusammengeführt wurden. Die zusammengeführten Zustandsmodelle wurden gemeinsam mit dem Referenzmodell mittels des Lagerstättensimulators ECLIPSE E300® und dessen integriertem Rückführungsalgorithmus simuliert, um zeitabhängige Sondenförderraten zu erlangen, welche detaillierte Komponenteninformation enthalten. Diese wurden anschließend von der Prozesssimulationssoftware Aspen HYSYS® simuliert, um Produkte wie Produktgas, Flüssiggas und Kondensat zu erlangen und sie zu untersuchen.

In dieser Arbeit konnte gezeigt werden, dass die Auswirkungen des Rückführens von Sondenförderraten einen vernachlässigbaren Einfluss auf die Menge der Prozessanlagenprodukte hat. Vielmehr wurde hervorgehoben, dass das sorgfältige und konsistente Zusammenführen von Zustandsmodellen oberste Priorität hat. Zusätzlich wurden einige wichtige Restriktionen seitens des Rückführungsalgorithmus gefunden, welche die Anwendbarkeit negativ beeinflussen.

Das Prozedere des Verknüpfens von Lagerstätten- und Prozesssimulator anhand der beiden Lagerstättenflüssigkeiten und hilfreiche Anregungen zu diesem Vorhaben sowie eine detaillierte Analyse der Ergebnisse werden in dieser Arbeit erläutert und beschrieben.

Abstract

This thesis is investigating the feasibility and impact of delumping production well streams which are used for prediction of process plant products, for a gas condensate and a volatile oil as reservoir fluids, by using coupled reservoir-surface simulation.

Because of the amount of equations which are solved during reservoir simulation, run-time is a crucial limitation. Therefore, it is commonly practised to lump components of a fluid model. In order to acquire detailed information about the system, delumping is applied afterwards.

The foundation of this thesis are phase behaviour models for both reservoir fluids with detailed component information. These models were used to create reference solutions. The detailed fluid models were then analysed by fuzzy clustering in order to realize lumping schemes which were implemented using PVTi® as fluid modelling software. These lumped fluid models were simulated with a reservoir model computed by ECLIPSE® E300, using its delumping facility to create time dependent well streams with detailed compositions. These well streams serve as input for the process simulation model calculated by Aspen HYSYS®. The obtained process plant products such as sales gas, liquefied petroleum gas (LPG) and condensate, were compared with the reference results and deviations from such were analysed and interpreted.

It was concluded that the impact of delumping compositional well streams for processing them in a gas treatment unit, to obtain process plant products, is almost negligible. The importance of a consistent lumping, and therefore sensitivity of fluid descriptions within a simulation environment, was proven. In addition, several, sometimes not well documented, limitations, of the available inbuilt delumping facility of ECLIPSE® E300, were found for using it in a coupled reservoir-process simulation approach.

The procedure on how to create a coupled subsurface-surface simulation for a gas condensate and a volatile oil are reviewed in this work as well as recommendations and remarks on the tasks and its influences are proposed.

Table of Content

Page

1 Introduction

The complete life cycle of a gas condensate production system consists of near critical hydrocarbon-mixtures which are produced from a reservoir through wells, then gathered and processed at surface facilities to generate saleable products. To be more specific a gas processing plant, also called gas treatment unit (GTU), is designed to produce sales gas, liquefied petroleum gas (LPG) and condensate - or intermediate-to-heavy fraction - in the most profitable quantities. Since companies have to ensure economical security, they are forced to evaluate how these saleable quantities will develop in the near future. This need for a prediction-tool was adapted to an idea of connecting reservoir simulators to process simulators. Such process simulators are highly dependent on the used fluid description (also called: pressure volume temperature (PVT) - , equation of state (EoS) - , fluid - model, …) which is a way of describing the thermodynamic phase behaviour of a fluid with a fixed distribution of chemical components [1]. Since process simulators need to cover calculations over a wide range of pressure and temperature conditions, a detailed fluid description is needed in order to predict the processed quantities correctly. [2]

With the todays' available computational power, modern process simulators can handle even complex models, in terms of number of modelled units, within a reasonable time. On the other hand, reservoir models are modelled by cells or blocks which can exceed millions in numbers for large fields. Because of the high number on equations to solve, reservoir simulators are limited in feasible runtime, especially when it comes to compositional reservoir simulation. Thus, a common approach is to decrease the number of components in a fluid model, used by the reservoir simulator. This approach is called lumping, where the lumped fluid model is approximating the same phase behaviour as the initial detailed fluid model but only consist of fewer components. Lumping is also referred as grouping, pseudo-grouping or pseudo-component generation. [3], [4], [5], [6], [7], [8]

When deciding to connect such a reservoir simulation model with a process simulator, one will face problems regarding the consistency of the fluid model, which should be coherent for the sake of above-mentioned intention. The process simulation will need detailed information of the produced well stream in terms of single component quantities to determine viable results, e.g. sales gas (high methane content), LPG, intermediate hydrocarbons, heavy fractions and non-hydrocarbons. The reservoir simulator, however, is calculating the well streams according to a lumped fluid description.

Delumping, or also called inverse-lumping in first place, component retrieval or splitting, is trying to recover the loss of detailed information due to lumping by use of different mathematical formulations. In other words, the delumping procedure will translate lumped information consisting of some pseudocomponents (PCS) to detailed information, in terms of single component quantities. [4], [8], [9], [10], [11]

This thesis will analyse the impact of lumping and delumping on sales product quantities. Therefore, Schlumberger's ECLIPSE® Compositional Reservoir Simulator 2018.1 (E300) is

used to calculate time dependent well streams with detailed compositional information, by applying its inbuilt delumping facility. Afterwards the detailed well streams are used to feed a GTU process plant model to calculate saleable products. As process simulator Aspen HYSYS® V10 (HYSYS) was used to model and calculate these.

The scope of this thesis will be constrained on the investigation of the upstream gas production cycle. It will be hereby declared that development of a new delumping technique, or application of any other delumping method apart from the E300 inbuilt facility is NOT a scope of this thesis. Additional to this it is mentioned that no full field simulation and no economic feasibility study will be undertaken, because it has little practical usage for the outcome of this thesis. Since the PVT fluid description was accomplished by Dr. Assareh there is also no requirement for tuning PVT data. The hands-on training, and guidance, for being able to use the process simulator HYSYS, was conducted by the PM Lucas (PML) process engineers, namely Dr. Sevic and Dr. Grubac, and the training for Schlumberger's Fluid Modelling Software PVTi® was conducted by PML-PVT Expert Dr. Assareh.

The analysis should consist of screening the used fluid models and their subsurface simulation result validity, comparison of central processing unit (CPU) times (since calculation time is a limiting factor when it comes to reservoir simulation), as well as interpretation of the whole process, from setting up the simulations to postprocessing the calculated results.

The thesis is structured in a way that provides guidance through the topic. It will start with a fundamental chapter where necessary theoretical background is explained, whereas some things will be briefly discussed e.g. the theory behind process simulation. The most general derivations are outsourced in the Appendices to keep the chapter concise. The literature review about lumping and delumping is conducted in chapter 3, where some of the different historical approaches for lumping and delumping are listed. The formulation used in E300 delumping facility is emphasized in more detail. Chapter 4 is describing the preparations for setting up the simulations as well as the description of the analysed cases which were conducted. Process simulation, reservoir simulation and fluid modelling will be separately treated. The results of the simulations are going to be discussed in chapter 5 and reviewed in blocks again. Finally, the last chapter will wrap everything up and the big picture will be interpreted along with an outlook for future studies as well as recommendations which were found during the work of this thesis.

2 Fundamentals

Because of the multi-disciplinary character of this thesis, the basic fundamentals are needed to be explained in the following subchapters It is mentioned that some explanations will be provided only briefly, while some are outsourced into the Appendices.

2.1 Production of Gas Condensate

With declining production rates of conventional hydrocarbon fields, contrary to increasing demand, and the ongoing low-price environment in the industry, gas condensate reservoirs are gaining more interest in hydrocarbon extraction. Gas condensate, or also called retrograde gas condensate, bears complex challenges during production, because of its near-critical fluid behaviour. It consists of light as well as intermediate-to-heavy components, making it therefore valuable for processing. [12]

The term “retrograde” gas condensate comes from the phenomenon that the gas will condensate during an isothermal pressure reduction until some point where the liquid will re evaporate by further pressure reduction. This happens only if the fluids’ temperature is in between its critical and cricondentherm temperature. [4]

Because of these heavier components within the fluid (ethane plus (C2+) ~ 30 %) a liquid will form during production which is called condensate. This condensate has an American Petroleum Institute density (API°) range between 50 and 60° and its colour can vary between transparent to light brownish and is sometimes called “white oil”. This dropped-out liquid can be used as natural gas liquids (NGL) products. [12], [13]

To create saleable products from a gas condensate, treatment is needed in form of a process plant. Gas processing in general can be categorized into four main tasks: [12], [14]

- Separation or Conditioning – Removing liquids and solids
- Treating – Sweetening or removal of acid (hydrogen sulphide (H2S) and/or carbon dioxide (CO2))
- Dehydration – Drying, removing vaporized brine
- Extraction – Recovery of sale specific components

2.1.1 Conditioning Unit

The first operation in gas processing after its gathering from the wellhead, is the physical separation of the fluid. This means unwanted constituents like liquid water (brine) and solids as well as the essential ones, gas and liquid hydrocarbons (condensate) are separated by using one or combinations of different separations units, schematically shown in Figure 1 as an example. [12]

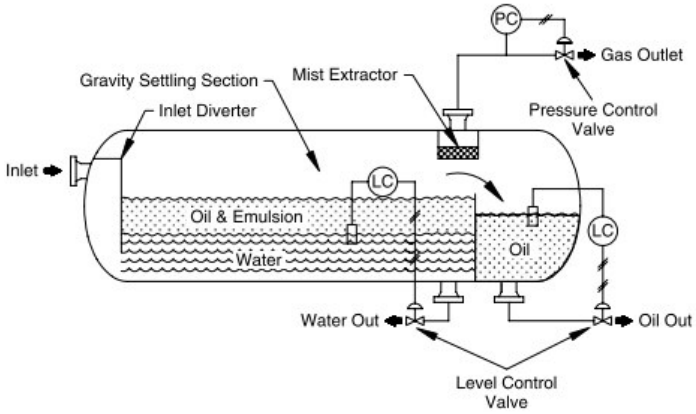

Figure 1 – 3-phase separator [15, p. 246]

2.1.2 Treating Unit

Since most of the reservoir fluids consist also of non-hydrocarbons, like e.g. CO2 and nitrogen (N2), with some of them even extremely toxic (mercury (Hg) or H2S), these have to be removed from the gas. The most common procedure is the removal of CO2 and H2S with a solvent, most commonly amines like methyl-diethanolamine (MDEA). An aqueous amine solution (namely lean solution) is fed into the top of an absorber column, where it becomes in counter-current contact with the sour gas. This is also called “amine washing”. The emerging products are sweet gas and contaminated amine solution (rich solution). This rich solution leaves the bottom of the column, at an increased temperature due to the reaction between the amine and the acid gases and enters then a splitter column where the acid gas is stripped out of the rich solution and the lean amine can be reused. The acid gas can then be flared or processed otherwise. The whole unit can be seen schematically in Figure 2. [12], [14], [16]

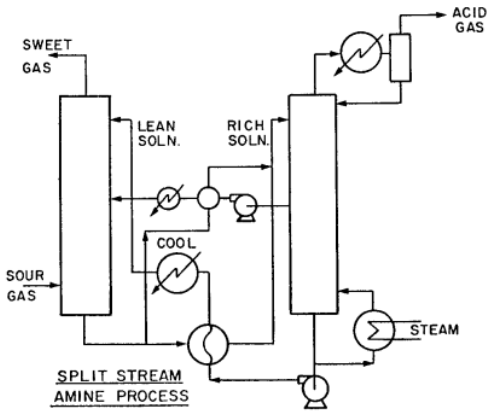

Figure 2 - Amine Unit [16, p. 67]

2.1.3 Dehydration Unit

Since either produced gas is saturated with brine vapour or has become “wet” because of the amine washing in the treating unit, the water vapour contaminant has to be removed. This can be done by a dehydration unit. [12]

Gas dehydration works either by absorption, adsorption, condensation, or membrane separation[1].

Absorption is the most common choice of dehydration method because of its simple and effective process design. For the dehydration process, a liquid absorbs the water from a wet gas stream. This liquid should meet specific criteria: [17]

- Highly hygroscopic,
- Non-corrosive,
- Non-soluble in liquid hydrocarbons,
- Stable along sulphuric compounds,
- Should not densify,
- Should not precipitate with gas compounds.

Therefore, glycol or to be specific triethylene glycol (TEG), comes closest to meet these demands. [17]

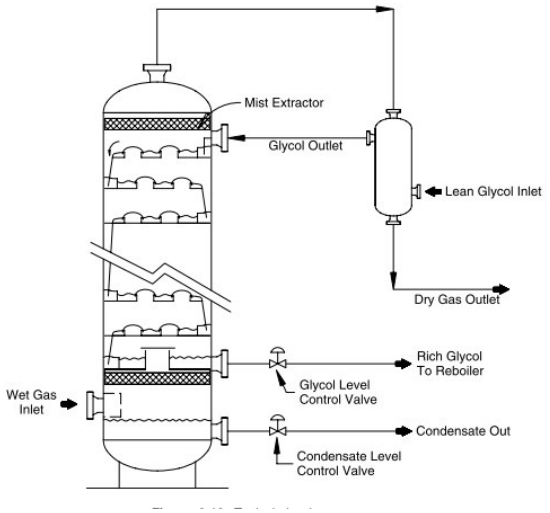

Figure 3 - Schematic of glycol-dehydration column [15, p. 50]

The process of dehydration itself can be simplified by cooling the wet gas and a glycol rich solution (lean glycol stream) at least below the freeze point (0 °C) and let the glycol solution then strip the water out of the gas when mixed in a column (contractor) or a flash tank. This will create dry gas and the “wet” glycol stream (rich glycol stream) after the stripping process. The rich stream will be put into a regeneration unit to recover the glycol for economic reasons. This regeneration unit uses glycol filters, distillation and vaporization flash tanks to recover the glycol. [17]

[1] Since the GTU model, which will be discussed in the upcoming chapters, works with a glycol adsorption dehydration technique, the others are not explained.

2.1.4 NGL extraction unit

The NGL unit is a term for the fractionation of the separate components from the treated and dried gas stream, e.g. Ethane, Propane (C3) and Butane (C4). The processes behind the term are absorption, adsorption and condensation which can be broken down to different pressure and temperature conditions inside a column, also called fractionation towers. The setting of these conditions influences the product compositions, which are tuned according to the demanded product specifications. These different conditions can be achieved in a combination of flash tanks stacked on top of each other. Every stage (:= tray) is responsible for a vapour-liquid-equilibrium (VLE) flash calculation, see Figure 4 and Figure 5. [18]

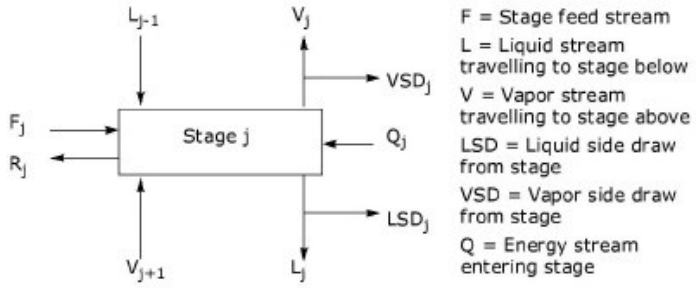

Figure 4 - Principle of a column tray or stage [18]

NGL fractionation units consist of absorber-, distillation-, refluxed absorber- or reboiled absorber columns. For comprehensibility of later chapters, these 4 types are briefly explained here. [17], [18]

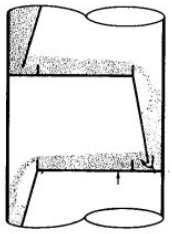

Figure 5 - Schematic flow of a fluid through a column - Vapor rises to the top and liquid travels towards bottom; adopted from Campbell [17]

A typical fractionation tower can be seen in Figure 6. This tower consists of stages where the feed is fed into at a specific tray position. At the top and the bottom, the exit streams are connected to a condenser and a reboiler.

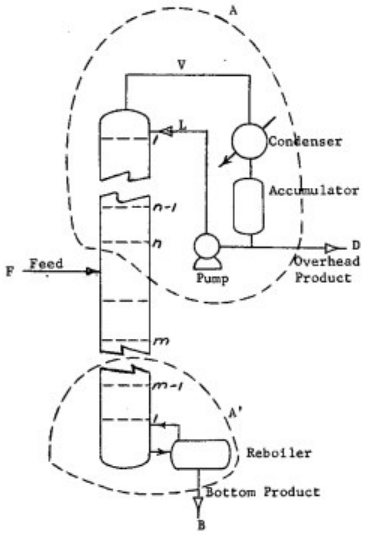

Figure 6 - Schematic of a Column with a Condenser and a Reboiler attached at the top and bottom [17, p. 282]

The condenser at the top of the tower ensures a better separation of the vapour stream due to different reflux settings. The condenser can be designed as either a total condenser, where the product stream (distillate) will be a saturated liquid, or as a partial condenser, where the distillate will be a saturated vapour. It is also possible to connect a reboiler to the bottom liquid stream, which operates at its bubble point temperature, and feed the generated vapour back into the column. This setup of a fractionation tower with a condenser and a reboiler attached, is termed “distillation column”. Towers with only either condenser or reboiler attached are called “refluxed-absorber” and “reboiled-absorber” respectively. At last the simplest fractionation tower design is the “absorber column” without any of these two attached. [18]

2.2 Process Simulation

Because of the sheer number of different units, equipment and calculation steps needed to analyse such a treatment plant, process simulation is a vital part in the production of gas condensate and in chemical engineering as a whole.

In general, process simulation can be described by calculating mass and energy balances of a steady state (time-independent) process at thermodynamically equilibrium. In a model-based representation of chemical, physical and other technical processes by use of a software, the real behaviour should be approximated. [19]

Especially in the oil and gas industry, the calculation of physical and transport properties as well as the phase behaviour of the produced fluid is particularly important for simulating the real behaviour. [20]

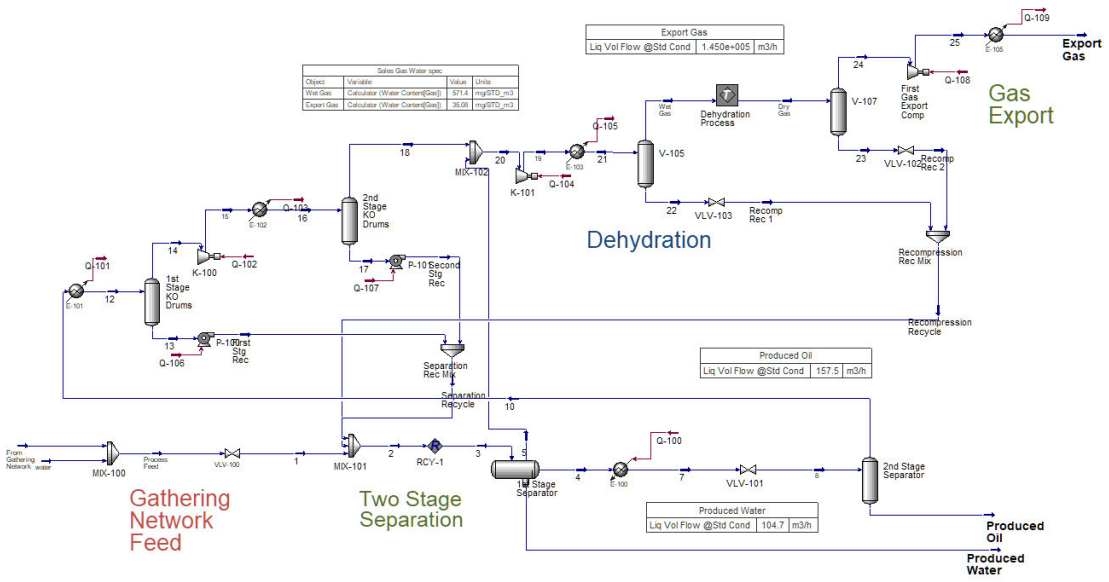

Figure 7 - HYSYS Gas Dehydration & Compression Unit, Tutorial Example [18]

Within a process plant model every vessel and every change in thermodynamic condition is calculated - e.g. the above-mentioned columns operations need to be calculated iteratively - in order to find a converging solution which honours the mass and energy balance. The complete process is modelled using flow diagrams as exemplary shown in Figure 7.

For this thesis, the industry's leading process simulator HYSYS was used. HYSYS, in general, is built for designing, analysing and optimizing either up-, mid- or downstream operations in one environment [21]. HYSYS is formulated intuitively for designing a process plant. It is separated in different environments.

The two most important are "property" and "simulation" environment. In the "property" environment the particularly crucial fluid model (explained in the upcoming chapter) is set up. A fluid description with as many as possible single components and its physical properties ensures accurate modelling of the fluid phase behaviour. Because of the broad range of different PVT conditions in a process model and the particular stream specifications, which are related to individual component concentrations and are also very sensitive to phase equilibrium calculations, lumped fluid descriptions are not feasible to be processed accurately [22].

The simulation environment is the part where the plant and its processes are designed and visualized by flowchart sheets, unit and model analysis sheets and other input masks. This set-up and its real-time calculation environment make HYSYS an advantageous simulator of choice. But since HYSYS, as a process plant simulator, is modelling the end of the hydrocarbon production life cycle, it is highly dependent on the GIGO principle – Garbage in, Garbage out. Using it for prediction of the future in terms of saleable quantities, it is depended on accurate detailed compositional hydrocarbon production streams from the reservoir itself.

2.3 Reservoir Simulation

In order to generate these streams, the hydrocarbon production from the field needs to be modelled too. That is where reservoir simulation comes in handy.

Numerical reservoir simulation is used to model or predict the fluid flow through a subsurface hydrocarbon reservoir. The underlying principles are conservation of mass, fluid phase behaviour, Darcy's filtration law and Fick's laws of diffusion. For modelling all the relevant physical and chemical processes, a set of partial differential equations are assembled which account for mass and heat transfer inside the reservoir. As can be seen from Figure 8, the formulation of the physical model has to consider all relevant processes and properties. This mathematical model consists of balance equation, property functions, constitutive equations as well as constraints. But since this set of equations is highly non-linear and thus not able to be solved analytically, one has to replace the differential equations with difference equations, which is called discretization (finite -difference, -element or -volume). [23]

As mentioned above, the mathematical model is set up by using conservation laws and constitutive relations. Both derived together, one can find the balance equation for fluid flow in porous media. A detailed derivation can be found in *"Systematic of Reservoir Flow Equations"* by Heinemann and Mittermeir [24]. A typical mole balance would look like **eq.** (1).

$$\nabla\left(\sum_{\pi}^{\Pi}\lambda_\pi\bar{\bar{k}}(\nabla p_\pi-\rho_\pi\bar{g})c_\pi z_{\pi,i}\right)+\nabla\left(\sum_{\pi}^{\Pi}\phi S_\pi c_\pi D_{\pi,i}\nabla z_{\pi,i}\right)+q_i=\frac{\partial}{\partial t}\left(\phi\sum_{\pi}^{\Pi}S_\pi c_\pi z_{\pi,i}\right) \quad (1)$$

Where Π is the number of phases, λ_π is the phase mobility, c_π molar concentration (molarity) for each phase, $z_{\pi,i}$ mole fraction of component i in phase π, and $D_{\pi,i}$ is the diffusion coefficient for component i in phase π. All other variables are listed in the Nomenclature.

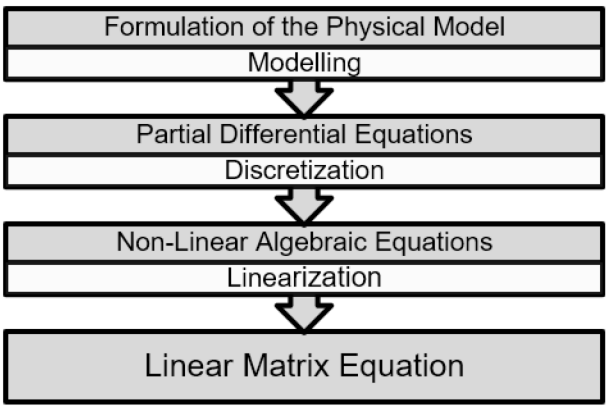

Figure 8 - Workflow for building a simulation model; after Heinemann and Mittermeir [23]

Discretization is a method which is splitting a continuous function into finite steps. If these finite steps now become infinitesimally small the discretized function equals the continuous function

and is therefore valid. This means that the discretization approximates a continuous function, namely algebraic function, which is easier to solve. As an example, the discretized form of **eq.** (1), which would be used in a reservoir simulator, for an orthogonal grid, looks like the following:

$$\sum_{I_1=1}^{N} \tau_{I_0 I_1} \left[\sum_{\pi}^{\Pi} \left(z_{\pi,i} \lambda_{\pi} c_{\pi} \right)_{I_0 I_1}^{m+1} \left(\Phi_{\pi,I_1} - \Phi_{\pi,I_0} \right)^{m+1} \right] + \sum_{\pi}^{\Pi} \left(q_{\pi} c_{\pi} z_{\pi,i} \right)_{I_0}^{m+1} \tag{2}$$
$$= \left\{ \frac{V_{I_0}}{\Delta t} \left[\phi \sum_{\pi}^{\Pi} \left(S_{\pi} c_{\pi} z_{\pi,i} \right) \right]_{I_0}^{m+1} - \frac{V_{I_0}}{\Delta t} \left[\phi \sum_{\pi}^{\Pi} \left(S_{\pi} c_{\pi} z_{\pi,i} \right) \right]_{I_0}^{m} \right\}$$

A graphical representation, of a discretized three-dimensional, heterogeneous, anisotropic rock body containing fluids of different composition, can be seen in Figure 9, but the reservoir is not only spatially discretized but also in its time domain.

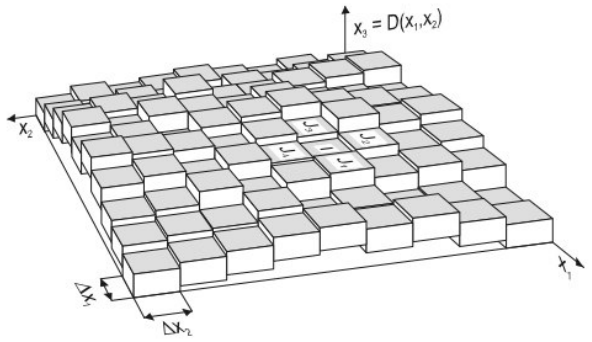

Figure 9 - block model of a reservoir [23, p. 2.8]

Beyond the mathematical complexity and usefulness of reservoir simulation, the model is highly dependent again on the input. Heinemann et al. [23] described numerical simulation in reliance to Figure 10. The computer program (simulator itself) is dependent on the input data which are based on measurements and observations of reality and the parameters which are uncertain and need to be matched. Such input data reaches from geological and seismic surveys to drilling- and production data.

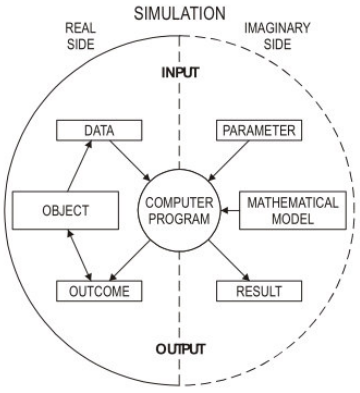

Figure 10 - Schematic description of a simulation model [23, p. 1.3]

2.3.1 Compositional Formulation

In reservoir simulation two main formulations are common. The black oil (or β -) model and the compositional model. The black oil model handles oil, gas and water as three pseudo components with internal composition at standard (stock tank) conditions and no mass transfer between water and the other two phases is possible. However, the black oil model is not suitable for calculating near critical fluids in its standard formulation, although there is an extension of the black oil model formulation which includes oil vaporization into the gaseous phase. [1], [25]

The compositional reservoir simulator is calculating the isothermal flow of single components within a hydrocarbon mixture, by determining the movement of a phase via equilibrium calculations. It can account for compositional variations and therefore miscibility calculations, e.g. of gas injection, as well as depth and pressure variations due to the presence of a near critical fluid, e.g. volatile oil or a gas condensate as reservoir fluid. It uses an EoS to calculate the distribution of the mixture's component for each phase due to the stable thermodynamic equilibrium. [1], [22]

The compositional reservoir simulation has more equations to solve, per block and timestep, which results in an increasing demand on computational power to solve the system compared with the black-oil-simulation. However, with today's increase in getting cheaper availability of computational power, compositional reservoir simulators are the method of choice. [1]

To accurately approximate the production of a near critical fluid with a compositional simulator, e.g. a gas condensate, a PVT model needs to be matched to experimental data of the reservoir fluid.

2.4 Phase Behaviour

Both above introduced disciplines, process and reservoir simulation, are highly dependent on the fluid description, since it is describing, as a mathematical model, the phase behaviour of a fluid during different pressure and temperature conditions. Cubic EoS are mainly used in the petroleum industry to describe the PVT behaviour of a mixture [7]. The derivation of a cubic EoS and additional information about EoS can be reviewed in Appendix A.

For analysing the phase behaviour of reservoir fluids, which are consisting of a mixture of hydrocarbons and often other non-hydrocarbons, experimental studies of the fluids are crucial to understand the behaviour during recovery. In Figure 11, below, the variation of the phase envelope for different binary mixtures, and thus the dependence of different composition can be seen. The critical locus shows the range of a critical point on the phase envelope for different compositions of the two pure compounds. [4]

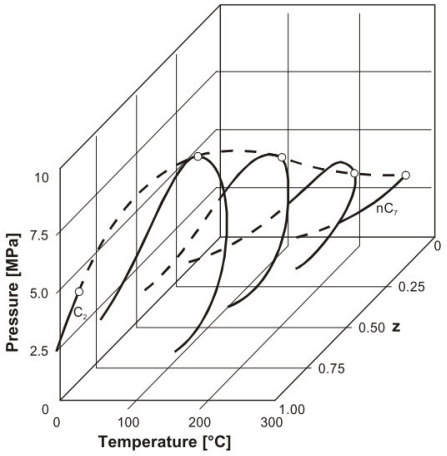

Figure 11 - Phase envelopes for different compositions of a binary mixture [26, p. 14]

Although reservoir fluids consist of a vast number of different components, they all have similar molecular structures. Thus, a general phase envelope, which can be seen in Figure 12 for a binary mixture, has all the details contained to describe the majority of reservoir fluid types. The maximum pressure and temperature are called cricondenbar and cricondentherm respectively and are defined by the maximum pressure and temperature where two-phases can be present. The point where bubble point line and dew point line are connected is called the critical point. Within the two lines the two-phase region is found, where, depending on the pressure and temperature of the system, different liquid and vapour states of equilibrium are quantified. Above and near the critical point there is only one phase present which is barely identifiable. Another important process which takes place near the critical point is called the retrograde condensation. Retrograde condensation is a phenomenon where an initial gaseous fluid will drop out of liquid with decreasing pressure, which is a characteristic of a gas condensate. The same can happen on the other side of the critical point where the process is named retrograde vaporization, which is defined by vaporizing liquid through decrease in temperature. Reservoir fluid conditions found near the left side of the critical point are classified as volatile oils. [7]

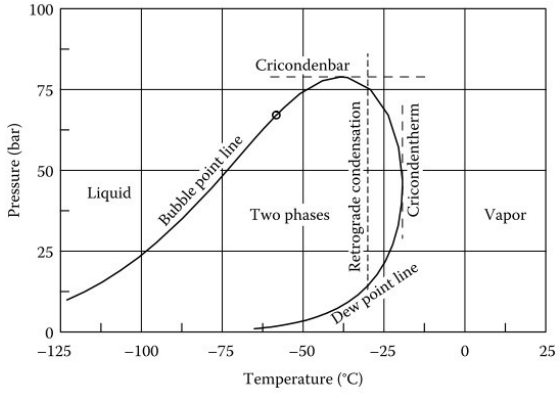

Figure 12 - general phase envelope for a gas (mainly CH_4) [7, p. 6]

For the simulation of the recovery process, knowledge about the phase equilibrium is essential, and thus explained in the upcoming subchapter.

2.4.1 Phase Equilibrium

Both, reservoir and process simulation, are dependent on VLE calculations. Since reservoir fluids are mixtures of hydrocarbons consisting of several thousand different components, it is vital for the fluid model to meet the experimental measurements in order to be able to calculate a good approximation of the real fluid phase behaviour via simulators.

In general, there are three basic phase-equilibrium calculations: (1) bubble point, (2) dew point and (3) equilibrium-flash. The first two determine phase envelopes and the third one is calculating the number of phases as well as molar amount and composition of each phase (if pressure, temperature and the mole fractions of the feed $(z_1, z_2, \dots z_{N_c})$ are known). [7], [12], [14]

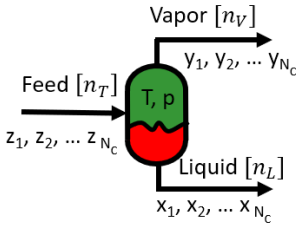

Figure 13 - Schematic of 2-phase flash

Phase equilibria, in general, work extensively with a quantity called equilibrium ratio or simply K-value which is defined as the ratio of vapor to liquid mole-fraction:

$$K_i = \frac{y_i}{x_i} \tag{3}$$

When a mixture is flashed at specific pressure and temperature conditions, a material balance for total moles of feed n_T would be as follows:

$$n_T = n_V + n_L \tag{4}$$

Now expressed for each component

$$z_i n_T = x_i n_L + y_i\, n_V \tag{5}$$

Where the sum of every fraction for all components equals unity,

$$\sum_i^{N_c} x_i = \sum_i^{N_c} y_i = \sum_i^{N_c} z_i = 1 \tag{6}$$

Which can be rearranged to:

$$\sum_i^{N_c} (y_i - x_i) = 0 \tag{7}$$

Substituting **eq.** (3) into **eq.** (5) gives with respect to x_i

$$x_i = \frac{n_T\, z_i}{n_L + n_V\, K_i} \tag{8}$$

Replacing n_L by $n_L = n_T - n_V$, where $\frac{n_V}{n_T} = \mathrm{F_V}$, which is named either vapour split factor or vapour fraction, gives:

$$x_i = \frac{z_i}{1 + F_V(K_i - 1)} = \frac{y_i}{K_i} \tag{9}$$

By proper substitution, **eq.** (7) can now be solved as below:

$$\sum_i^{N_c} \frac{z_i(K_i - 1)}{1 + F_V(K_i - 1)} = 0 = f(F_V) \tag{10}$$

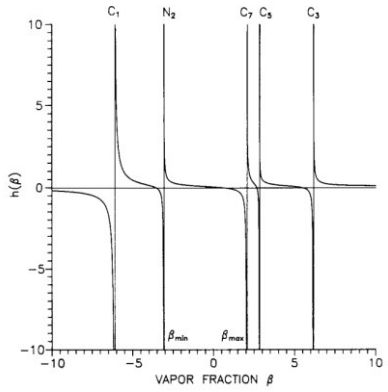

Figure 14 - monotonic series for five component mixture [27, p. 4.7]

In Figure 14, one can see the monotonic $f(F_V) = h(\beta)$ function versus $F_V = \beta$. **Eq.** (10) is the well-known Rachford-Rice equation [28].

With known feed composition and approximated K-Values, $K_i = f(p_{c_i}, T_{c_i}, \omega_i)$, one can determine the unknown F_V by using the Newton-Raphson method, to find the roots of the function iteratively by $F_V^{new} = F_V^{old} - f(F_V^{old})/f'(F_V^{old})$. [29] It can be shown that the only physical meaningful solution corresponds to values:

$$F_{V_{min}} < F_V < F_{V_{max}} \tag{11}$$

The approximation is usually done by the Wilson equation, which can be found in **eq.** (12). [29]

$$K_i = \frac{p_{c_i}}{p} \exp\left(5.37\,(1 + \omega_i)\left(1 - \frac{T_{c_i}}{Z}\right)\right) \tag{12}$$

Using the converged F_V, the corresponding mole fractions x_i and y_i can be calculated with **eq.** (9). The issue with this method is the numerical stability for **eq.** (10). Because the equilibrium ratio estimations are poor for high pressures, an EoS based method is usually applied, in order

to converge and give an accurate approximation of the state of the system. With above introduced **eq.** (3) and the definition derived by **eq.** (116) in Appendix A.6 pg. 100, it can be stated that the K-values can also be approximated by the ratio of fugacity coefficients of the mixture $\hat{\phi}_i^{l,v}$:

$$K_i = \frac{y_i}{x_i} = \frac{\hat{\phi}_i^l}{\hat{\phi}_i^v} \tag{116}$$

Which can also be written as:

$$\ln K_i = \ln \phi_i^l - \ln \phi_i^v \tag{13}$$

Using now the cubic Peng-Robinson-EoS (PR-EoS) consistent **eq.** (22), which was derived in Appendix A.6 starting at pg. 100, for approximating the K-value for every component, the flash equation **eq.** (10) can be solved.

A schematic of this process can be seen in Figure 15. The equations for setting up the EoS for every phase can be found in Table 1, pg. 16, with **eq.** (14) to (23). The detailed derivation from Appendix A to Appendix A.6 is suggested to be reviewed here since delumping, especially the in the upcoming chapter explained LSK delumping algortihm, is explained in the next chapter 3 and highly dependet on the EoS-VLE calculations.

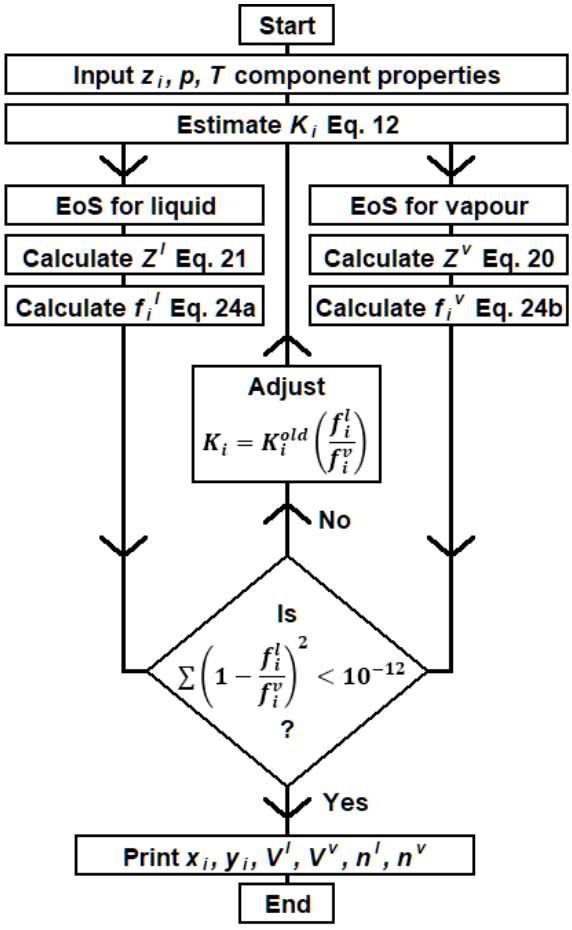

Figure 15 - VLE process flowchart; adopted from Danesh [4]

Table 1 - Summary of VLE equations; adopted from Smith et al. [30]

1.) Mixing rules for liquid and vapour phase

$$a^l = \sum_i \sum_j x_i x_j \sqrt{a_i a_j} \qquad a^v = \sum_i \sum_j y_i y_j \sqrt{a_i a_j} \tag{14}$$

$$b^l = \sum_i x_i b_i \qquad b^v = \sum_i y_i b_i \tag{15}$$

2.) Dimensionless parameters for liquid and vapour phase

$$\beta^{l,v} = \frac{b^{l,v} p}{RT} \tag{16}$$

$$q^{l,v} = \frac{a^{l,v}}{b^{l,v} RT} \tag{17}$$

$$\bar{q}_i^{l,v} = q^{l,v}\left(1 + \frac{\bar{a}_i^{l,v}}{a^{l,v}} - \frac{b_i}{b^{l,v}}\right) \tag{18}$$

3.) Calculate Z factor for vapour

$$Z^v = 1 + \beta^v - q^v \beta^v \frac{Z^v - \beta^v}{\left(Z^{v2} + 2Z^v\beta^v - \beta^{v2}\right)} \tag{19}$$

4.) And for liquid

$$Z^l = \beta^l + \left(Z^{l2} + 2Z^l\beta^l - \beta^{l2}\right)\frac{\left(1 + \beta^l - Z^l\right)}{q^l\beta^l} \tag{20}$$

5.) Calculate VLE

$$I^{l,v} = \frac{1}{2\sqrt{2}} \ln\left(\frac{Z^{l,v} + \beta^{l,v}\left(1+\sqrt{2}\right)}{Z^{l,v} + \beta^{l,v}\left(1-\sqrt{2}\right)}\right) \tag{21}$$

$$\ln \hat{\phi}_i^{l,v} = \frac{b_i}{b^{l,v}}\left(Z^{l,v} - 1\right) - \ln\left(Z^{l,v} - \beta^{l,v}\right) - \bar{q}_i^{l,v}\, I^{l,v} \tag{22}$$

$$f_i^l = x_i \hat{\phi}_i^l p \qquad f_i^v = y_i \hat{\phi}_i^v p \tag{23}$$

3 Lumping & Delumping

Reservoir fluids consist of thousands of constituents which are impossible to be all characterized by a PVT laboratory. Today's fluid reports vary between detailed component information up to carbon numbers of 7 to 30 [29]. Since computing time is a major restriction in reservoir simulation, the number of components in fluid models for reservoir simulation is usually held at a minimum. Because simulation time for a compositional reservoir model is already high due to more governing equations to be solved, the iterative nature of flash calculations and the associated additional computing time is limiting the practical capabilities even for modern hardware and their computational power. Because of the rather small ranges of pressure conditions during isothermal reservoir simulation, it is common to lump or group single components to PCS in order to decrease the overall number of components in the fluid model. [4]

The selection of the lumping scheme defines which components to group. It usually depends on the application. Whereas a gas injection will probably need 10 components to capture the physical process, two components are probably enough to model the phase behaviour of depletion simulation runs, accurately. This is not valid for near critical fluids. Lumping down to two components would result in a black-oil model with only oil and gas as explicit components. In literature the satisfactory number of components is reported between 4 and 10 for reservoir modelling purposes. [4], [9], [31]

3.1 Lumping

Lumping as a process is by definition of Pedersen et al. [7]:

> "Deciding what carbon number fractions to lump (group) into the same pseudocomponent.
> Averaging T_c, p_c and ω of the individual carbon number fractions to one T_c, p_c and ω representative for the whole lumped pseudocomponent" [7, p. 117]

This definition is congruent with Danesh's [4]. The first part consists of deciding how the lumping scheme should look like. There are many recommended approaches in the literature which will be listed below. A practical oriented approach is, to combine N2 and C1 to one PCS and CO2 and C2 to another PCS, in addition obvious candidates like iC4 and nC4 to C4, and iC5 and nC5 to C5. [4]

If a proper scheme was selected, the unanswered question is how to determine the properties for the pseudocomponents in order to achieve a consistent fluid model. This is usually done by averaging, which can be applied in diverse ways, although it should be mentioned that even the most carefully selected lumping schemes will still result in a loss of information because of the nature of lumping itself.

The simplest averaging method would be molar averaging, **eq.** (24), for all properties also known as Kay's rule. [4]

$$\theta_k = \frac{\sum_i^k z_i \theta_i}{\sum_i^k z_i} \tag{24}$$

Where θ is an arbitrary property and k stands for the number of detailed components within one PCS.

Other scheme selection and averaging methods are listed here:

- Weight-based grouping, each lumped PCS should weigh the same, this ensures equal importance for phase behaviour calculations. [32]
- Logarithmic weight-based method, where Danesh et al. [9] proposed an automatable lumping/delumping scheme generation procedure, for use during a reservoir simulation to account for compositional changes within PCS and therefore prevent failure of valid prediction of phase behaviour calculations. Ordering of components according to their true boiling point (TBP) is necessary and then, PCS with equal $\sum_i^k z_i \ln MW_i$.are getting grouped and their properties will be averaged using **eq.** (24). [9]
- Grouping PCS on basis of volatility was proposed by Li et al. [33]. The lumping-scheme is accomplished by selecting intervals on an equilibrium ratio scale. [33]
- Montel and Gouel [31] proposed a method (see Figure 16, pg. 19) which uses a partition algorithm that tries to minimize the distance between properties of components iteratively and hence increase the similarity of components belonging to a group. This is also called clustering. They used molar weighting from the single components later to calculate the centre of clusters, which acts then as property for the PCS.
- Leibovici [6] proposed a fundamental approach in 1993. He used the mixing rules from an EoS to derive the EoS parameters for PCS analytically. This means that the EoS parameters for the detailed and lumped fluid will be almost identical (low loss of information due to lumping compared to other methods). It is emphasized that the analytical solution is only valid if no binary interactions coefficients (BIC) between components are assigned. However, he did not suggest any group selection method.
- A flow based lumping approach was conducted by Rastegar and Jessen [34], [35]. They included the displacement dynamics into the lumping scheme selection and stated that components with similar K-values should be lumped together according to their variation over the displacement length. They stated that the objective function of $obj = \int_0^L \left(K_{iI_0} - K_{jI_1}\right) dx$ should be minimized in order to find a lumping scheme.
- A kind of combination of [31] and [6] was proposed by Assareh et al. [3] in 2014. They proposed to use fuzzy clustering to find the similarities between the critical properties and define the clusters and calculate the respective cluster properties by use of EoS based mixing rules. Assareh et al. [3] made also a comparison between automated group selection (direct approach) and excluding important components from grouping (screening approach), where the latter was found to be more precise for a gas condensate mixture.

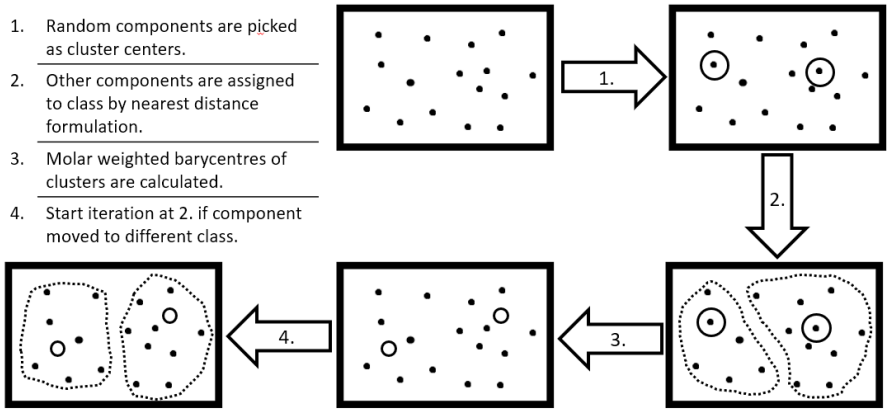

Figure 16 - Lumping algorithm based on similarities adopted from Montel and Gouel [31]

As already mentioned above, the lumping scheme also depends on the recovery process from the reservoir simulation viewpoint. In e.g. gas injection simulation, the fluid behaviour cannot be modelled correctly using a black oil formulation.

In a process plant however, the number of different units and their different pressure and temperature conditions are more sensitive to an EoS model and therefore the fluid model should be as detailed as possible to predict the fluid phase behaviour accurately. Therefore, to satisfy both contrary demands, a method which is retrieving detailed component information from lumped components as a result from a reservoir simulator is of interest. [7]

3.2 Delumping

Composition retrieval, or delumping, should compensate the loss of detailed information about the system. Not only in regards for process simulation but also to review the state of the compositional reservoir simulation. If large compositional variations are expected, the lumped fluid description could lose its validity because the pseudo component properties are linked to the composition of its grouped single components [11].

In general, delumping is a term for translating compositions of lumped systems into compositions of detailed systems. [8]

In 1988, Schlijper and Drohm [8] introduced the term inverse lumping, as one of the first delumping methods. They proposed a method by which results from a flash calculation of the lumped system (lumped equilibrium K-values) are obtained to approximate detailed compositions by the use of EoS- and split-parameters (determined by feed composition and expected change in composition) through Gibbs energy minimization. A different type of correlation was applied by Danesh et al. [9], as already introduced above in the Lumping subchapter. They used the linear trend of the lumped K-values, given by **eq.** (25), to retrieve the detailed K-values.

$$\ln K_i = c_0 + c_1(1+\omega_i)\left(1-\frac{T_{ci}}{T}\right) \tag{25}$$

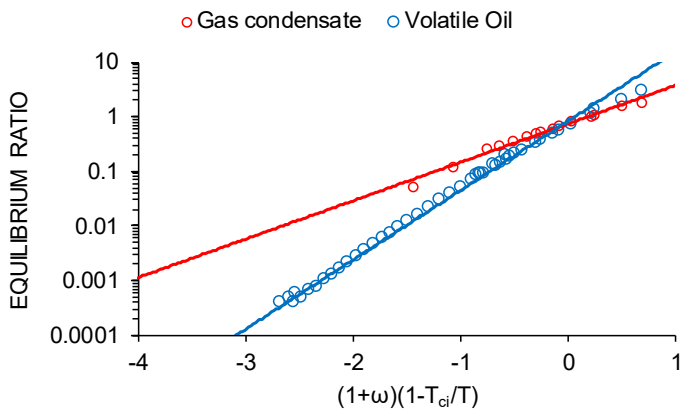

Figure 17 - Example of the linear trend of the equilibrium ratios of a 46-component volatile oil and a 15-component gas condensate

Visualized by Figure 17, the idea of their thought of delumping can be seen. If the lumped mixture would have well approximated properties assigned to the PCS the trend of the lumped equilibrium ratios obtained by flash calculations, should be the same for the detailed mixture as well.

To approximate detailed equilibrium ratios out of the $\ln K_i$ trend calculated from the lumped system, c_0 and c_1 in **eq.** (25) are constants which are determined by fitting the trend to the lumped data. It is mentioned that this approach was presented as a combination of lumping-delumping- (and regrouping, if necessary) algorithm in an automated process for application in reservoir simulators. [9]

An extension of the back translation from lumped to detailed composition via the $\ln K_i$ trend, done by Danesh et al. [9], was proposed by Leibovici et al. [10]. They stated that the fugacity coefficients of components in a mixture can be expressed as linear combinations of the EoS parameters $\theta_{i,j}$ of that components.

$$\ln \hat{\phi}_i^{l,v} = c_0 + \sum_{j=1}^{\eta} c_j \theta_{i,j} \quad \eta\text{…number of EoS parameter} \tag{26}$$

This means that at equilibrium, **eq.** (112), in Appendix A.5 pg. 99, applies and therefore **eq.** (116), in Appendix A.6 pg. 100, can be used to express **eq.** (26) further.

$$\ln K_i = \ln \hat{\phi}_i^{l} - \ln \hat{\phi}_i^{v} = \Delta c_0 + \sum_{k=1}^{k=\eta} \Delta c_k \, \theta_{i,k} \tag{27}$$

Where the differences are calculated from the respective phase coefficients, shown in **eq.** (28) and the two PR-EoS parameters are mentioned in **eq.** (29).

$$\Delta c_k = c_k^{l} - c_k^{v} \qquad c_k^{l,v} = f(p, T, \pi) \tag{28}$$

$$\theta_{i,1} = \sqrt{a_i} \qquad \theta_{i,2} = b_i \tag{29}$$

Leibovici et al. [10] found that the analytical expressions for c_0, c_1 and c_2, respectively for each phase, derived for the PR-EoS, are:

$$c_0^{l,v} = \ln\left(\frac{p}{RT}\, V^{l,v} - b^{l,v}\right) \tag{30}$$

$$c_1^{l,v} = \frac{\sqrt{a^{l,v}}}{\sqrt{2}b^{l,v}RT} \ln\left(\frac{V^{l,v} + \left(1+\sqrt{2}\right)b^{l,v}}{V^{l,v} + \left(1-\sqrt{2}\right)b^{l,v}}\right) \tag{31}$$

$$c_2^{l,v} = \frac{Z^{l,v} - 1}{b^{l,v}} + \frac{a^{l,v}}{2\sqrt{2}{b^{l,v}}^2 RT} \ln\left(\frac{V^{l,v} + \left(1+\sqrt{2}\right)b^{l,v}}{V^{l,v} + \left(1-\sqrt{2}\right)b^{l,v}}\right) \tag{32}$$

With **eq.** (29) substituted into **eq.** (27) we get the formulation of the well-known LSK-algorithm (Leibovici-Stenby-Knudsen), which is a thermodynamic consistent delumping method [2], [10], [36].

$$\ln K_i = \Delta c_0 + \Delta c_1 \sqrt{a_i} + \Delta c_2 b_i \tag{33}$$

The EoS parameter honour the consistency for lumped and detailed mixture by:

$$a^{lumped} = a^{detailed} \quad \text{and} \quad b^{lumped} = b^{detailed} \tag{34}$$

If all BIC between components in the mixture are zero, the Δc_k coefficients can be calculated analytically with **eq.** (30), (31) and (32). If BIC are non-zero, then a bypass solution was recommended by which the Δc_k coefficients can be approximated, by using any least square regression method.

The proposed delumping procedure using LSK-algorithm is following: [10], [36]

1.) The detailed system should be lumped into minimum $\eta + 1$ components, where η is the number of EoS parameters, and the critical properties should be calculated for the lumped PCS, favourable with a consistent lumping method like Leibovici proposed in [6].
2.) A Flash calculation is performed on the lumped system in order to obtain the lumped components K-values.
3.) Find Δc coefficients by either
    a. Analytical expressions, **eq.** (30), (31) and (32), only if all BIC are zero
    b. Use regression if BIC are non-zero
4.) The lumped system is delumped using Δc_k coefficients of the lumped system and **eq.** (33) to calculate the detailed component K-values.
5.) Detailed K-values are used in a flash calculation to receive molar composition and vapour fraction of the detailed system. This can either be done by using **eq.** (10) again and find the detailed vapour fraction [36], or assume that $F_V^{lumped} \equiv F_V^{detailed}$ and calculate the mole fractions directly with **eq.** (9). [2]

It should be mentioned that the assumption, using the lumped equilibrium ratios for approximating the detailed system is limiting the accuracy of the delumping algorithm since the delumping is, thus, dependent on the lumping itself. [36]

Leibovici et al. [2] additionally proposed a method of how to implement the LSK algorithm in a reservoir simulator using the delumping algorithm as a post processor. By storing the data of the lumped simulation for every cell and timestep to delump the calculated equilibrium ratios of the lumped system for every cell afterwards with a fully explicit finite difference scheme. Since the reservoir simulator calculations were executed using an adaptive implicit scheme, they had to reduce the timestep for delumping because of stability reasons, but found nevertheless, satisfying results [2].

They used the stored:

- molar fluxes between each grid block I_0 and its neighbour I_1 ($l^m_{I_0I_1}, v^m_{I_0I_1}$),
- molar fluxes between blocks into or out of wells ($q^m_{oI_0}, q^m_{gI_0}$),
- vapour fraction $F_V^{lumped,m}$ for each grid block,
- mole fractions $z^m_{iI_0}$ for every component in every phase,
- lumped equilibrium ratios for every grid block $K^{lumped,m}_{iI_0}$,

from the lumped system (lower case variables) and assumed that these are equal to values of the detailed system (upper case variables) for each time step m.

For molar fluxes between grid blocks:

$$L^m_{I_0I_1} = l^m_{I_0I_1} \qquad V^m_{I_0I_1} = v^m_{I_0I_1} \tag{35}$$

For fluxes into or out of wells

$$Q^m_{oI_0} = q^m_{oI_0} \qquad Q^m_{gI_0} = q^m_{gI_0} \tag{36}$$

After approximating the detailed equilibrium ratios with the LSK-algorithm, and the assumption $F_V^{lumped,m} = F_V^{detailed,m}$ one can evaluate the normalized detailed mole compositions for each phase X_i^m and Y_i^m, with **eq.** (9). By knowing the composition for both, lumped z_i and detailed fluid Z_i and overall moles of fluid n_T, for the initial state of the reservoir, the composition of detailed components for every timestep can be calculated with:

$$\begin{aligned} Z^{m+1}_{iI_0} = \frac{Z^m_{iI_0} n^m_{TI_0}}{n^{m+1}_{TI_0}} &- \frac{\Delta t}{n^{m+1}_{TI_0}}\left(X^m_{iI_0} Q^m_{oI_0} + Y^m_{iI_0} Q^m_{gI_0}\right) \\ &- \frac{\Delta t}{n^{m+1}_{TI_0}} \sum_{I_1} \left(X^m_{iI_1} L^m_{I_0I_1} + Y^m_{iI_1} V^m_{I_0I_1}\right) \end{aligned} \tag{37}$$

After the above described delumping procedure for reservoir simulators, proposed by Leibovici et al. [2], was implemented into E300 by Schlumberger, Vignati et al. [37] used the E300

delump facility to create a fully integrated asset model, by using E300 as subsurface- and HYSYS as surface simulator, not focused on the plant products but more on gas cycling purposes for production network optimization reasons. [37]

A different proposal was published by Faissat and Duzan [22] after Schlijper and Drohm [8] and Leibovici et al. [10]. They addressed the fluid description discrepancies between reservoir and surface simulation and proposed to use varying PCS split factors, contrary to at that time commonly used constant split factors, in order to obtain single component information. They used single-cell simulations with both lumped and detailed fluid descriptions to find the varying representation of the split factors for the whole simulation. They showed that this approach makes it possible to decrease the error of lumped full field simulation results for use in process simulations. [22]

Since Leibovici et al. [10] established their method for mixtures without any BIC, the regression method for non-zero BIC yields to inaccurate results. To compensate this issue Nichita and Leibovici [38] developed a delumping method, based on a reduction approach. This should reduce the problems' dimensionality by reformulation of the problem. They derived a thermodynamically consistent method by which the fugacity coefficients of the components are only dependent on pressure, temperature and reduction parameters $Q = \{\alpha, B, \gamma^T, \theta^T\}^T$ and not on compositions directly. They proved that their method applies to mixtures with:

- non-zero BIC between single components and PCS,
- zero BIC between PCS,
- non-zero BIC between PCS,

on condition that BIC of components within groups are zero. The latter is no severe restriction since the lumping is anyway accounted for similar components which are having zero BIC with each other normally [38]. The algorithm and procedure of the reduction method is not straight forward and needs also specific adherences for calculation but, for the sake of keeping things simple in this thesis, it is not explained here in more detail, but can be found in the referred paper.

The delumping method based on reduction was one of a variety of developments in phase equilibria calculations. The fundamental principle of the reduction method was also used to develop a multiphase flash calculation technique by Nichita and Graciaa [39] as well as other VLE applications such as: phase stability analysis, and critical point calculations. [39]

Nichita et al. [40] accomplished a detailed comparison of the PVT-behaviour of fluid mixtures by whether using LSK-delumping or the reduction-delumping approach. De Castro et al. [5] published a comparison for application in a full compositional reservoir simulation, between the LSK-algorithm using regression and the reduction approach from Nichita and Leibovici [38]. Both papers concluded that the reduction approach outperforms the LSK-regression method and showed excellent agreement between delumped and detailed reservoir simulation, as well as PVT behaviour, results for non-zero BIC mixtures. [5], [40]

The most recent developments in delumping methods were conducted by Assareh et al. for both cubic EoS [11] and non-cubic EoS [41]. The two methodologies are using the same approach, but the non-cubic EoS will not be explained here any further since it is outside the scope of this work.

For the cubic EoS delumping technique Assareh et al. [11] proposed introducing a delumping coefficient array. In this array every component in the lumped system has three delumping coefficients where the first two coefficients are the same for all single components and PCS (mixture properties) and the last one is dependent on the BIC and is used to retrieve the detailed information from the PCS. They tested the new delumping technique on two real reservoir fluids and proved that the phase behaviour of their delumping method is more accurate than the proposed one's from Danesh et al. [9] and Leibovici et al. [10]. Still an important remark comes from the fact that the accuracy of the delumping technique is only as good as the lumping technique itself. [11]

4 Model and Simulation Setup

This chapter will explain the steps taken to set up the simulation models and everything needed to utilize the investigation of the product streams of the GTU. The chapter is built on the foundation set up in the fundamentals chapter. Practical aspects will be added in this section as it was not covered in the theoretical part. The structure of the subchapter will differ from the fundamental part since it will start with fluid modelling because it is crucial for both, reservoir and process simulation, and the sequence of operations also followed this structure.

4.1 Fluid Descriptions

The initial fluid description and its characterization was already done by PML PVT expert Dr. Assareh. This fluid description is considered as detailed and acts as reference for all the delumping simulation cases. The first task was to analyse the two different fluids. One is a gas condensate and the other a volatile oil, both near critical reservoir fluids. In the following subchapter both fluids are separately treated. The fluid modelling and lumping itself was done by using PVTi, which is also used to generate the PVT input files for E300. In order to attain consistency between the simulation models, the detailed fluid descriptions were translated from PVTi to HYSYS, which will be investigated in the last sub-chapter.

4.1.1 Gas Condensate Fluid Modelling

The gas condensate consists of 15 components with a composition, as shown in Table 2. In Figure 18, it can be seen that the phase envelope has an open shape without a critical point. The reservoir temperature was reported at $106\ °C$ and the initial reservoir pressure at $583\ bar$.

Table 2 - Gas condensate composition

Component	Mole Percent [%]
N2	1.9971
CO2	0.84903
C1	68.671
C2	11.581
C3	4.8182
iC4	0.86203
nC4	1.5101
iC5	0.64003
nC5	0.62703
PC6	0.93404
PC7	0.91304
PC8	0.81503
PC9	0.42102
C10+	5.0403
C18+	0.32091

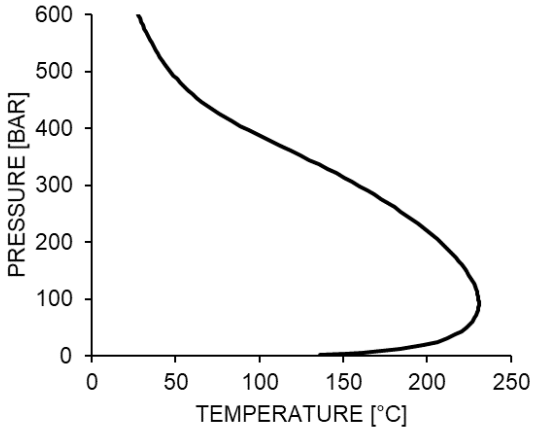

Figure 18 - Phase envelope of gas condensate

The fluid description was split by Dr. Assareh to extend the detailed composition. The lab report consists of proven data up to C10+. This extension is a common approach which is achieved by approximating an exponential decline of the heavier fraction-mole concentrations, further information can be looked up in *“Phase Behaviour of Petroleum Fluids” by* Pedersen et al. [7].

Using the above introduced detailed fluid description, the selection of the lumping scheme was undertaken. Together with a proposed lumping scheme from Dr. Assareh, there were 5 different lumping schemes in addition.

- Dr. Assareh Lump – Lump_ME (see Appendix C.1, Table 11, left side)
- Lump_2 (see Appendix C.1, Table 11, right side)
- Lump_ML_10A (see Appendix C.1, Table 12, left side)
- Lump_ML_5A (see Appendix C.1, Table 12, right side)
- Lump_ML_10B (see Appendix C.1, Table 13, left side)
- Lump_ML_5B (see Appendix C.1, Table 13, right side)

The lumping scheme selection, besides Dr. Assareh's proposal, was based on the approach from Assareh et al. [3], where a fuzzy clustering algorithm was used to determine groups of similar components. The fuzzy clustering script was set up with MATLAB® and consists of two different modes. The first mode, A, searched for similarities in a two-dimensional domain using the attraction and repulsion EoS parameter of every component a_i and b_i (see Appendix C.1 - Figure 65, pg. 106). The second mode, B, searched for similarities between single component properties p_{ci},T_{ci} and ω_i (see Appendix C.1 - Figure 66, pg. 106). The fuzzy clustering algorithm was used from the already inbuilt `fcm` option from MATLAB®, the short clustering script can be found in Appendix B.

There were two lumping schemes created using the first mode A (Lump_ML_10A and _5A, with 10 and 5 overall components, respectively) and two using the second mode B (Lump_ML_10B and _5B). In addition to the four generated schemes and one proposed scheme (Lump_ME) there was an attempt to exclude the sensitive light components from lumping (Lump_2) by myself, analogously to the screening approach of Assareh et al. [3], but this case was discarded because the lumping resulted in an inaccurate fluid description. The tabulated forms of the lumping schemes for the gas condensate can be found in Appendix C.1, Table 11 - Table 13.

The lumping of the remaining five models was completed by using PVTi's inbuilt lumping procedure, using EoS based mixing rules for generating PCS. This ensures thermodynamically consistency, as already mentioned in the last chapter by proposal of Leibovici [6]. But since these mixing rules are only exact for zero BIC, there will still be an approximation involved and this leads to some inaccuracy. This inaccuracy, can be seen in the summary with all phase envelopes for the gas condensate fluid descriptions, Figure 19. It becomes clear now why Lump_2 was discarded since the lumping of all heavy fraction compounds led to a crucial shrinking of the phase envelope on the dew point side. This effect was also reported by Assareh et al. [11], and it will be experienced the other way too, where immense lumping of light components leads to shrinking of the bubble line of the phase envelope, as will be seen in the next subchapter 4.1.2.

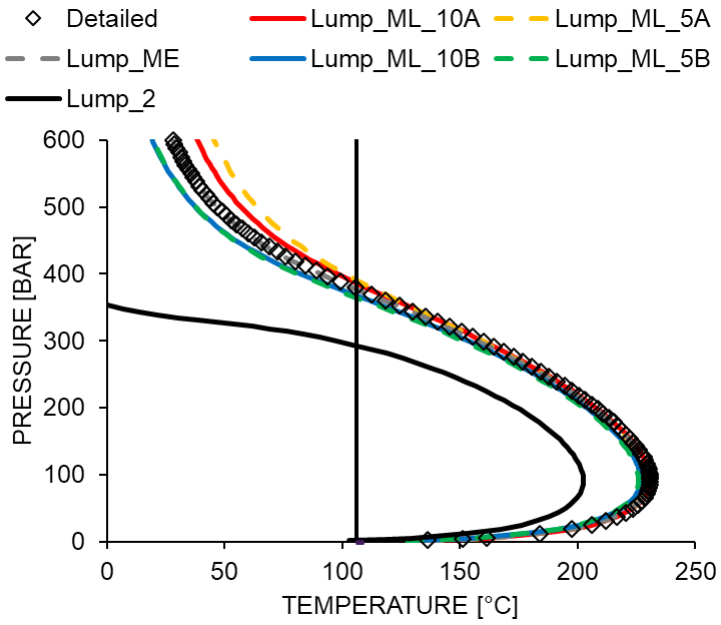

Figure 19 - Phase envelopes of different lumping schemes of gas condensate

After neglecting Lump_2 for further analysis a quality check was performed in order to quantify the deviations for later interpretability. The different fluids were flashed at different stages and some key properties - $F_V, MW^{v,l}, Z^{v,l}$ and $\rho^{v,l}$ - were compared with each other. The results of the flash stages and the detailed error analysis, with a brief explanation, can be found in Appendix C.2. A summary as graphical representation of these deviations can be seen in Figure 20.

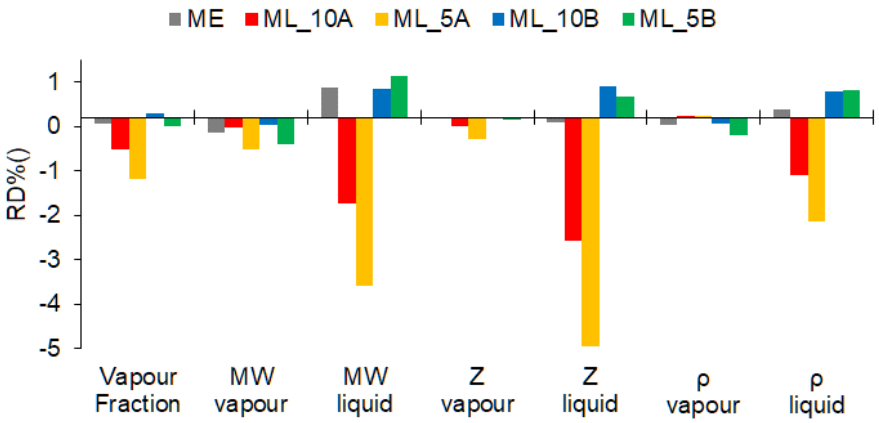

Figure 20 - Deviations of the quality check for gas condensate fluid description (values from Table 16, pg. 108)

In Appendix C.2 - Table 15, pg. 108, the deviations $RD\%\,()$ of the key parameters are summarized as geometric average $\emptyset_{geo}$, which should quantify the accuracy of the fluid model as a single measure. The absolute value of $\emptyset_{geo}$ should be interpreted with care since the PVT behaviour of the fluids will be different for different measurements and is more complex as stated by a single value. As already seen in Figure 19, at $106\,°C$, the liquid drop out during depletion will be less since the dew point is overestimated for e.g. Lump_ML_5A, during a constant volume depletion experiment (CVD) (see Figure 21).

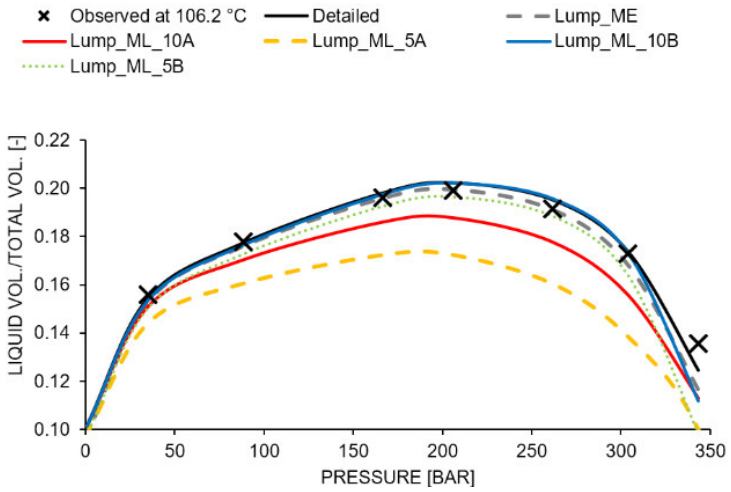

Figure 21 - Liquid saturation plot from a constant volume depletion experiment

The trend of Figure 21 is directly linked to the findings of Figure 20 and thus deviations especially for the gas-oil ratio (GOR) are expected for the reservoir simulation since less liquid will form during the phase transition in lower pressure regimes.

4.1.2 Volatile Oil Fluid Modelling

For the volatile oil, the same procedure, as done for the gas condensate, was undertaken. Since the PVT lab report for the volatile oil is more detailed, the proven data consists of 48 characterized components in total. The reservoir temperature was like the gas condensate at $107.9\,°C$ with an initial pressure of $533\,bar$. The 48 components will be referred to as initial fluid description (see Table 3). The initial fluid model was again established by Dr. Assareh. Although it was planned to use this as reference fluid, internal limitations of E300 were prohibiting it for use as reference description. It was found that the maximum number of components, allowed for the E300 delumping facility, is 46. This issue was bypassed by setting up a detailed fluid description where the latter three components of the initial one, C33, C34 and C35, are lumped to one PCS which is named C33+. The created detailed fluid description was again analysed and an exact agreement was obtained (see Figure 22).

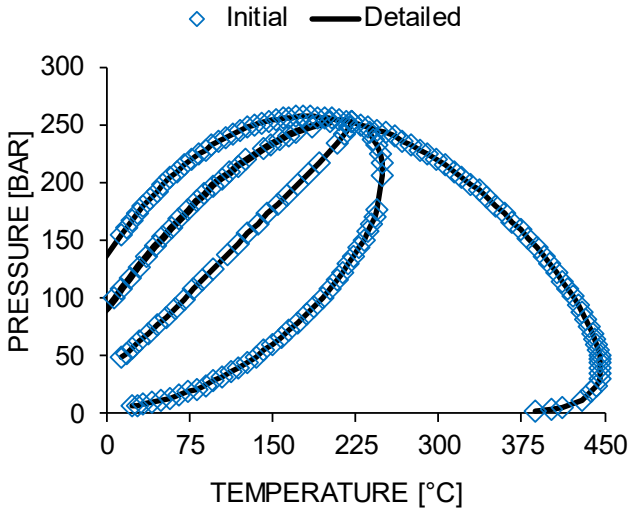

Figure 22 - Initial and Detailed phase envelope with three quality lines $F_V = 0.25, 0.50\ \&\ 0.75$, for the volatile oil

Table 3 - Initial composition of the volatile oil

Component	Mole Percent [%]	Component	Mole Percent [%]	Component	Mole Percent [%]
N2	0.388	C2BE	0.105	C21	0.218
CO2	0.747	MPXY	0.439	C22	0.187
C1	49.519	OXYL	0.112	C23	0.158
C2	14.955	C8	1.814	C24	0.136
C3	8.383	C9	1.426	C25	0.120
IC4	1.323	C10	1.787	C26	0.104
NC4	3.231	C11	1.313	C27	0.093
IC5	1.223	C12	1.050	C28	0.082
NC5	1.376	C13	0.950	C29	0.071
BEN	0.058	C14	0.726	C30	0.061
C6	1.833	C15	0.654	C31	0.055
MCC5	0.264	C16	0.492	C32	0.049
CC6	0.281	C17	0.423	C33	0.043
MC6	0.699	C18	0.373	C34	0.038
TOL	0.240	C19	0.315	C35	0.034
C7	1.625	C20	0.252	C36+	0.178

Table 4 - Detailed composition of the volatile oil

Component	Mole Percent [%]	Component	Mole Percent [%]	Component	Mole Percent [%]
N2	0.388	C2BE	0.105	C21	0.218
CO2	0.747	MPXY	0.439	C22	0.187
C1	49.518	OXYL	0.112	C23	0.158
C2	14.955	C8	1.814	C24	0.136
C3	8.383	C9	1.426	C25	0.120
IC4	1.323	C10	1.787	C26	0.104
NC4	3.231	C11	1.313	C27	0.093
IC5	1.223	C12	1.050	C28	0.082
NC5	1.376	C13	0.950	C29	0.071
BEN	0.058	C14	0.726	C30	0.061
C6	1.833	C15	0.654	C31	0.055
MCC5	0.264	C16	0.492	C32	0.049
CC6	0.281	C17	0.423	C33+	0.115
MC6	0.699	C18	0.373	C36+	0.178
TOL	0.240	C19	0.315		
C7	1.625	C20	0.252		

The total number of lumping schemes was defined as five cases again. One proposed by Dr. Assareh, and four schemes, created using the fuzzy clustering approach from Appendix B, using again mode A and B. The lumping schemes can be found in Appendix D.1, pg. 111. It should be mentioned that the lumping was done on the initial fluid description as starting point

in order to keep the error propagation, introduced by generating C33+ for the detailed description, as small as possible. The lumping schemes are following:

- Dr. Assareh Lump – Lump_ME (see Appendix D.1, Table 20)
- Lump_ML_18A (see Appendix D.1, Table 22)
- Lump_ML_10A (see Appendix D.1, Table 21)
- Lump_ML_18B (see Appendix D.1, Table 24)
- Lump_ML_10B (see Appendix D.1, Table 23)

The initial approach for overall component number selection was to create lumped fluid models with 20 and 10 components but during accomplishing the simulations it was found that the E300 delumping facility has again a limitation regarding maximum delump-able components. This was, maybe arbitrarily, set to 18 by Schlumberger.

In the following the comparison between the phase envelopes will be split up visually, to ensure the visibility of the deviations of the lumping schemes. In Figure 23, we can see the compared phase envelopes for the detailed and the lumped fluid descriptions, clustered with mode A where only a_i and b_i are the similarity parameters. ML_18A has sufficient accuracy compared to the detailed envelope, while ML_10A has a highly deviated critical point and thus shifted envelope lines. This comes from the fact that ML_10A consists of a PCS where 17 components are lumped together.

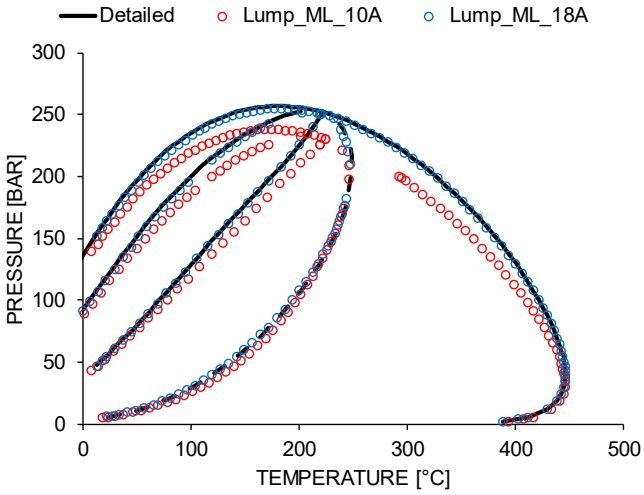

Figure 23 - Phase envelope of detailed, ML_18A and ML_10A for volatile oil

The comparison with mode B, is shown in Figure 24. The envelopes are matching much better, only ML_10B has a slightly decreased phase envelope due to the heavy lumping from 48 down to 10 components. But as it can be seen in Appendix D.1 - Table 23, pg. 112, the fuzzy clustering distributed the components to all PCS more uniform in ML_10B, compared to ML_10A.

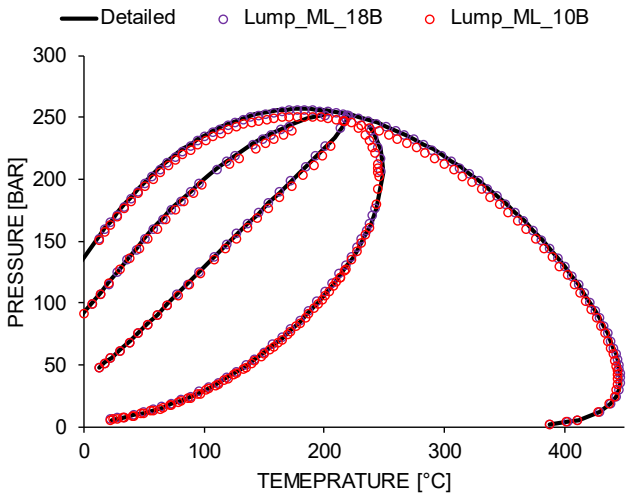

Figure 24 - Phase envelope of detailed, ML_18B and ML_10B for volatile oil

Last but not least, Figure 25 shows the proposed lumping scheme by Dr. Assareh. It is matching the detailed envelope almost exactly. Only small deviations on the dew line side can be explained by the lumping of heavy components, since 25 single components are lumped to four PCS, Appendix D.1 - Table 20, pg. 111.

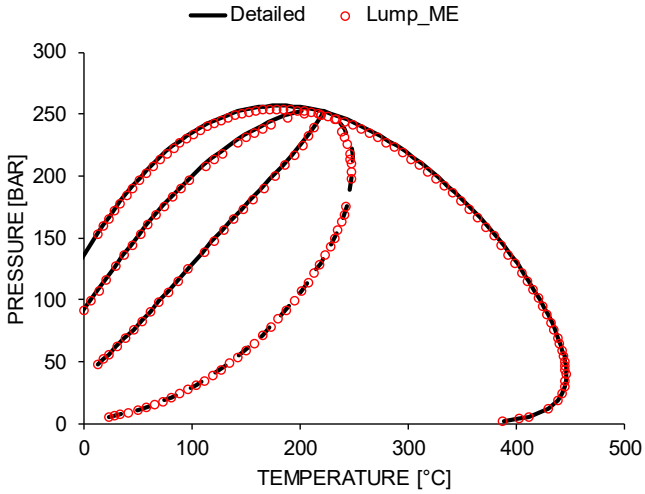

Figure 25 - Phase envelope of detailed and Lump_ME for volatile oil

The explicit data for the quality check, of the volatile oil fluid descriptions, can be found in Appendix D.2, from pg. 114 and pg. 115. As summary of this, Figure 26 is showing the geometric averaged relative error $\emptyset_{geo}(RD\%)$ for all variables with the three flash stages averaged.

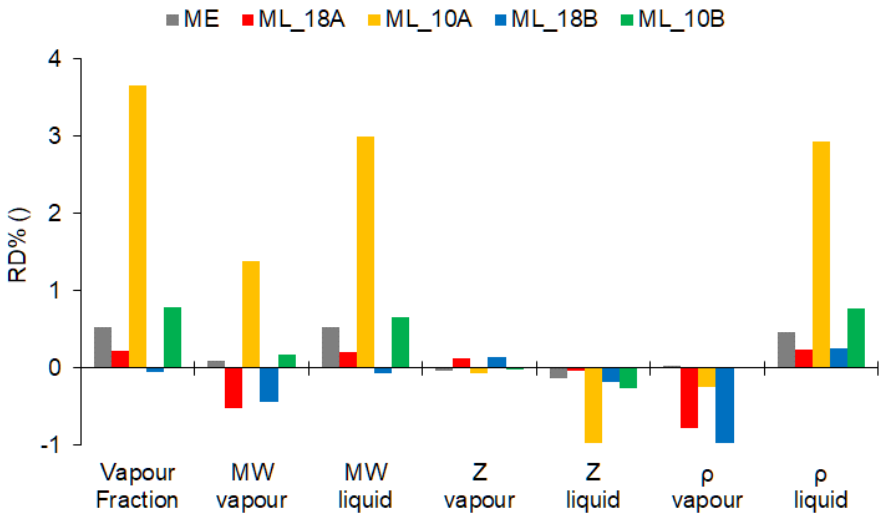

Figure 26 - Deviations of the quality check for volatile oil fluid description (values from Table 27, pg. 115)

Except for the outliner case ML_10A all errors are below 1 % which is a sufficient range of deviations for the fluid descriptions which are used in this thesis.

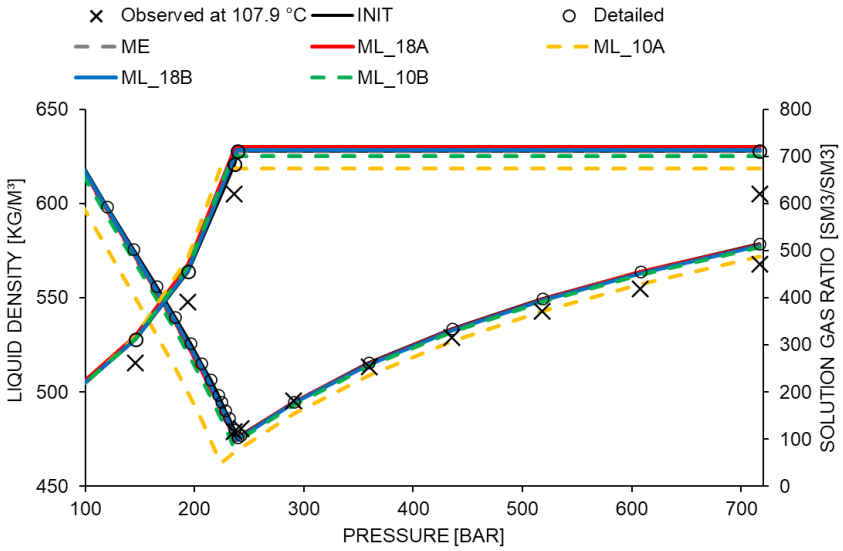

Figure 27 - Experimental result comparison of liquid density (lower series) from a differential liberation and the solution gas ratio (upper series) of a constant volume depletion

Figure 27 shows simulated differential liberation experiment (DLE) results, together with real observed datapoints. Although all fluid models are overestimating the solution gas ratio R_s, compared to the observed data, the agreement of the different cases are similar to the calculated $\emptyset_{geo}(RD\%)$ values. The accuracy trend of the different fluid models to the reference is: $ML\_10A < ML\_10B < ME < Detailed < ML\_18B < ML\_18A$, for both liquid density and solution gas ratio. Noting the small deviations of ME, 18A and 18B it is expected that these will show good agreement in the upcoming simulations too.

For summarizing the lumping schemes and reviewing the scheme selection, there were many lumping schemes presented throughout the in chapter 3 introduced literature. Some of them propose a lumping ratio $\mathcal{R}$ (see **eq.** (38)) of ~ 18 % [3], [8], [9], but also as high as $\mathcal{R}$ ~ 40 %

[2], [37] are mentioned. Taking every reviewed lumping ratio as average it can be proposed that:

$$\mathcal{R} = \left(\frac{N_c^{lumped}}{N_c^{detailed}}\right)_{avg\ for\ literature} * 100\ \% = 26\ \% \tag{38}$$

This means, that the in this thesis selected five lumping schemes for both, gas condensate and volatile oil with $30\ \% < \mathcal{R}_{gas\ condensate} < 60\ \%$ and $20\ \% < \mathcal{R}_{volatile\ oil} < 37\ \%$ respectively, are covering a reasonable range in order to investigate the impact of delumping on the surface facility product streams.

4.1.3 Fluid Description for Process Simulation

Since fluid modelling consistency is one of the most important element in coupling of reservoir and surface simulation and was already discussed by Faissat and Duzan [22], it was ensured that the detailed fluid description was identical for both E300 and HYSYS. Although the process simulation itself will be explained later the fluid modelling within HYSYS is going to be explained here.

HYSYS is intuitively built for setting up a simulation. There are two main working environments as already mentioned. For setting up the fluid model the “property” environment has to be adjusted. As a first step, the components get added to the component list. N2, CO2, C1 – nC5 can be inserted using library components from the HYSYS database. For the PCS we need to define hypothetical components (hypos), which is just another term for PCS. The hypos are created by using the PVTi calculated PCS properties, which can be found in Table 5. Since water is handled in E300 as a separate phase routinely, H2O needs to be added to the component list too. In addition, since glycol is needed for the glycol dehydration unit, ethylene glycol (EGlycol) is added too. After these additions, the HYSYS component list is completed.

Table 5 - Hypo properties as input for HYSYS fluid model

Name	Boiling Temp [°C]	MW [g/mol]	ρ^l [kg/m³]	T_c [°C]	p_c [bar]	V_c [m³/ kmol]	ω
PC6	57.25	86.2	660.70	225.56	31.605	0.360	0.250
PC7	86.57	100.2	684.70	255.17	28.146	0.415	0.315
PC8	114.65	114.2	708.20	285.88	25.961	0.469	0.366
PC9	139.60	127.0	729.90	312.94	24.359	0.517	0.411
C10+	196.70	153.6	801.35	379.85	23.012	0.602	0.496
C18+	263.96	196.9	837.87	443.97	18.696	0.768	0.636

Next step, the fluid package is necessary to be defined. Since PR-EoS with volume correction was used in PVTi, it is also selected in HYSYS. To account for the volume correction, the HYSYS option “EoS-Density” needs to be modified. Dr. Assareh provided a worth-mentioning tip: it is required to change the sign of the volume-translation values extracted from PVTi for

proper implementation into HYSYS [18]. This is due to the internal handled definition of the parameter “EoS-Density” in HYSYS.

All other values were kept by default. For securing the above-mentioned consistency a comparative analysis, similar to the fluid model quality check, was conducted on the PVTi and HYSYS fluid models which can be found, in detail, in Appendix E - Table 31 till Table 35. The generated phase envelopes from both software-packages for the detailed gas condensate and volatile fluid descriptions are plotted in Figure 28.

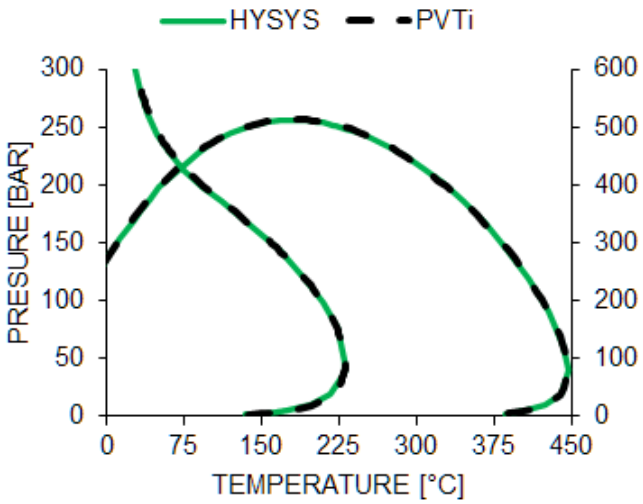

Figure 28 - Phase envelopes of PVTi and HYSYS fluid models

Both phase envelope comparisons, see Figure 28, showing almost exact agreement which is supported by the results of the comparative analysis, located in Appendix E. The summary of this can be found in Table 6.

Table 6 - Summary of comparative analysis from Appendix E

$\emptyset_{geo}^{Gas\ Condensate}(RD\%)$ [%]	-0.03
$\emptyset_{geo}^{Volatile\ Oil}(RD\%)$ [%]	-0.11

4.2 Reservoir Simulation Model

Full field reservoir models are consisting of millions of cells. This is limiting the practical usage of reservoir simulation, because of the long simulation time needed. Therefore, well spot models are commonly used to investigate certain behaviours. These well spot models are cut-outs of grid blocks near wells from a full field model commonly or are created from the scratch.

Also, in this thesis the simulation was conducted by using such single-well-models (SWM), since it has no advantage in conducting the reservoir simulation on a full-field scale for generating time dependent well streams as input for HYSYS.

4.2.1 Gas Condensate Single Well Model

The full-field simulation model of the high-pressure gas condensate reservoir consists of around one million cells. Such number is not unusual for full-field models. But because of run-time reasons, a SWM was used to obtain a simulated well stream.

The well was selected beforehand, and the grid was cut out a certain distance around the well. This cut-out, see Figure 29, has only 7680 cells and is therefore much faster to simulate.

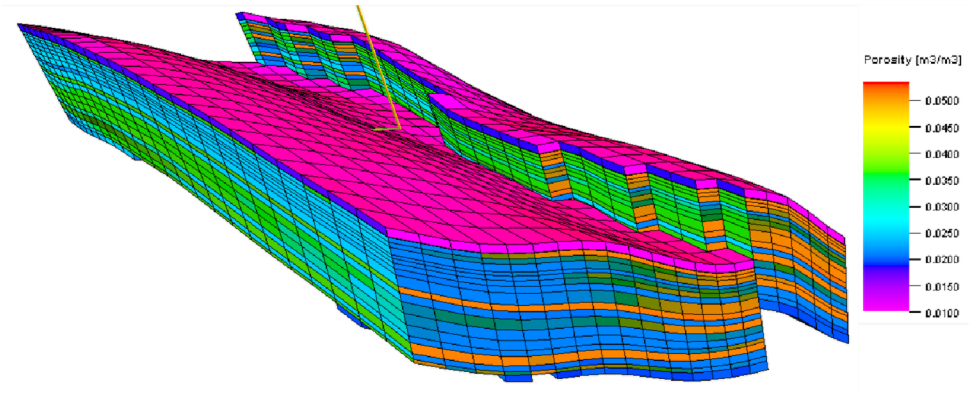

Figure 29 - cut out SWM of Well W1 from the high-pressure gas condensate full-field model, porosity coloured (first four layers not shown)

The model consists of about 24 layers where the first four layers are taken as non-productive (not shown in Figure 29 for better visualization reasons). The areal grid consists of $16x20$ blocks. The maximum horizontal and vertical permeability is about 4 and $0.03\ mD$ (millidarcy) respectively, with an average porosity of about $3\ \%$ making this part of the reservoir to a poor-quality reservoir. The SWM is penetrated by well $W1$ almost horizontal with a small down-dip and has only perforations in high productive intervals. The field is connected to a bottom-up aquifer, see Figure 30, with minor pressure support; thus, it was neglected for the purpose of simplification in this SWM. The water gas contact was determined at $5067\ m$ with an initial pressure of about $583\ bar$, as already mentioned in the fluid description chapter. The connate water saturation is about $S_{wc} = 0.3$.

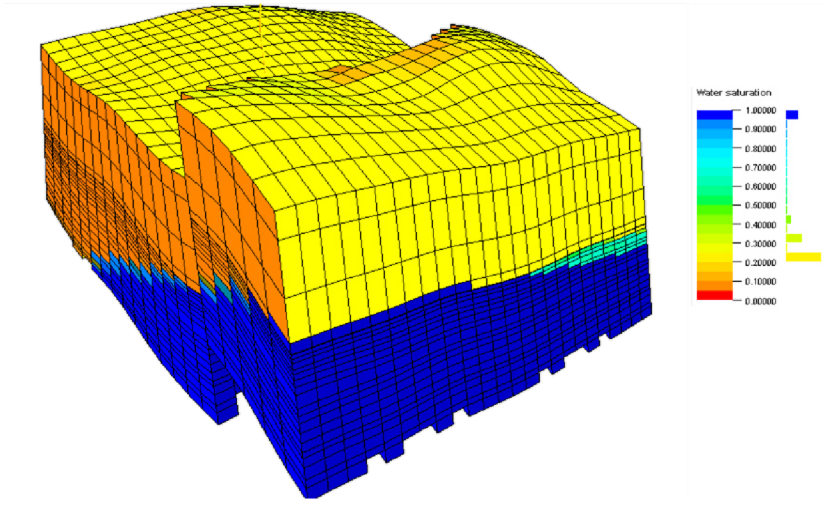

Figure 30 - Water saturation of SWM W1

The SWM simulation model was set up using vertical flow performance (VFP) tables, to relate tubing-head-pressure (THP) to the calculated bottom-hole-pressure (BHP) using sets of flowing conditions [42].

According to the surface equipment a two-stage separator was included where the flash conditions are following:

1. Stage: $p = 39.2\ bar$ and $T = 38\ °C$
2. Stage: $p = 1.01325\ bar$ and $T = 20\ °C$

The well $W1$ started production on August 2010 and the history included monthly production rates until October 2017.

The reference case was simulated by using the detailed fluid description (exported by PVTi) of the gas condensate, which consists of 15 components. The detailed main simulation (`*.DATA`) file can be seen in Appendix F.1. The specific options and keywords for the main simulation file were set by PML reservoir simulation specialists and are not reviewed here further. The keyword structure for the delumping cases are built on the detailed `*.DATA` file and only extended for the specific mentioned keywords, needed for the delumping facility.

The delumping facility is switched on by the keyword `LUMPDIMS` in the `RUNSPEC` section. The two entries for this keyword determine the number of lumped components (first entry) and the maximum number of detailed components per PCS (second entry) [43].

```
LUMPDIMS
  8   4 /
```

The itemised delumping keywords within the `PROPS` section can be found in Appendix F.2 [42]. The delumping section contains all necessary information about the detailed component properties as well as the lumping scheme. For example, as shown in Appendix F.2, for the Lump_ME case, the `LUMPING` keyword would look like the following:

```
LUMPING
N2C1   2   _1 _3 /            -- PCS N2C1 consists of 2 detailed
CO2C   2   _2 _4 /            -- components which are N2 & C1, which
C3     1   _5 /               -- are the first (_1) and third (_3)
C4     2   _6 _7 /            -- components in the detailed fluid
C5     2   _8 _9 /            -- description. Etc.
C6+    4   _10 _11 _12 _13 /
C10+   1   _14 /
C18+   1   _15 /
```

The first entry of a line in the `LUMPING` keyword refers to the specified lumped component name in the PVT file of the lumped description which the simulator uses for allocation to the fluid model. It should be mentioned that E300 is only processing the first four characters of the name, thus it was taken care of that the name of components is not exceeding this limit (e.g. CO2C, which would be more comprehensible if it would be named CO2C2). The second entry defines the number of detailed components in this lumped component and the last entries refer to an arbitrarily user defined name given in order to determine these detailed components in a PCS. The processing of the names from the third entry is also restricted to four characters [43].

After setting up the lumping scheme the simulator needs an initial detailed component state of the reservoir, as mentioned in chapter 3 by [2]. This is entered via a table of mole fraction or

make-up fraction (DETAILMF or DETAILVD respectively) of the detailed components in the lumped simulation. Following physical properties of the detailed components are mandatory to include:

- acentric factor (ACFDET),
- molecular weight (MWDETAIL),
- critical temperature (TCRITDET),
- critical pressure (PCRITDET),
- Ω_a EoS coefficient (OMEGAADE) and Ω_b EoS coefficient (OMEGABDE).

They are needed to approximate the detailed information by the delumping facility. It should be mentioned, as proposed in Appendix F.2, the order of input (according to scheme in LUMPING) is important since it is the only way to refer to the correct detailed components from the lumped components [42].

The last thing which needs to be specified is the output for a delumped simulation. Only the molar production concentration for delumped components are available, either for field (FTPC), group (GTPC) or well (WTPC) quantities. [42]

This is a limiting factor for convenient use of the delumping facility since it is necessary to manually calculate the molar flow rates of detailed components with the produced concentration results, to obtain usable detailed quantities.

This calculation was done by PML-ESYS which is a PML proprietary developed software. Since this was used as a tool, to translate E300 results towards HYSYS input, PML-ESYS is not reviewed here further in detail.

The above procedure for setting up the delumping cases was applied for all lumping schemes mentioned in chapter 4.1.1 as well as Appendix C.1.

4.2.2 Volatile Oil Single Well Model

For the volatile oil cases an approach, using a cut-out of the related full-field model was conducted as well. Unfortunately, the simulation results were not usable since the volatile oil SWM would have needed extensive tuning for simulating the real behaviour (production history was too short and not able to be matched). Since tuning of reservoir models is not the scope of this thesis, it was, together with the PML supervisors, decided to build a shoebox model (SBM) with a pressure-controlled production history for use as volatile oil reservoir model.

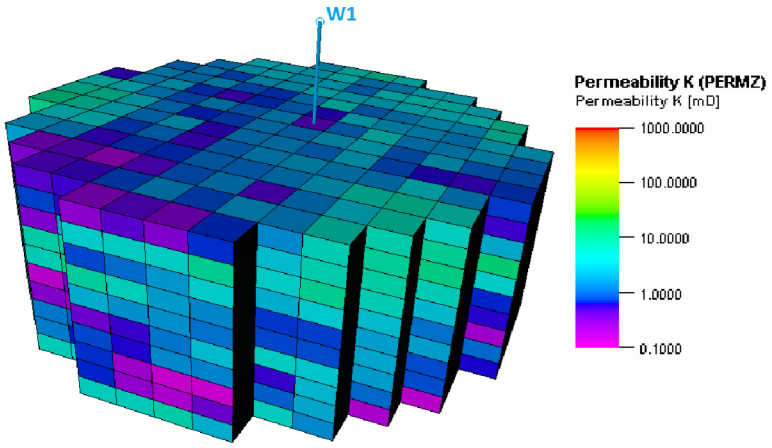

Figure 31 - SBM for simulating the volatile oil reservoir (vertical permeability coloured)

As it can be seen in Figure 31, the volatile oil SBM consists of a circular area (14 cells in every direction) around a single vertical well, penetrating all 10 layers over a vertical extension from $3000\ m$ to $3100\ m$ depth. This equals 1960 grid cells for the whole SBM. Reservoir parameters like permeability and porosity are calculated using gaussian random distribution. As rock type, PETREL's default values for consolidated sandstone were used. The water-oil-contact was arbitrarily set at $3080\ m$ with an equivalent initial reservoir pressure at this reference depth of $400\ bar$ in order to ensure that the system will reach two-phase behaviour during a practicable simulation time and hence trial the delumping facility, since the bubble point pressure is about ~ $250\ bar$ for the volatile oil, as it was seen in chapter 4.1.2.

Because there is uncertainty involved about the PVT report of the volatile oil fluid as well as the reservoir history (currently not in production), this reservoir SBM should be taken as a synthetic high component case only for the purpose of testing the E300 delumping facility.

The model was set up otherwise same as the gas condensate using same two-stage separator conditions. The simulation was conducted via BHP control mode of $150\ bar$ which lasts from 01.01.2019 for 20 years ongoing simulation time.

The delumping simulations are set up same as for the gas condensate, only the amount of data has increased since there are 46 detailed components. As mentioned already in chapter 4.1.2, during the set-up of this case it was found out that the delumping facility in E300 can handle only 46 detailed and 18 lumped components maximum.

As an example, the `LUMPING` keyword for the volatile oil case 10A is shown here:

```
LUMPING
N2C1   2    _1 _3 /
CO2C   2    _2 _4 /
C3     1    _5 /
C4     2    _6 _7 /
C5     2    _8 _9 /
PS1    8    _10 _11 _12 _13 _14 _15 _16 _20 /
PS2    8    _17 _18 _19 _21 _22 _23 _24 _25 /
PS3    10   _26 _27 _28 _29 _30 _31 _32 _33 _34 _35 /
PS4    10   _36 _37 _38 _39 _40 _41 _42 _43 _44 _45 /
C36+   1    _46 /
```

All other delumping cases can be utilized and understood based on the procedure of the previous chapter as well as information from Appendix D.

4.3 Process Simulation Model

HYSYS was used for modelling the surface treatment, to be specific a GTU. The GTU prepared by the PML process engineers consists of several duplicate units in order to model the real equipment used in the actual surface facility. This GTU was designed to meet full field specifications which made the results and underlying principles hard to interpret and comprehend. Thus, the process model was recreated using the full-field model specifications, in order to obtain the same result, but on a simplified model. The specific data about the PML-GTU process simulation model, abbreviated here as INIT_GTU, are confidential.

4.3.1 PML-GTU Process Simulation Model

The INIT_GTU includes following features:

- High pressure manifold
- Separation unit
- Several multi-stage compression units
- Associated gas treatment unit, coming from oil treatment surface facility
- Amine unit
- Sulphur recovery unit
- Two identical conditioning units consisting of
    - Full gas-dehydration unit (dehydration + glycol recovery unit)
    - De-Ethanizer (De-C2) fractionation tower
    - De-Butanizer (De-C4) fractionation tower
- Total product streams
    - Sales gas
    - LPG
    - Condensate

The scope of this thesis was not to model the real physics and catch the complexity of such a real surface treatment facility. Hence, several simplifications can be done e.g. neglecting multi-

stage compressor units and use instead a single stage compressor for the purpose of gas compression. This is valid in this case since the material losses due to compression were small for the two reservoir fluids. Furthermore, since no H2S and only low concentrations of CO2 are present, the amine- as well as sulphur recovery unit are becoming obsolete, and in addition the glycol recovery unit is also not mandatory to model, because it has no influence on the plant products.

However, it should be mentioned that these simplifications are only true for this setup. Since the amine unit would also remove CO2 from the feed it does have an influence on the results but the concentration of CO2 for both fluids is low (meeting the specifications of sales products after processing) it was found out that the deviations are not severe at such concentrations and therefore the amine unit negligence is valid.

The first approach was to modify the INIT_GTU in a way to simplify the above-mentioned obsolete units. But unfortunately, the complexity of the whole model was too overwhelming for matching the specifications by modification (the deviations in composition of the results were greater than 20 % for some cases). Therefore, it was agreed on creating an own GTU model which is simplified in physics but meeting the demanded specifications, composition wise, for the processed products, for purpose of this thesis. The detailed results of the deviation analysis can be found in Appendix G - Table 36, pg. 125. The geometric weighted relative errors of specific streams from the modified GTU can be found in Table 7.

Table 7 - Summary INIT_GTU modification deviation analysis

	$\emptyset_{geo}(RD\%)$ [%]	$\emptyset_{geo}^{all}(RD\%)$ [%]
Dried Gas Stream	1.18	0.86
De-C2 vapour product	-0.31	
Total Sales Gas	2.50	
Total LPG	0.16	
Total Condensate	0.02	

Although the geometric average of e.g. the condensate product stream is almost negligible, the sales gas deviation is too high for usage of the INIT_GTU as reference case. Therefore, another approach was initiated, by modelling a synthetic GTU which ensures meeting the specifications together with the above-mentioned simplifications.

4.3.2 Synthetic GTU

The synthetic GTU, named from now on MF_GTU, was set up by using the specifications of the units from the INIT_GTU and was simplified as much as possible. The heat-exchangers are replaced by heaters and coolers in order to modify the streams similar as in the INIT_GTU. Multi-stage compressor units are simplified by a single stage and since the glycol recovery unit has no influence on the products, it was neglected as well. The result can be seen in Figure 32.

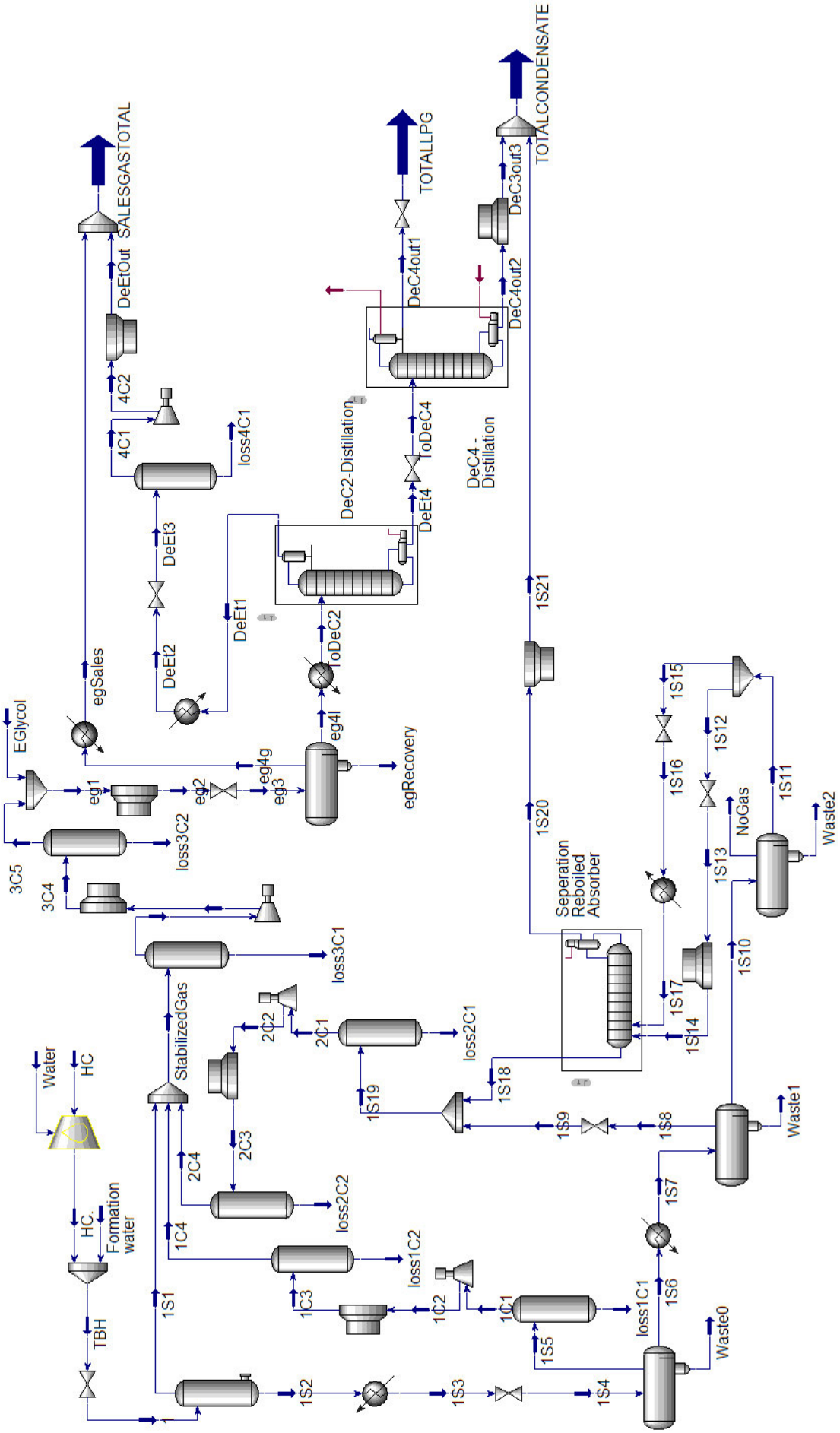

Figure 32 - Flowchart of recreated MF_GTU

For being able to compare the INIT_GTU with the MF_GTU, the GTU was partitioned into several stages of the "treatment" process. The confirmation of MF_GTU validity was proven by analysing crucial fluid streams which are listed below and additional information shows the location of the stream in the coloured process model, visible in Figure 33:

1. Tubing head (TBH) (transition from red to yellow)
2. Separated (conditioned) gas (yellow to blue)
3. Dried gas (blue to grey)
4. De-C2 feed (blue to grey)
5. De-C2 top
6. De-C4 feed (grey to green)
7. Total sales gas
8. Total LPG
9. Total condensate

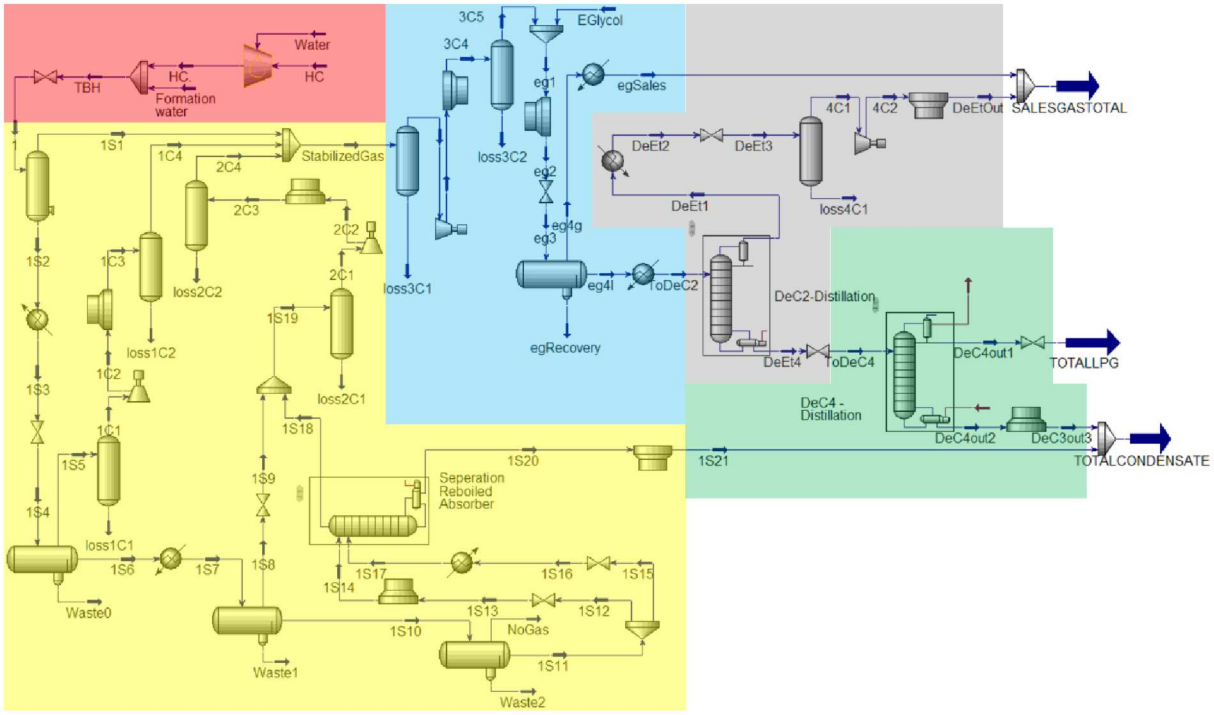

Figure 33 - treatment sections/ units; Red=Tubing Head; Yellow=Separation; Blue=Dehydration; Grey=De-C2; Green=De-C4

The detailed comparative deviation analysis for the MF_GTU can be found in Appendix G - Table 37, pg. 126, and are summarized as geometric weighted averages in Table 8.

Table 8 - Summary MF_GTU comparative deviation analysis

	$\emptyset_{geo}(RD\%)$ [%]	$\emptyset_{geo}^{all}(RD\%)$ [%]
TBH	0.00	-0.02
Conditioned Gas	0.58	
Dried Gas	0.56	
De-C2 Feed	-1.46	
De-C2 Top	0.00	
De-C4 Feed	0.11	
Total Sales Gas	-0.25	
Total LPG	-0.30	
Total Condensate	0.00	

Although the LPG deviation was doubled in the other direction, compared to the INIT_GTU in Table 7, the overall result is almost exact since everything below 1 % is acceptable including the amount of complexity in the simulation model. The simplification also provides the basis for an easier interpretation of the results since the different processes are better distinguishable.

The whole MF_GTU can be categorized into five parts, coloured in Figure 33. The red area represents the well stream which consists of the stream HC, which is the hydrocarbon production rate coming from E300. It is connected to a saturation unit which saturates the stream with H2O, to ensure that the after added formation water stream (also from E300) has a consistent material balance. This application was done because otherwise, the formation water would vaporize into the HC stream and the flow rates for both mixed together would differ.

The conditioning block is included by the yellow area. This was one of the least simplified stages since the different separation stages led to molar losses and this was detrimental in order to meet the INIT_GTU specification requirements. But overall, the conditioning unit can be summarized as a 3-stage separation unit followed by a reboiled absorber column whose bottom products are condensates. The product of the whole conditioning unit is gas which needs to be dried. Since the operation conditions for the gas dehydration unit requiring high pressures and extremely low temperatures ($-35\ °C$), a compressor stage is inserted before. Both represented by the blue area. The product streams of the dehydration unit are dried gas, which flows directly to the sales gas manifold, and cold liquid, which needs to be heated up for fractionation in the next NGL extraction unit.

The grey area consists of a De-C2 column. All light-components (C1 and C2) are extracted from the feed stream and exerted as top product which flows directly to the sales gas manifold. The last stage is represented by the green area which involves another NGL extraction unit, namely a De-C4. The De-C4 splits intermediate and heavy fraction components which are saleable products namely LPG and condensate. The bottom product of the De-C4 and the separated condensate from the conditioning unit, are mixed to obtain the total condensate stream.

As already mentioned in chapter 4.1.3, the two fluids (gas condensate and volatile oil) require different fluid setups for HYSYS, but both are using the same process simulation model.

Summarizing this chapter, there are two different detailed fluid descriptions which are lumped using five different schemes for each, which makes six fluid descriptions as input for E300, simulating either a SWM or SBM. The lumped descriptions are delumped by the E300 delumping facility and forwarded to PML-ESYS which acts as a pre- and post-processor for HYSYS. After data has been organized by PML-ESYS, it is delivered to HYSYS which calculates the plant products for every timestep. After HYSYS finishes calculation PML-ESYS will gather the time dependent product streams and store them in a file on the local drive. This procedure makes again six results per fluid. For the concluding interpretation MS-EXCEL® was used. Schematically, the whole procedure is shown in Figure 34.

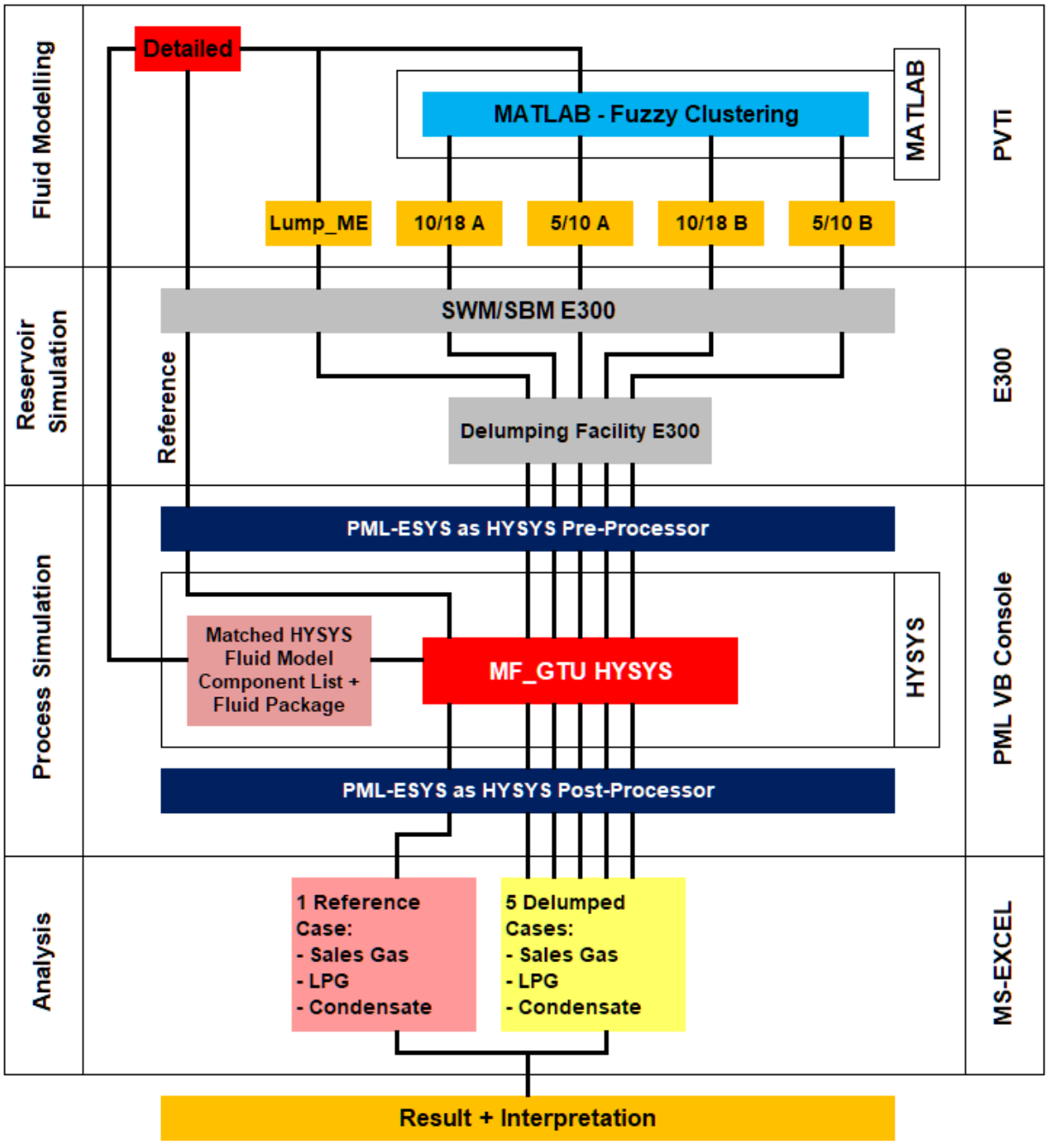

Figure 34 - Summary Simulation Procedure

5 Results and Discussion

This chapter will deal with the results of the prepared simulations, which were discussed in chapter 4. The interpretation of these results are summarized in the last subchapter as transition to chapter 6 where the conclusion of this thesis is written.

The results are split, which means that in order to catch the leitmotif through the whole procedure of combining reservoir simulation with process simulation, it is differentiated between intermediate results such as the E300 results and the HYSYS results which determine the final outcome of this thesis.

5.1 Reservoir Simulation Results

Since the reservoir simulation model chapter dealt with building and set-up of the SWM and SBM, the first results which are going to be discussed are the initializations of these reservoir models. This is a common approach to start analysing the reservoir model validity. Since E300 simulations were set up by using basic hydrostatic equilibrium initialization it is expected that there are deviations regarding the pore fluid quantities inside the model [42]. These need to be included in interpreting the whole procedure in the end.

For investigating the initialization of the model, five key parameters were selected for the initialization study. These are:

- hydrocarbon weighted average field pressure (FPR_{HC}),
- initial reservoir fluid volume for reservoir as well as surface conditions ($V_{g,o}^{res}$, $V_{g,o}^{surf}$),
- either gas for the gas condensate simulation or oil for volatile oil simulation,
- liberated or condensed volume at surface conditions ($V_{o,g}^{surf}$), either oil for the gas condensate or gas for the volatile oil,
- total moles of hydrocarbon (n_T) initially present.

The surface conditions should not be confused with standard conditions. It is worth to mention that E300 is calculating the liquid surface volumes and liquid well production rates according to the last specified separator conditions [43]. Fortunately, for the used reservoir models here, the surface conditions are set same as standard conditions

After the initialization analysis, the reservoir simulation end-results are inspected more explicitly, since the delumping is processed by E300 and therefore directly affect the results of the process simulation.

5.1.1 E300 Initialization – Gas Condensate

The initialization results for the key parameters of the reference run (detailed) for the gas condensate can be found in Table 9.

Table 9 - Initialization for the detailed E300 simulation for the gas condensate

	FPR_{HC} [bar]	V_o^{res} [rm³]	V_o^{surf} [sm³]	V_g^{surf} [sm³]	n_T [kmole]
Detailed	578.9	9.77E+06	2.07E+06	2.82E+09	1.29E+08

As the reported values for the volumes are too big to see deviations in tabulated form, only the deviations from the initialization parameters from the lumped simulations, compared to the reference case, are shown in Figure 35 (explicit values are located in Table 19 - Appendix C.3, pg. 110). The deviations for the surface volumes are again attributed, as already mentioned in chapter 4.1.1, to the accuracy of the fluid description since E300 is calculating the equilibrium for surface conditions on the basis of the EoS. Therefore, deviations after the flash calculation were expected.

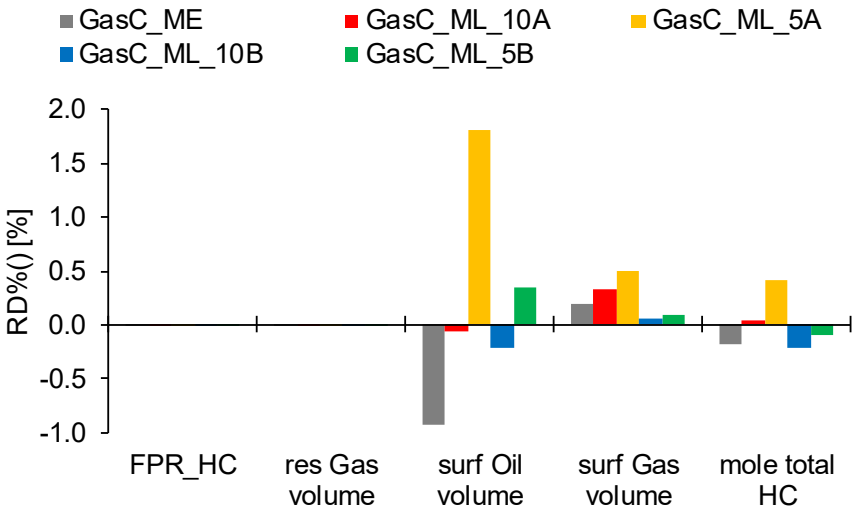

Figure 35 - Graphical representation of RD% from the initialization key parameters, tabular form in Table 19

Again ML_5A has the highest deviation and its expected that this will carry through all simulations. All others are well approximated since common uncertainties are exceeding 1 %, especially for fluid in place volumes.

5.1.2 E300 Initialization – Volatile Oil

The same was done for the volatile oil, where it is mentioned again that this case was a synthetic reservoir model.

Table 10 - Initialization of detailed reference reservoir simulation for volatile oil

	FPR_{HC} [bar]	V_o^{res} [rm³]	V_o^{surf} [sm³]	V_g^{surf} [sm³]	n_T [kmole]
Detailed	397.93	2.30E+07	9.96E+06	4.35E+09	2.37E+08

In Table 10 are the detailed initialization results shown and in Table 30 - Appendix D.3, pg. 118, the explicit values of lumped cases for volatile oil, in addition graphically represented by Figure 36.

Again we have a high deviation of ML_10A as expected since the fluid description has a strong shrunken phase envelope as discussed in chapter 4.1.2. The quantitative higher deviations are attributed to the doubled reservoir volume of the SBM compared to the SWM.

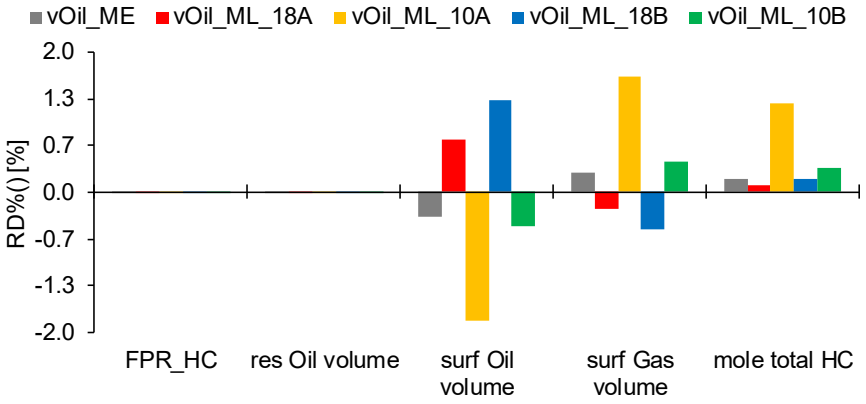

Figure 36 - Graphical representation of RD% from the initialization key parameters, tabulated in Table 30

Overall, both initializations are accurate enough in order to proceed since only ML10A of the volatile oil is taken as an outlier which is expected to fail correct product stream prediction.

5.1.3 E300 Simulation – Gas Condensate

Since the delumping is directly processed by E300 the following analysis will be more detailed. The gas condensate simulation was conducted using a real production history. The reference was conducted, and the lumped cases were processed with the delumping facility.

The BHP and GOR are shown in Figure 37. There it can be seen that the result is, for both parameters, in perfect agreement with the detailed reference case until the year 2013. Since after that time the BHP will fall below the dew point which is, as seen in chapter 4.1.1, around $\sim 380\ bar$, hence the small deviations of the different phase envelopes (differences in the EoS model) will become active and the system will transfer to a two-phase system since liquid will form first in the near well proximity and later in the whole reservoir since also the reservoir pressure will drop below the dew point pressure later. After passing the dew line and producing in the two-phase envelope region, pressure wise, the BHP for the different cases will align again, since the discrepancies are highest during transition (passing dew line). The same reason led to an increase of the GOR. The liquid which condensed has a very low mobility and is considered as immobile, thus intermediate and heavy fractions will not be produced and less oil will be reported at the surface. This is also a well-known process during depletion of a gas condensate reservoir which is called condensate banking.

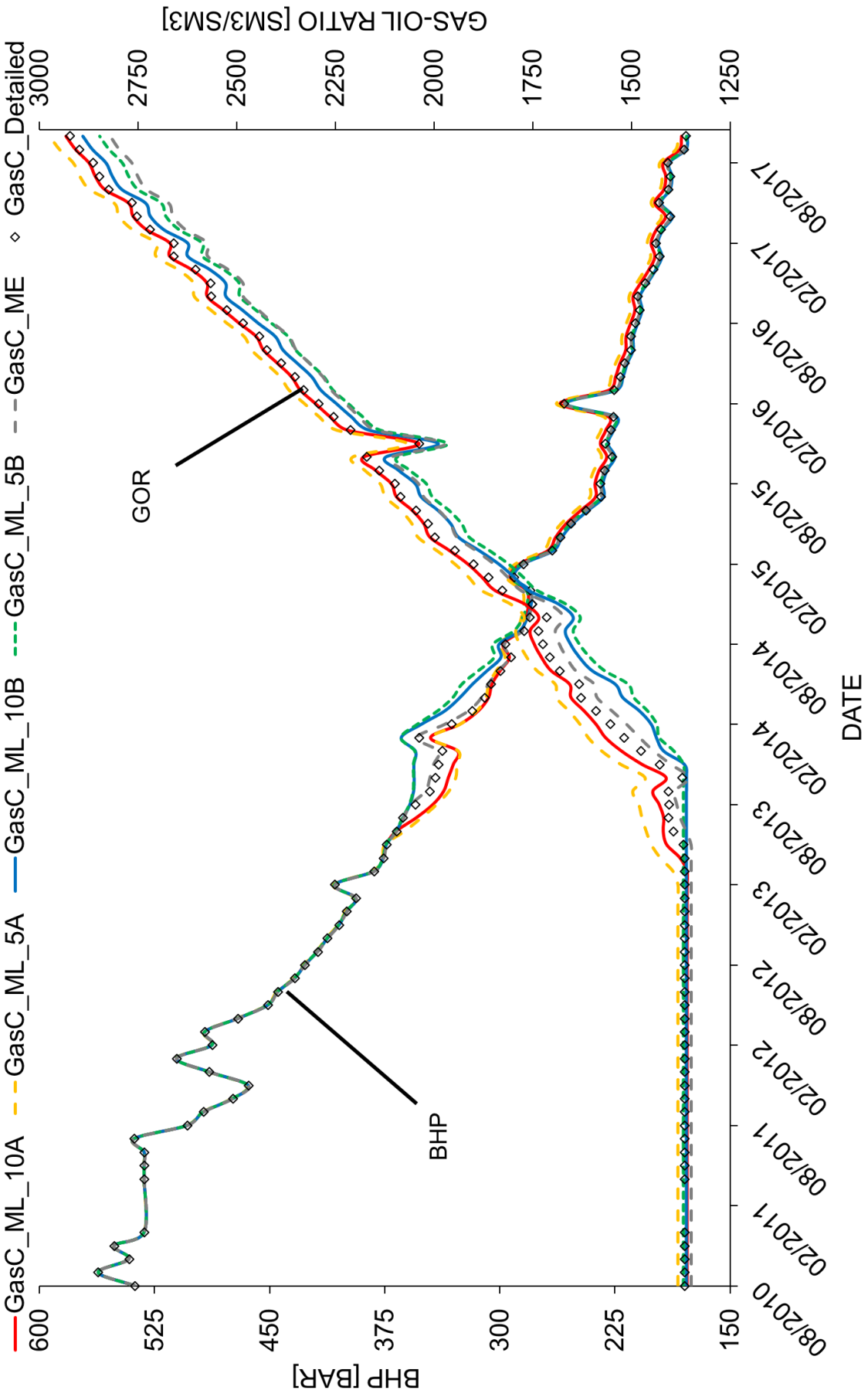

Figure 37 - Production plot for Gas Condensate Simulation

The field pressure, together with the simulation run-time is shown in Figure 38. Since the field pressure is hydrocarbon weighted and averaged through all blocks the small deviations because of different fluid models are not visible there. The second parameter, cumulative CPU-time, is plotted in addition with the run times of the lumped simulations without the delumping facility switched on. The obvious fact, that fewer components lead to less simulation time, was not proven here. The fact that delumped cases are exceeding the simulation time of the detailed reference case was not further investigated but it was assumed that the SWM model and its size is not representable for the – anyway, short - CPU time. In addition to the small model the lumping ratio of $\mathcal{R} = 60\%$ for the _10A and _10B cases, is maybe not sufficient in order to account for the extra CPU-time needed for the delumping calculations.

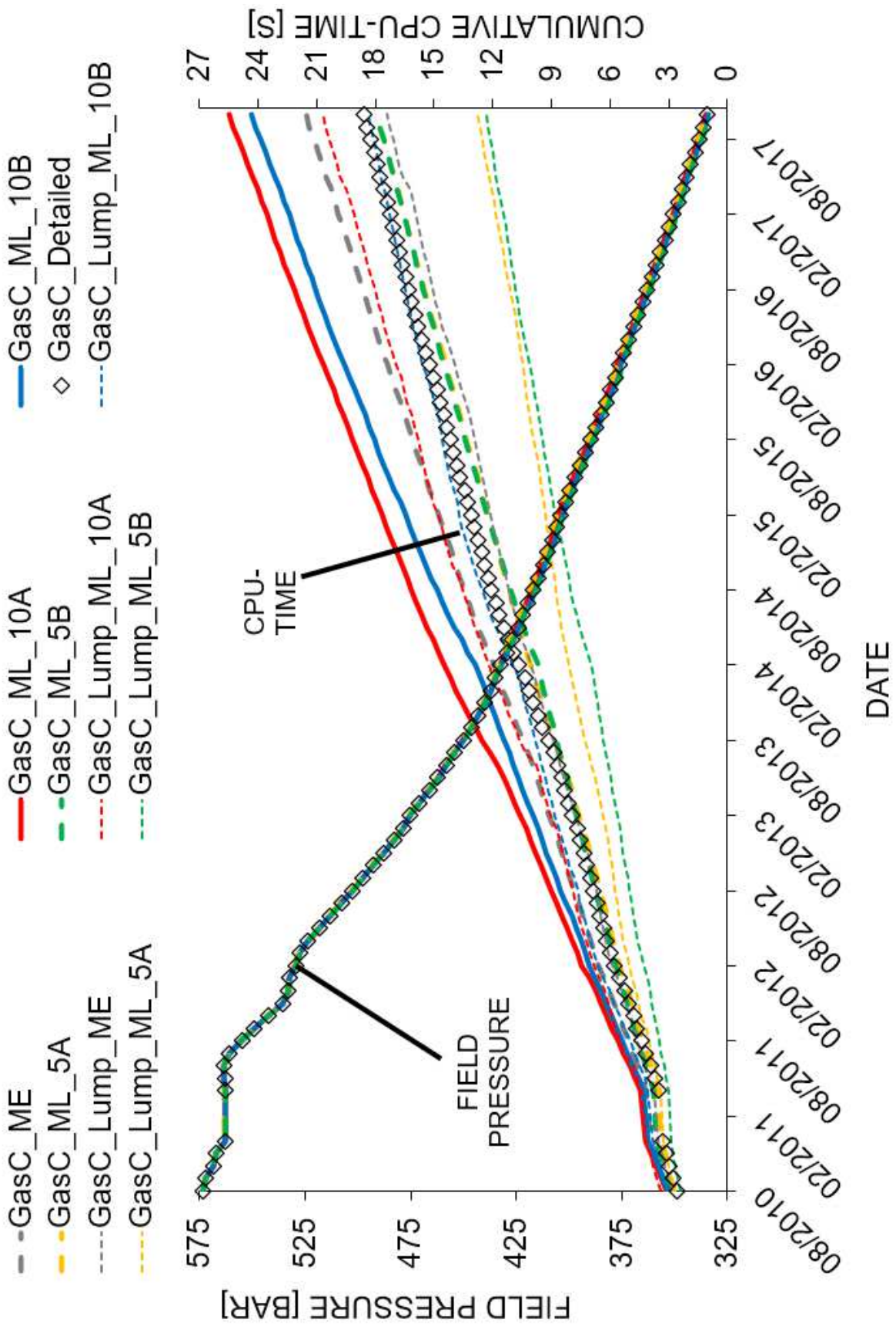

Figure 38 - Gas Condensate Simulation run-times

As an example, Figure 39 shows two components for all cases. The behaviour of the GOR is becoming clearer as, C1 has a high tendency to be in vapour phase and its produced mole fraction will increase during ongoing simulation, on the other side C3 as an intermediate component will condense in the reservoir and thus not be produced. That is why its trend is declining. It should be mentioned that the scales of both components are different by magnitudes. This is important for interpreting later but nevertheless, the two extremes _5A and _5B are again found, this can be explained by the small discrepancies between the slightly different EoS models.

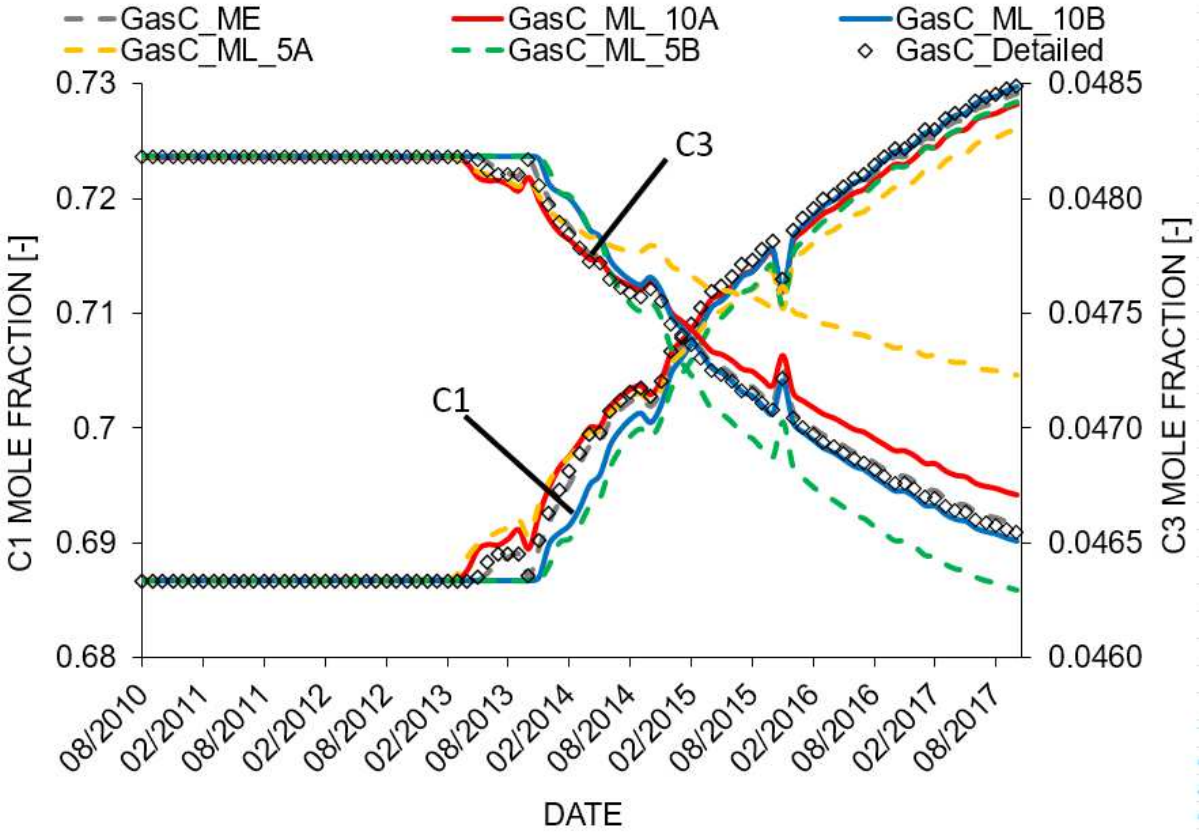

Figure 39 - produced molar fraction for gas condensate simulation

To generate an overview for all cases and all components, the bar chart in Figure 40 shows the relative errors per produced mole fraction, for every case. Recalling the lumping schemes used for creating the cases, it can be seen that lumping the heavy components leads to an underestimation of produced heavy fractions (tendentially generated with fuzzy clustering mode B), whereas lumping the light components (tendentially mode A) led to an overestimation for heavy components. Because Figure 40 shows the deviation at the last timestep, care should be taken regarding interpreting the values of the deviations since these deviations represent a cumulative behaviour of inaccuracy during calculation.

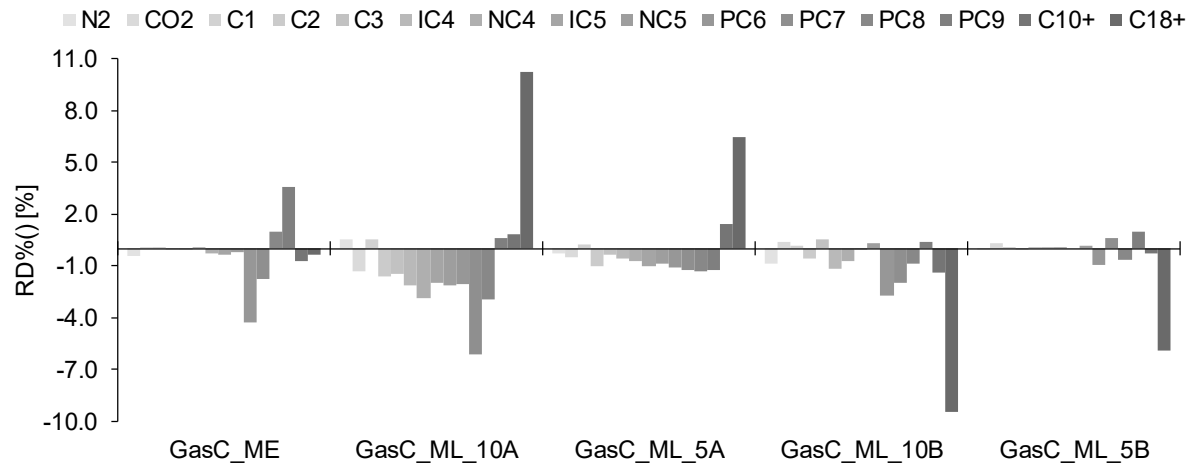

Figure 40 - RD% of produced delumped component mole fractions for the last timestep (01/07/2017) in the gas condensate E300 simulation

As final part, shown in Figure 41, the total hydrocarbon production rate can be seen. The same behaviour after year 2013 takes place.

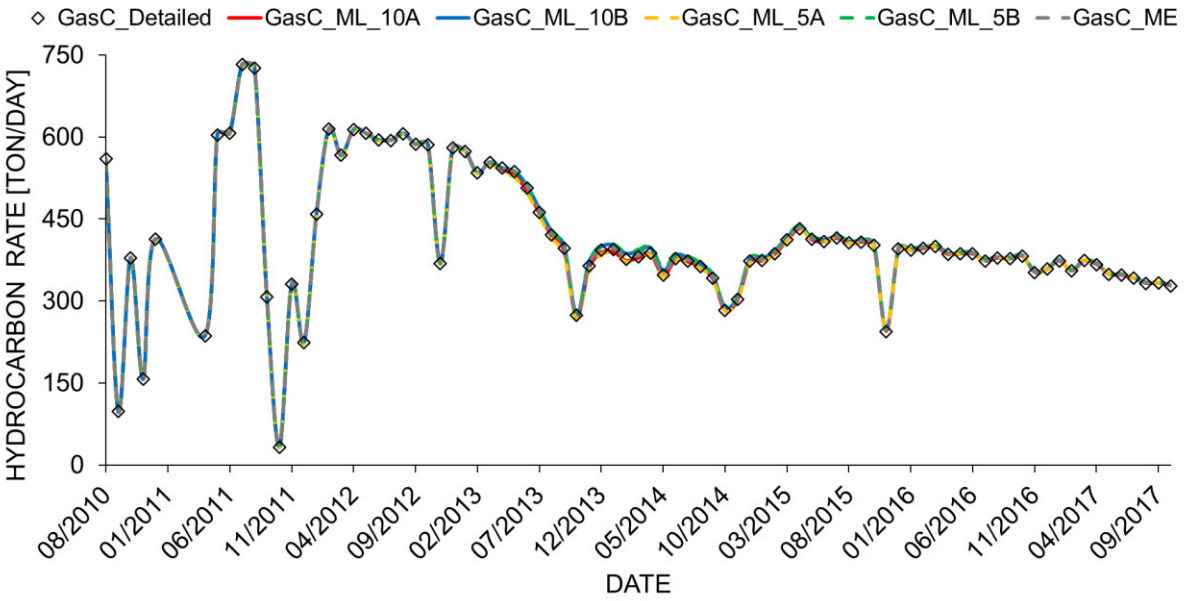

Figure 41 - hydrocarbon production rate of E300 simulation

The deviation analysis, shown in Figure 42, for the well production stream showed the same as discussed in correlation with Figure 37. Where the two opposite error amplitudes are attributed to the lumping schemes and the dew line transition.

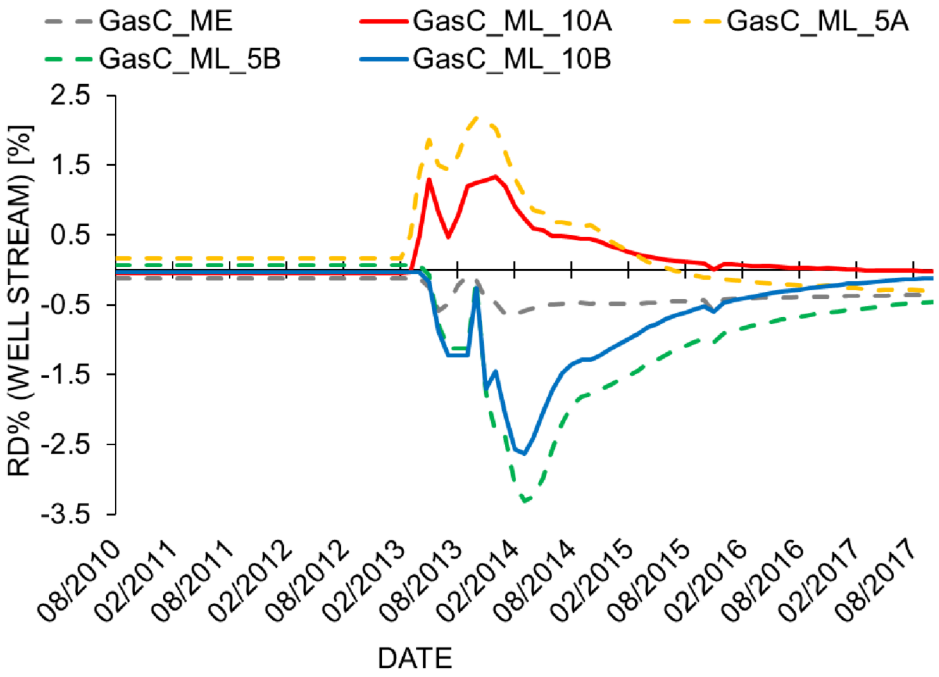

Figure 42 - RD% for well stream rate of gas condensate simulation

5.1.4 E300 Simulation – Volatile Oil

For the volatile oil - SBM a BHP production control was implemented. In Figure 43 the hydrocarbon weighted field pressure and GOR are plotted. As it was seen in the initialization subchapter 5.1.2, the number of hydrocarbon moles was highly overestimated due to the difference in ρ^l $(1.2\,\%)$, reported in Table 26 - Appendix D.2, pg. 115, for the reservoir conditions flash stage. This resulted in an overestimation in mole numbers for the hydrocarbons and thus a reduction in hydrocarbon field pressure. Since ML_10A was already classified as outliner it will be less attention paid during interpretation. The other cases are reasonable and accurate as expected. The GOR is having a minimal turning point at year 2026. This can be explained by the rather (too) low BHP production control of about $150\ bar$, which was set arbitrarily. Since the bubble point was observed at $\sim 230\ bar$ the whole reservoir will fall immediately below it. Hence, gas will liberate and be immobile at first, which leads to a small decrease in GOR. After the critical gas saturation is overcome (enough gas has liberated) the gas phase becomes mobile and will be produced which increases the GOR. The extended anti-climax period of ML_10A attributed to the excess of moles inside the reservoir fluid.

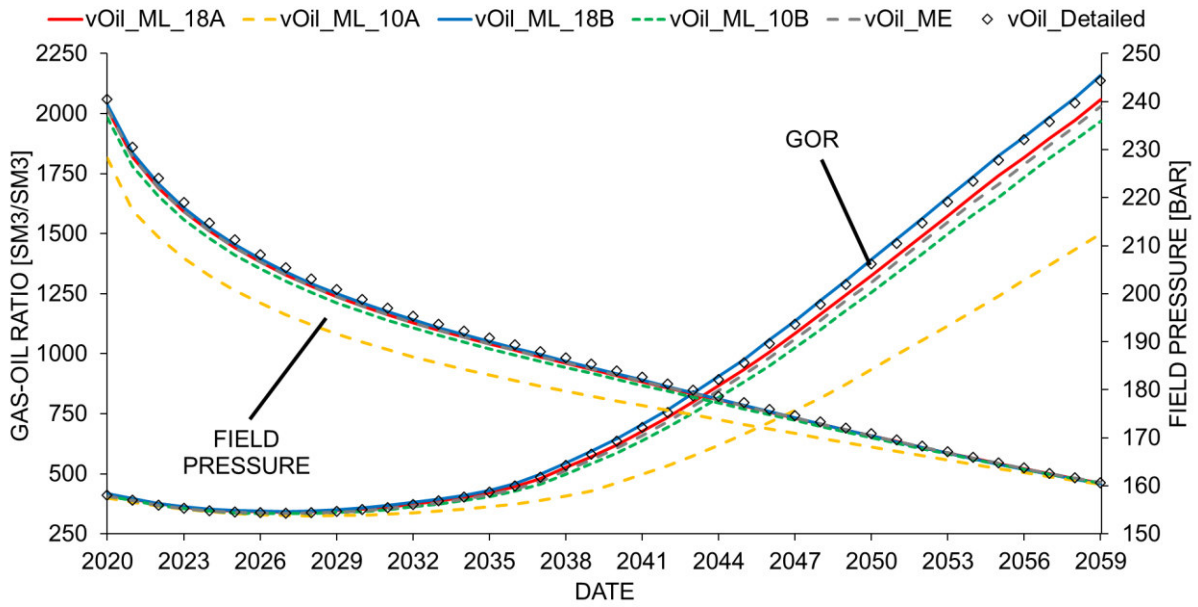

Figure 43 - Average Field pressure and Production GOR for Volatile Oil Simulation

The CPU-time for the volatile oil looks more reasonable, as it is shown in Figure 44. The lumped simulations are obviously the fastest and the detailed simulation lasts extensively longer. Here it is seen that the delumping calculations are only using a fraction of the detailed run-time. As mentioned several times in literature i.e. [9], [5], [2] and [37].

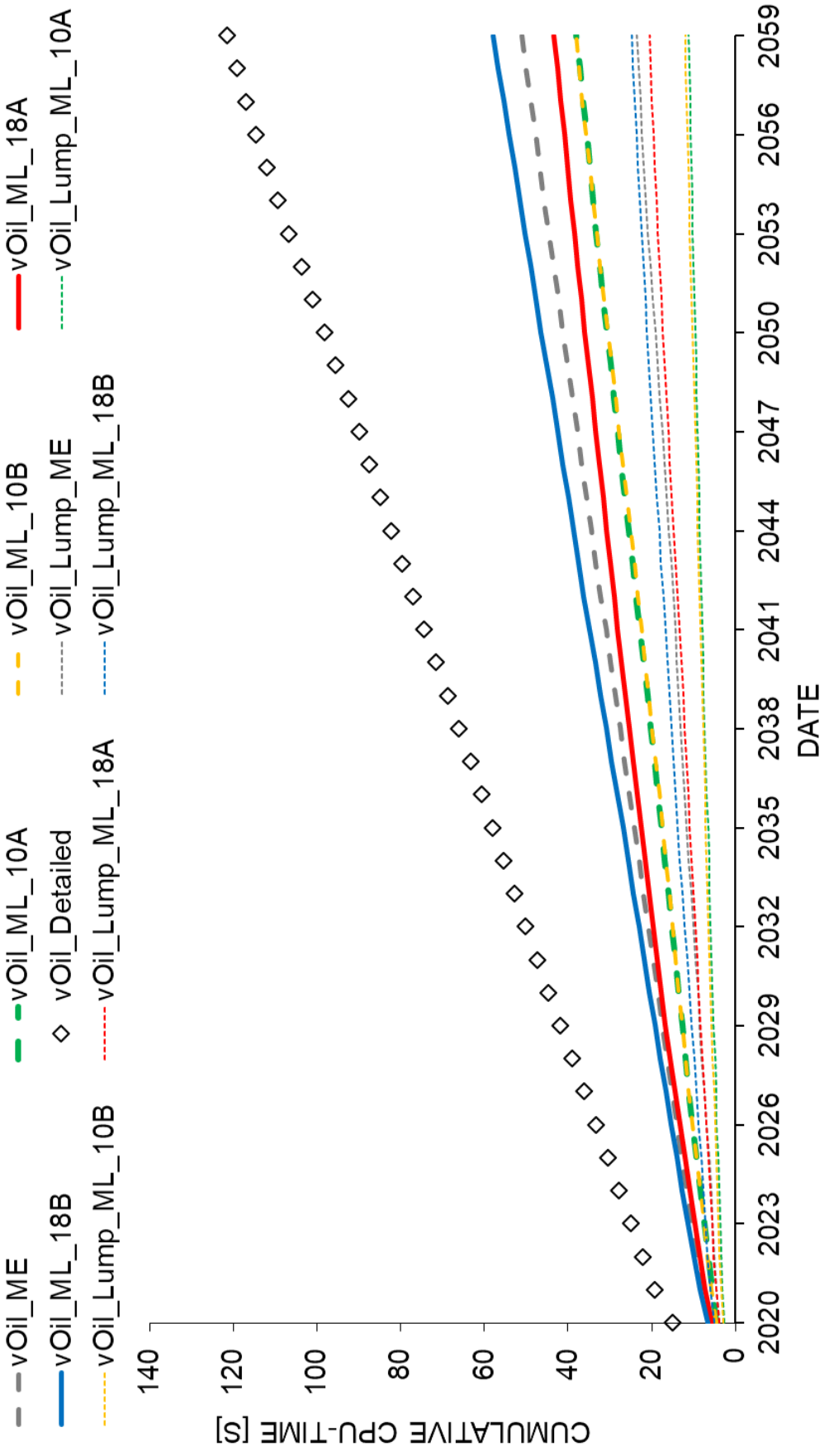

Figure 44 - Volatile Oil Simulation run-time

In Figure 45, there are the two contrary components C2 and C6 and their produced mole fractions shown. Both are again mimicking the GOR trend. After the gas liberation, less C2 and more C6 fraction will be produced, after gas mobilization the trends are turning inversely.

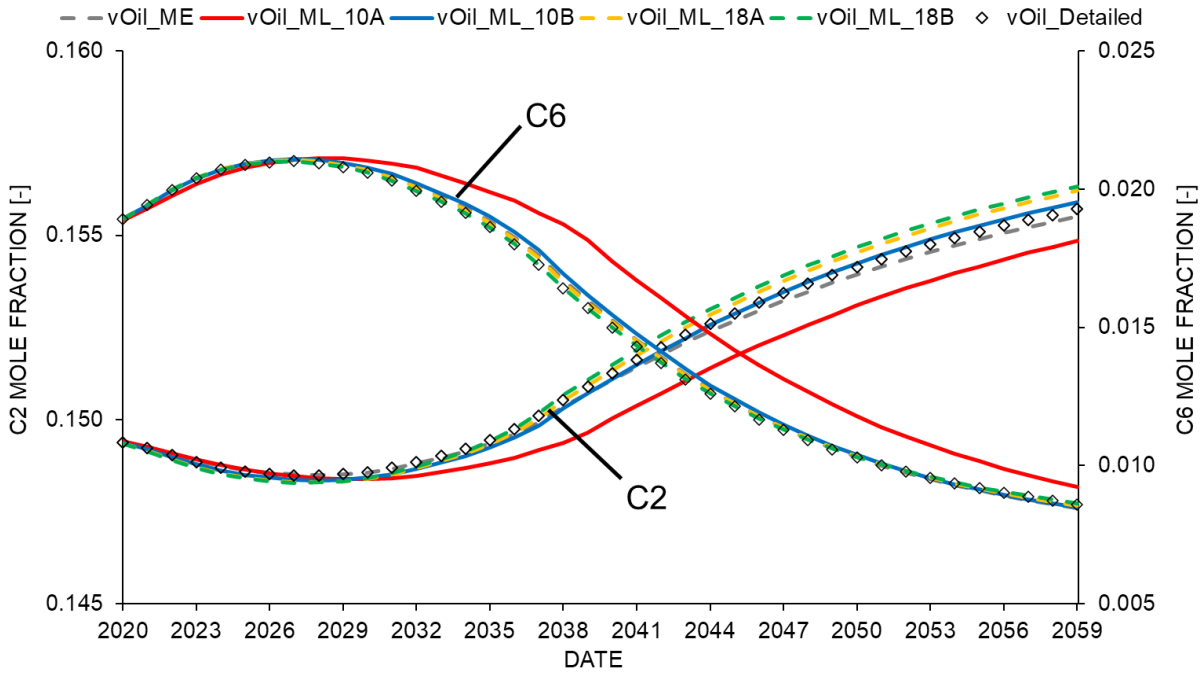

Figure 45 - produced molar fraction for volatile oil simulation

Since the reservoir gets heavily depleted during the SBM simulation, the volatile oil will undergo significant changes. This leads to high cumulative errors, mole fraction wise. The same as for gas condensate was applied here. Figure 46 and Figure 47 are showing the fraction errors at last simulation timestep. The plotted values can be reviewed in Appendix D.3, Table 28 and Table 29, pg. 116 and 117. A detail is catching the eye. In all cases the $RD\%$ of $C2Be$, $oXyl$ and $mpXy$ are increased contrary to the otherwise similar behaviour of components in their vicinity. A reason for this cannot be found straight-forward since it would need a more detailed review of the fluid model. It must depend somehow on the lumping scheme since these components are always forming a PCS together.

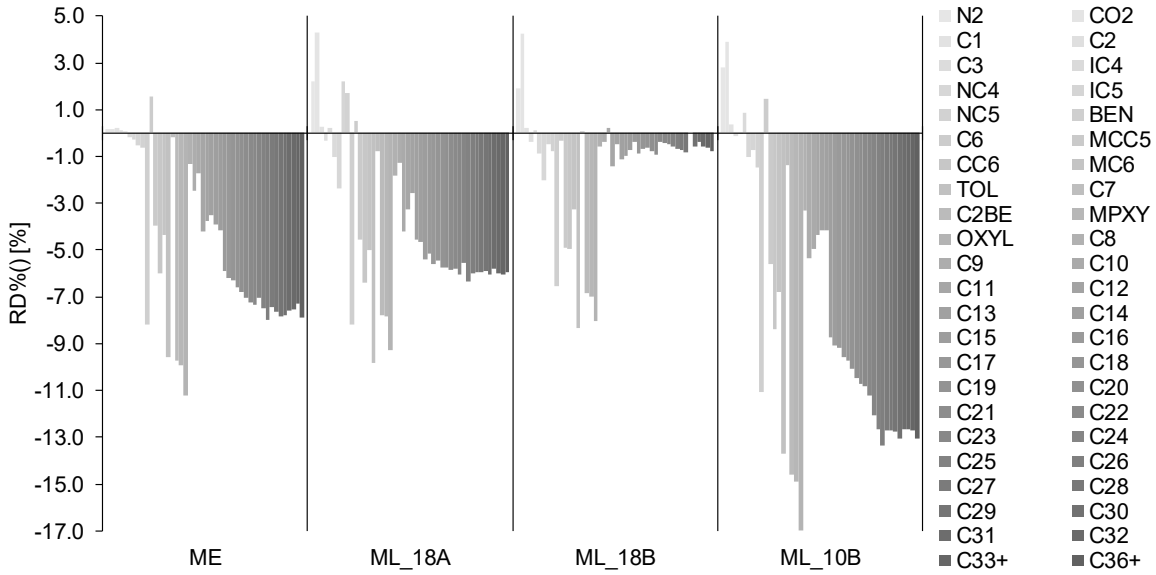

Figure 46 - RD% of produced delumped component molar fractions for volatile oil E300 simulations at last time step (01/01/2059)

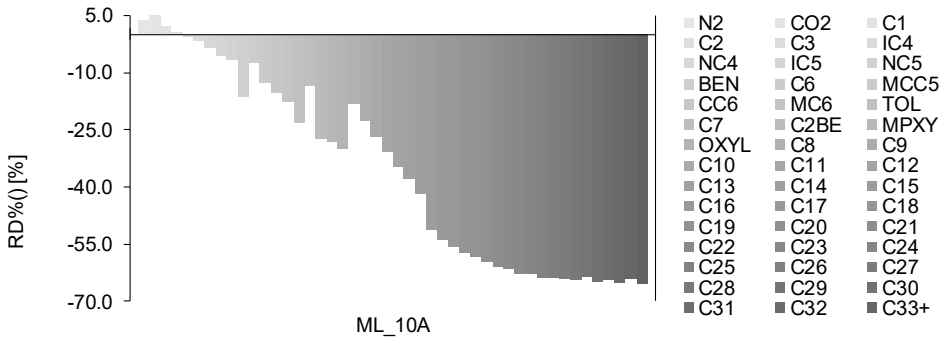

Figure 47 - RD% of produced delumped component molar fractions for volatile oil E300 simulations at last time step (01/01/2059), outliner case ML_10A

Since there was no production history in the SBM included, the time varying production rate from the model looks like Figure 48, as common depletion of a bounded reservoir with declining rate and asymptotic behaviour.

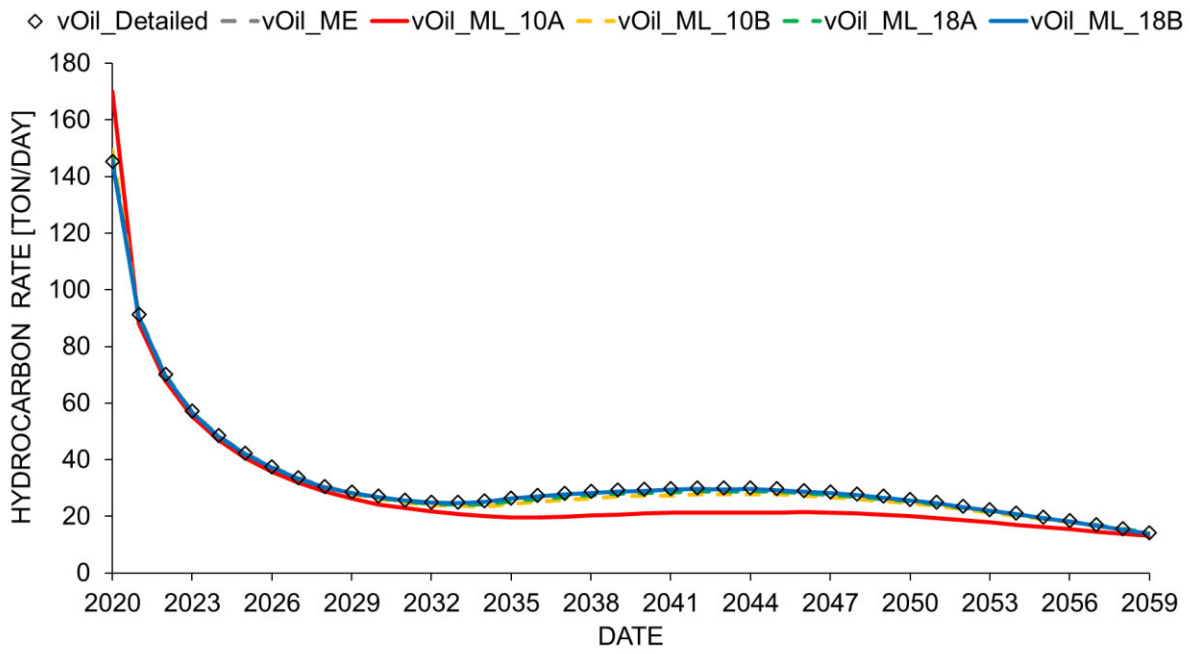

Figure 48 - Production rate for volatile oil reservoir simulation

For better interpretability, the deviations of the cases to the reference are shown in Figure 49. A fair agreement of the cases except for ML_10A can be seen.

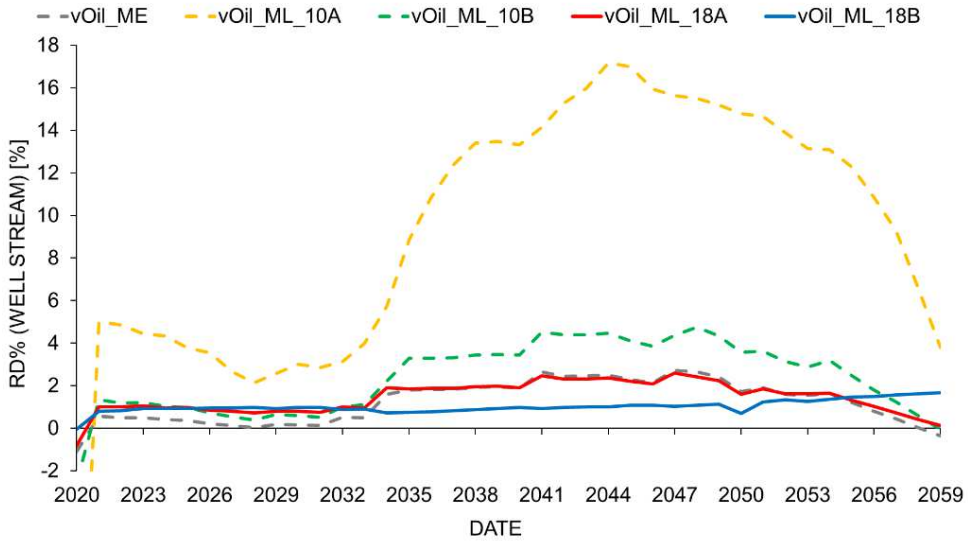

Figure 49 - Deviations of well streams for volatile oil

5.2 Process Simulation Results

Since the delumping is already done by E300, the analysis of the process simulation results will be analysed mostly on deviations since all HYSYS simulations were using the same detailed (beforehand) matched fluid model per different reservoir fluid, but only calculates with the different input values as examined by production plots in the subchapters 5.1.3 and 5.1.4.

Since the coupling of E300 with HYSYS was accomplished by a PML-ESYS by using it as a pre and post processor, as already mentioned in Figure 34, the result discussion is restricted

by three output streams which are the three total calculated product quantities (also visible in Figure 32) namely:

- Total sales gas
- Total LPG
- Total condensate

This is suitable since MF_GTU is a recreated hypothetical GTU and more detailed process simulation analysis would be outside the specified scope of the thesis.

5.2.1 Process Simulation – Gas Condensate

The three streams as a result of the HYSYS simulation will be discussed here. The total sales gas rate for all cases are shown in Figure 50.

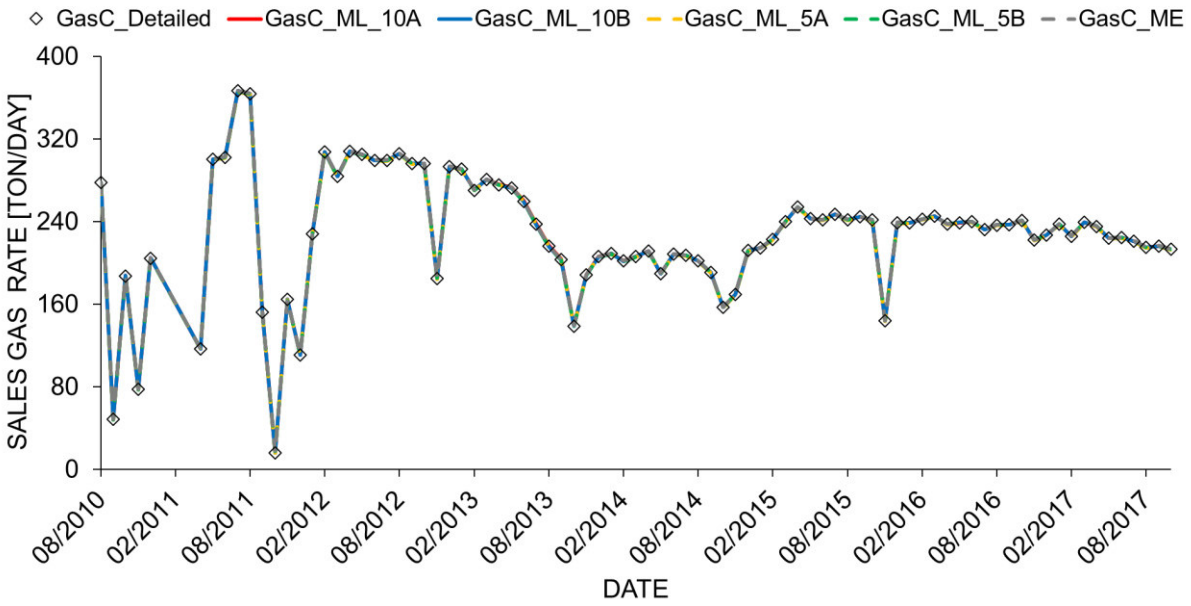

Figure 50 - HYSYS total sales gas rate for gas condensate

In order to account for the deviations in the quantity of the well stream, the ratio of the plant product streams, to the well stream for every case were calculated, in order to minimize the error propagation. The results are shown in Figure 51.

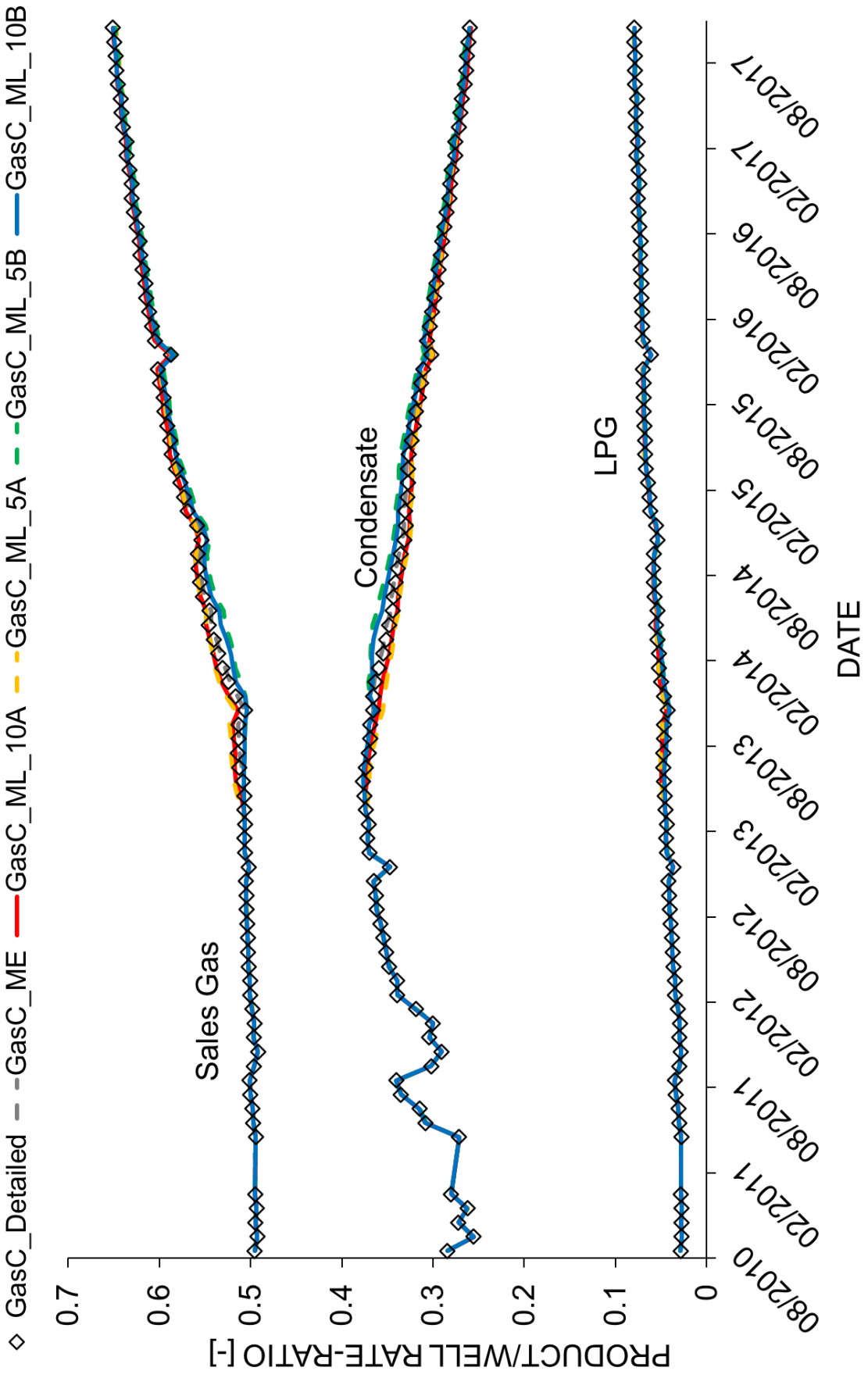

Figure 51 - stream rate ratio of HYSYS products for gas condensate simulation

These trends can be described by comparing them with the gas condensate production from the reservoir. The heavier components are decreasing, and light and intermediate components are increasing due to the retrograde condensation in the reservoir.

The discussed relative deviations for the plant products are therefore discussed on fractions of the well stream. The error analysis for the sales gas/well stream ratio is shown in Figure 52. The amplitudes for the error can be referred again to the two-phase transition of the system. Whereas the ME delumping case show almost exact agreement with the reference case due to already determined best approximated fluid model which was proven in subchapter 4.1.1.

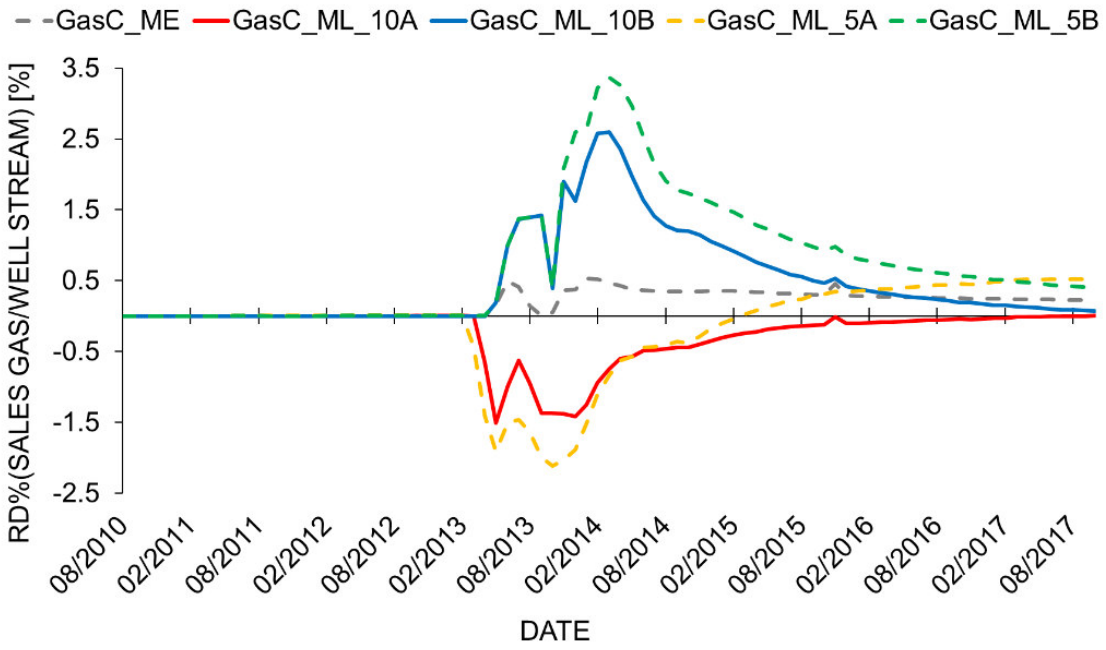

Figure 52 - RD% for total sales gas to well stream ratio

In addition, the contrary under- and overestimation of the lumped cases with either mode A and mode B, respectively, are again seen because of the lumping schemes with either lumping lighter or heavier components together.

Analysing the LPG stream, shown in Figure 53, the deviations around year 2013 are visible. The deviation errors can be found in Figure 54. The LPG is separated in the MF_GTU via the two fractionation towers, first going through the De-C2 as bottom product and afterwards leaving the De-C4 as top product. The De-C2 fractionation tower calculates its top and bottom products via a specified composition ratio. This composition ratio can be seen as an efficiency by which the feed stream composition gets separated, in other words a constant split factor, this means that its less prone to component variations. The De-C4, on the other hand, is component dependent since it calculates its products via a Reid Vapour Pressure[2] (RVP) specification applied at the condenser, which determines the top products (directly LPG). This

[2] Reid vapour pressure (RVP) is the vapour pressure measured at $100°F$, thus a measure of volatility for liquids specified by the American Society for Testing and Materials (ASTM) [15]

specification is prone to component variations since the RVP is based on the processed mixture.

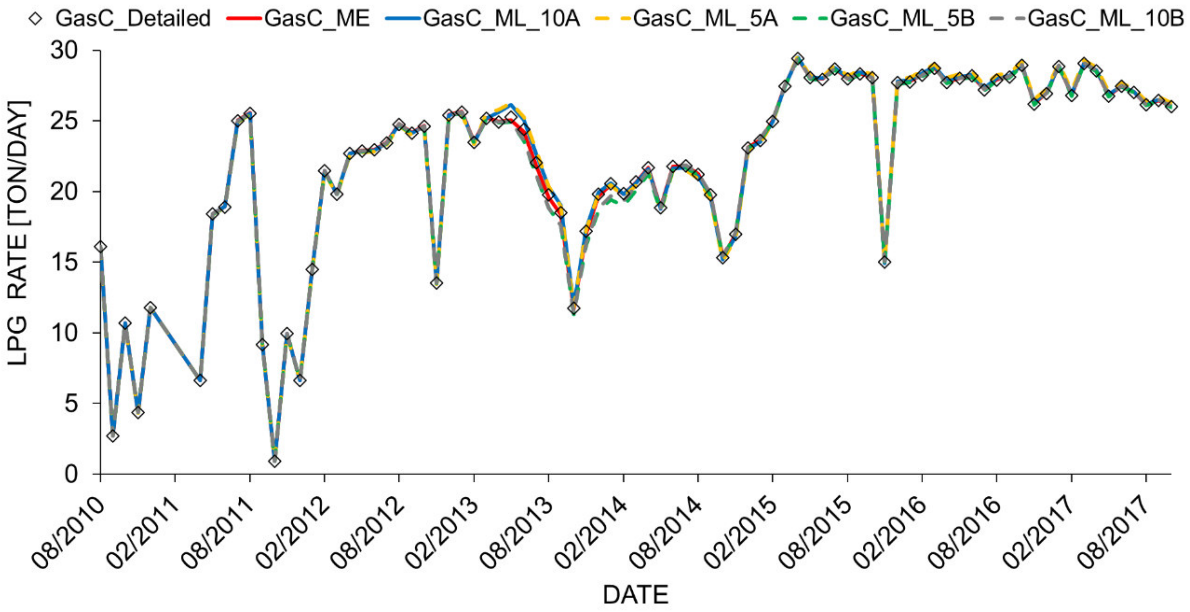

Figure 53 - HYSYS total LPG rate for gas condensate

The amplitude of these deviations during the passing of the dew point are quite high compared to the sales gas deviations this is assumed to be reasoned by the component dependency of the above mentioned De-C4 column and the fact that the LPG consists mainly of C3 which is only produced in small concentrations (3 %) and therefore calculation errors are preponderated.

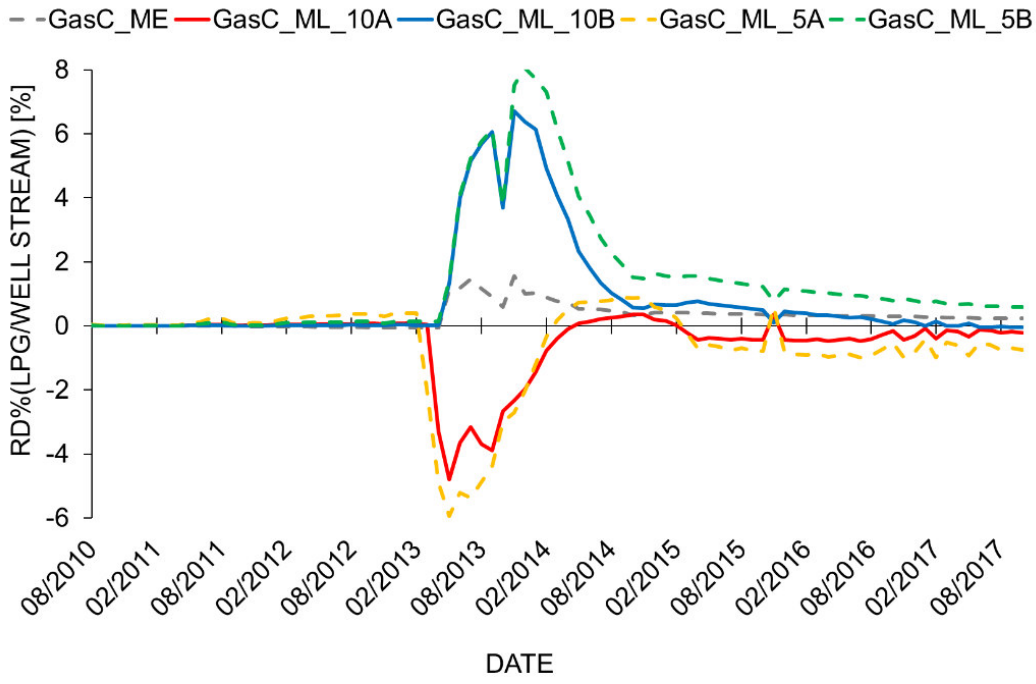

Figure 54 - RD% of LPG stream for gas condensate

The condensate as the third and last product stream can be found in Figure 55. The variations of the stream quantities are delayed a bit, compared to the LPG stream. Whereas the LPG deviations start before 2013 the condensate deviations will do so after 2013. It was first thought that the retardation comes from different composition variations of the well streams, that the C10+ (main fraction of condensate) variations are happening later than C1 (sales gas) or C3 (LPG). But after investigation no proof was found for this statement. There would be a detailed compositional analysis through the whole MF_GTU processing units needed in order to come up with an explanation.

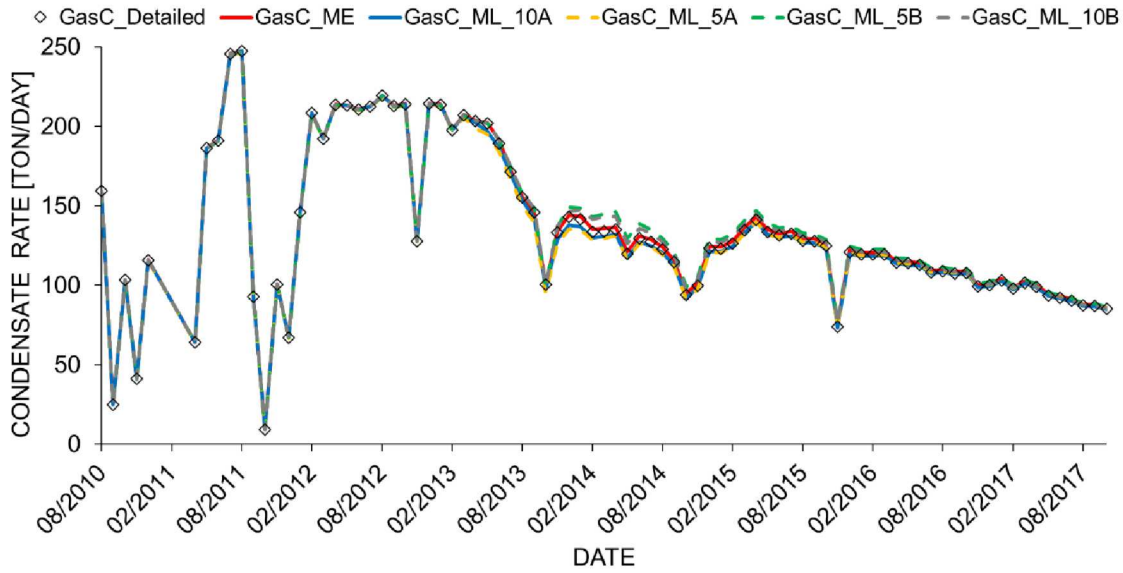

Figure 55 - HYSYS total condensate rate for gas condensate

As mentioned the deviations of the gas condensate will kick in delayed as shown in Figure 56. It is seen that the amplitude of deviations for the cases are contrary in sign compared to sales gas and LPG.

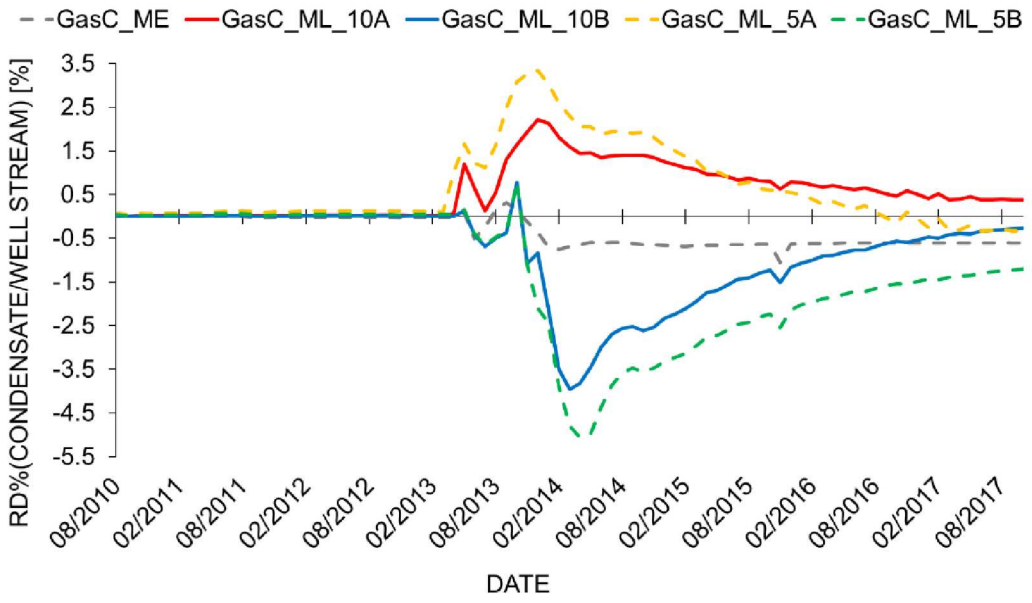

Figure 56 - RD% of Condensate stream ratio deviation for gas condensate simulation

For summarization, it can be concluded that the errors are rather small. With maximum average deviations of $\sim 1\ \%$ overall, they are similar to the average discrepancies between the fluid models. The high deviations of LPG are related to the rather small quantities and hence care should be taken when comparing the absolute values of the analyses in general.

5.2.2 Process Simulation – Volatile Oil

The plots of the absolute produced stream quantities are not supportive for interpreting here. All of them having the same declining trend as shown in Figure 48. That is the reason only Figure 57 displays an overview of the plant products in relation to the well stream. As expected for a volatile oil as produced fluid, the produced condensate is at highest in the earlier simulation. With ongoing depletion, the gas will liberate from the high shrinking oil and, is at first immobile and will then be produced more favourably since the heavy components will stay behind due to lower mobility, as already discussed with Figure 43.

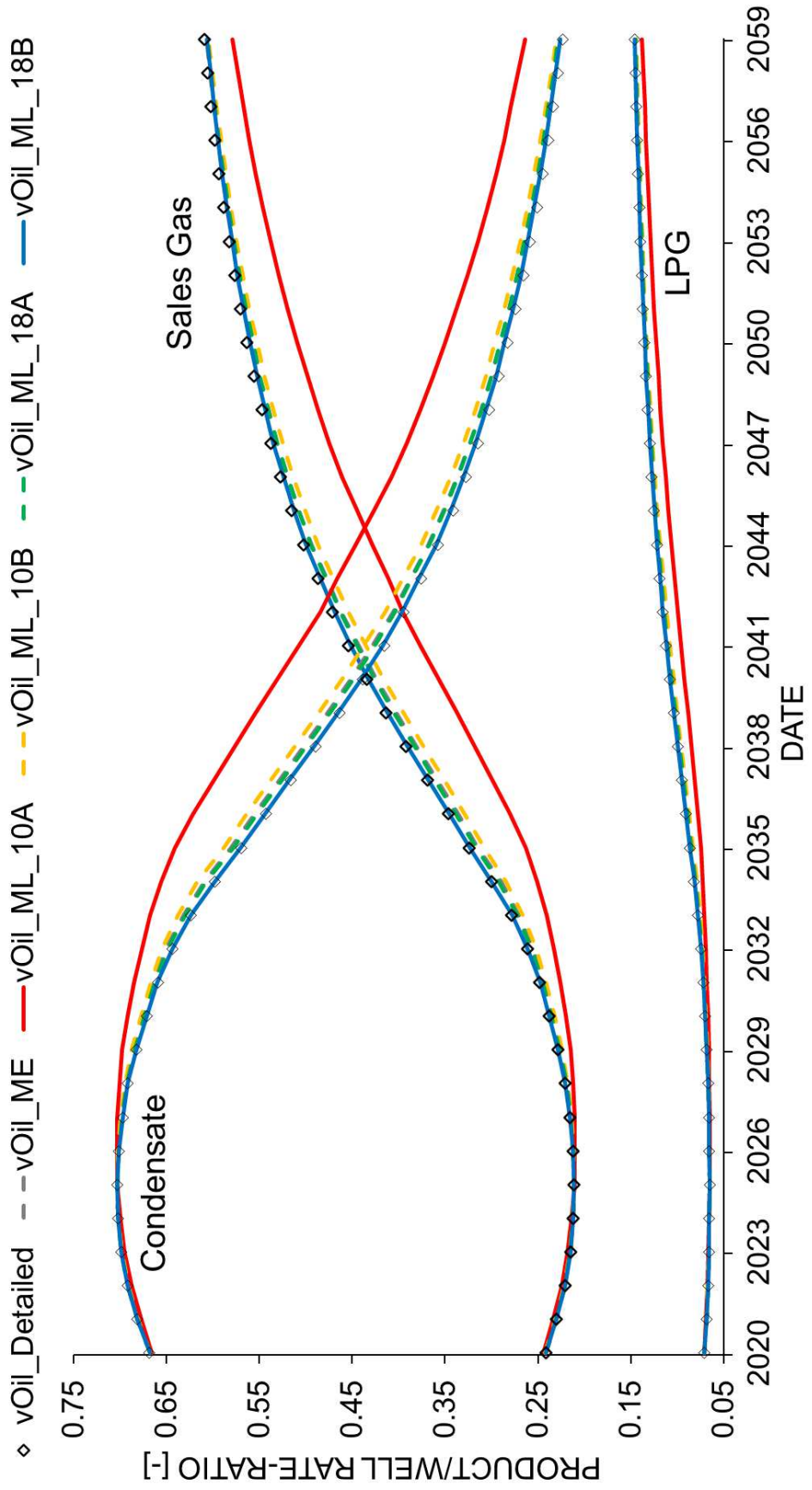

Figure 57 - stream rate ratio of HYSYS products for volatile oil simulation

The same analysis, as proposed in subchapter 5.2.1, is done with the volatile oil - process simulation results. In Figure 58 the deviations for the sales gas streams relative to the well stream are shown.

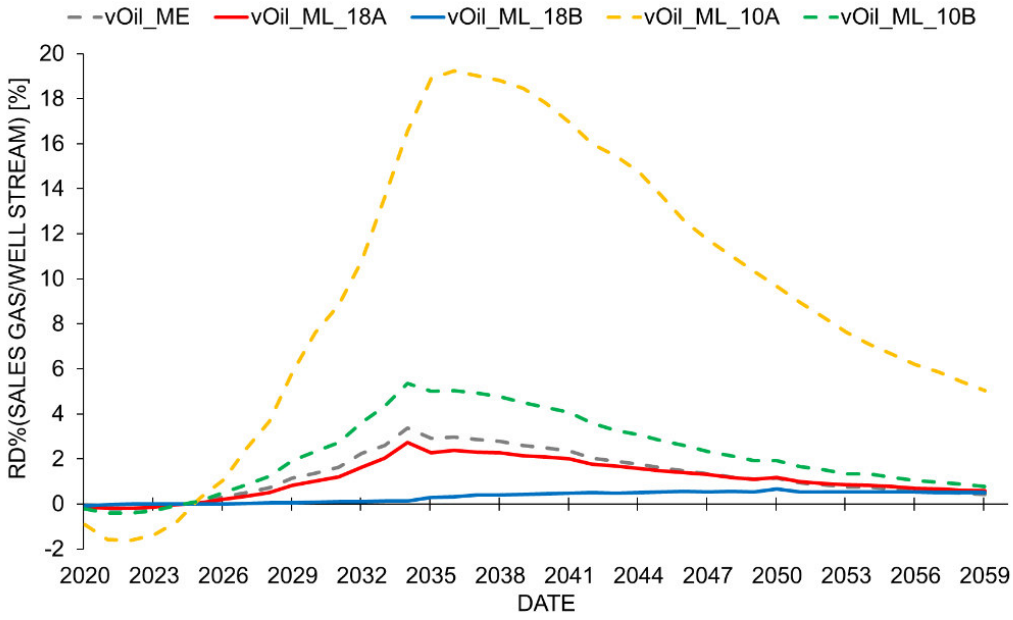

Figure 58 - RD% of sales gas stream ratio deviation for volatile oil simulation

The magnitudes of the deviations are similar to the deviations in the well streams from Figure 49. But it is again mentioned that the deviations from the streams are taken out from this analysis, since the product quantities divided by the well streams were calculated and interpreted.

The high amplitude for the deviations at year 2035 are attributed to the mobilization of the gas, when the critical gas saturation inside the reservoir is overcome. Since there are small discrepancies in the fluid model and therefore in the reservoir simulation itself, this gas mobilization will start at separate times, making the compositions varying during production. This can be seen in Figure 45 as an example for light and intermediate-to-heavy components.

The results for the LPG quantities are, as expected, similar to the sales gas comparison. The deviations are shown in Figure 59 and even the magnitudes of deviations are similar.

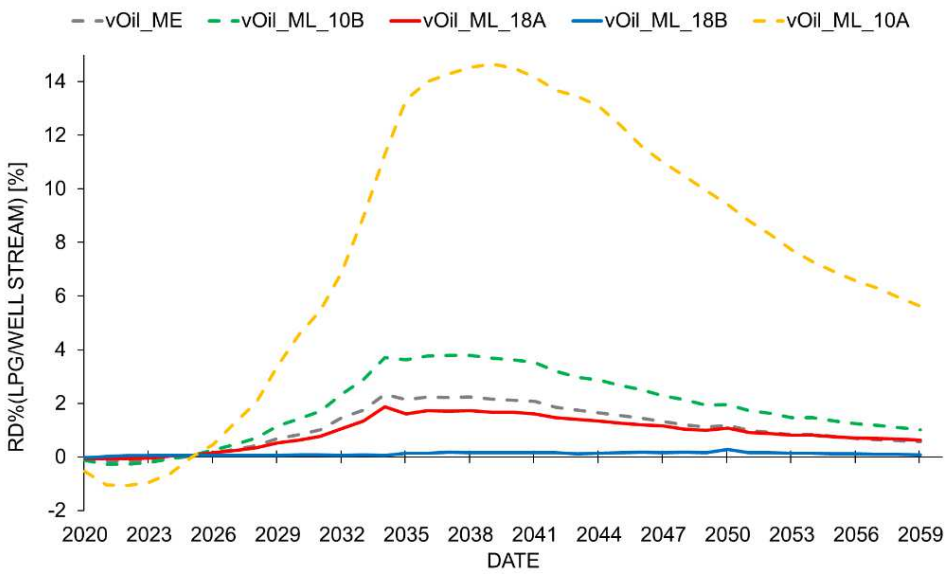

Figure 59 - RD% of LPG stream ratio deviation for volatile oil simulation

The condensate deviations (Figure 60) are, as expected, opposite in amplitude direction and magnitude. A statement about the compositional behaviour of the deviations cannot be made since the condensate is consisting of the majority of components from the volatile oil since its component number is so high, this means that no single component can be found for representing the condensate (contrary to the sales gas (C1) and LPG (C3, C4)), which makes it difficult to find a reasonable and correct answer.

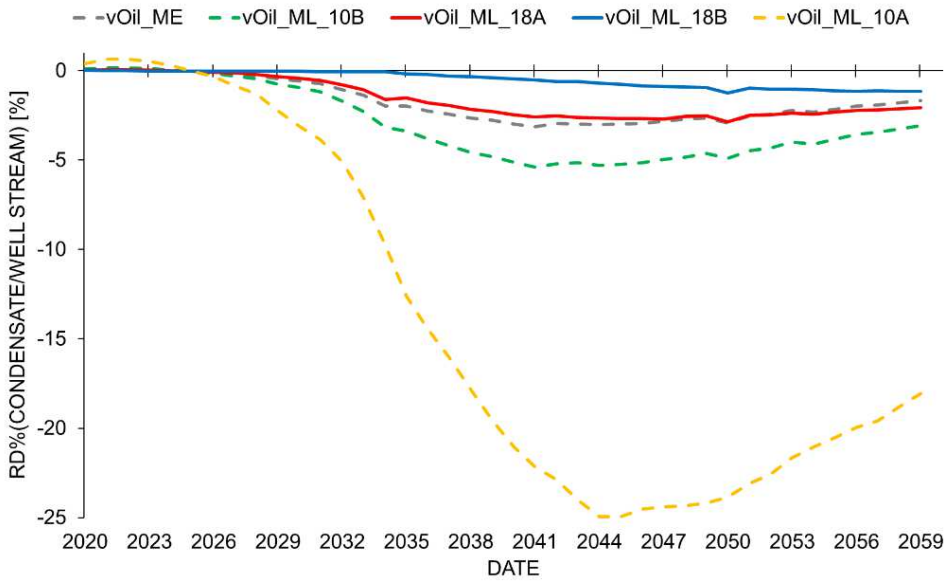

Figure 60 - RD% of Condensate stream ratio deviation for gas condensate simulation

In general, for the volatile oil, it can be conducted that the investigated streams are in good agreement with the reference. Although it is emphasized that compared to the gas condensate the deviations are either over or underestimated. This comes from the fact that because of the lumping of such high detailed component number the phase envelope was always shrunk which was not the case for the gas condensate where mode A overestimated the envelope.

6 Conclusion and Recommendations

For the conclusion of this thesis, Figure 34 at the end of chapter 4 is recalled in order to remember the setup and workflow. The scope of this thesis was to analyse the impact of delumping on the results of surface facility simulations. This was done by setting up different lumping schemes for two different fluids with 15 and 48 components in its full initial description. These created lumped-, together with its detailed-, fluid descriptions were then simulated with SWM/SBM reservoir models by E300. In addition, the simulations using the lumped schemes were delumped by the integrated delumping facility of E300 to obtain detailed system information. The results of the delumped simulations were then compared with the detailed simulation which acts as the reference solution, and all are then handed over to HYSYS which simulate a gas treatment facility in order to obtain three product streams which are sales gas, LPG and condensate for the reference and all delumped cases.

6.1 Conclusion

The following statements and conclusions were found during development of this thesis. Whereas indented paragraphs quoted by "»" are meant to be explanations, and additional information for the introduced conclusions, which are quoted by "✓".

- ✓ Delumping is, as already proposed by the literature, highly dependent on the quality of lumping. Most findings and errors can be traced back to discrepancies introduced when lumping detailed components to PCS by different lumping schemes. Therefore, it is emphasized that the delumping accuracy of the used E300 delumping facility is sufficient for engineering practice since the biggest difficulty is to lump properly.
  - » The analysis of the deviations induced by lumping were carried out for all steps undertaken in the procedure. After the fluid modelling and after the reservoir simulation was a deviation analysis conducted in order to quantify the errors. The deviations determined after the fluid modelling, where consistently carried through the simulation. Most of the other errors detected afterwards, after reservoir and process simulation, were able to be explained with reasoning and no case was found were delumping explicitly had failed.
  - » The issues of inaccurate lumping are thought to be exponentially increasing with increasing field size. Since this thesis handled only single well models it is believed that initialization and production quantity errors are evolving due to the cumulating nature of error propagation. That is the reason the conclusions and quantifications of this work cannot be taken as same for all reservoirs, fluids etc.
- ✓ Several limitations were found regarding the practicable implementation of connecting E300 with its delumping facility with a process simulator such as HYSYS.
  - » Maximum number of lumped components handled by the delumping facility is 18.
  - » Maximum number of delump-able components is 46.

  - » No straight-forward application of dynamic process simulation when connecting E300 with HYSYS.
  - » Different fluid modelling correlations within each software (e.g. viscosity correlations).
  - » Limited output information from E300 is available (only produced concentration via e.g. `WTPC`), since the delumping facility is not extensively implemented.
  - » Poor documentation from E300 delumping facility is available – therefore the above findings were mostly found by trial and error.
- ✓ Delumping gives an excellent opportunity for integrated asset management if conducted properly. It speeds up reservoir simulation time and provides accurate detailed simulation results.
  - » Limited in creating a fluid model which is valid for the real reservoir in a full field is not as easy as it seems by matching a lab report. Since the composition within reservoirs can vary, there is also uncertainty included in the lab report and knowledge of the reservoir fluid itself. In addition, the fluid model needs to be investigated and monitored throughout the simulation, since it is possible that the lumping scheme itself becomes invalid (e.g. with varying mole concentration of a single component, the affinity towards an initial PCS cluster can change). Therefore, delumping enables such monitoring of the composition state.
  - » Lumped fluid descriptions are often not applicable in process simulations. If single components are lumped, e.g. in this thesis N2C1, the GTU cannot process the simulated PCS properly, e.g. fractionation tower specified via component-ratio. Delumping however, makes such lumping possible and still gives detailed results which can be processed by a process simulator.
  - » Nevertheless, the used delumping facility from E300 (using LSK-method [2]) is sufficient for engineers' practice. Although other methods in literature show promising results and should be investigated further.

6.2 Recommendations and Future Developments

There are some interpretations left which can only be investigated by detailed component tracking through all simulations, which was not scope of this thesis and would also burst the limit of this master thesis. However, such analysis could be important e.g. in gas cycling assets and general process model optimization studies.

Another recommendation is the comparison of different delumping techniques, since this is possible, and was already applied, by using the lumped simulation and apply other delumping methods as post-processing.

References

[1] Z. Chen, G. Huan and Y. Ma, Computational Methods for Multiphase Flows in Porous Media, Philadelphia: Society for Industrial and Applied Mathematics, 2006.

[2] C. Leibovici, J. W. Barker and D. Wache, “Method for Delumping the Results of Compositional Reservoir Simulation,” *SPE Journal,* vol. 5, no. 02, pp. 227-235, 2000.

[3] M. Assareh, C. Ghotbi, M. R. Pishvaie and G. M. Mittermeir, “Development of a new workflow for pseudo-component generation of reservoir fluid detailed analysis: a gas condensate case study,” *International Journal for Oil, Gas and Coal Technology,* vol. 7, no. 3, pp. 275-297, 2014.

[4] A. Danesh, PVT and Phase Behaviour of Petroleum Reservoir Fluids, Elsevier Science, 1998.

[5] D. T. De Castro, D. V. Nichita, D. Broseta, M. Herriou and J. W. Barker, “Improved Delumping of Compositional Simulation Results,” *Petroleum Science and Technology,* vol. 29, pp. 1-12, 2011.

[6] C. Leibovici, “A Consistent Procedure for the Estimation of Properties Associated to Lumped Systems,” *Fluid Phase Equlibria,* vol. 87, pp. 189-197, 1993.

[7] K. S. Pederson, P. L. Christensen and J. A. Shaikh, Phase Behaviour of Petroleum Fluids, Boca Raton: Taylor & Francis Group, 2015.

[8] A. G. Schijper and J. K. Drohm, “Inverse Lumping: Estimating Compositional Data From Lumped Information,” *SPE Reservoir Engineering,* 1988.

[9] A. Danesh, D. Xu and A. C. Todd, “A Grouping Method To Optimize Oil Description for Compositional Simulation of Gas-Injection Processes,” *SPE Reservoir Engineering,* vol. 7, no. 03, pp. 343-348, 1992.

[10] C. Leibovici, E. H. Stenby and K. Knudsen, “A Consistent Procedure for Pseudo-Component Delumping,” *Fluid Phase Equilibria,* vol. 117, no. 1-2, pp. 225-232, 1996.

[11] M. Assareh, C. Ghotbi, G. Bashiri and E. Roayaie, “An improved component retrieval method for cubic equations of state with non-zero binary interaction coefficients for natural oil and gas,” *Journal Petroleum Exploration and Production Technology,* vol. 6, pp. 243-251, 2016.

[12] F. S. Manning and R. E. Thompson, Oilfield Processing of Petroleum, Natural Gas ed., vol. 1, Tulsa: PennWell, 1991.

[13] “Gazprom Info,” Gazprom, [Online]. Available: http://www.gazprominfo.com/articles/condenced-gas/. [Accessed 17 January 2020].

[14] J. M. Campbell, Gas Conditioning and Processing: The Basic Principles, 7 ed., vol. 1, Norman: Campbell Petroleum Series, 1984.

[15] K. Arnold and M. Stewart, “Design of Oil Handling System and Facilities,” in *Surface Production Operations*, 3 ed., vol. 1, Burlington, Gulf Professional Publishing, 2008.

[16] R. N. Maddox, Gas Conditioning and Processing: Gas and Liquid Sweetening, 3 ed., vol. 4, Norman: Campbell Petroleum Series, 1982.

[17] J. M. Campbell, Gas Conditioning and Processing: The Equipment Modules, 7 ed., vol. 2, Norman: Campbell Petroleum Series, 1984.

[18] Aspen Technology Inc., “Aspen HYSYS V10 Help,” Aspen Technology Inc., Bedford, 2017.

[19] C. L. Rhodes, “The Process Simulation Revolution: Thermophysical Property Needs and Concerns,” *Journal Chemical Engineering Data,* no. 41, pp. 947-950, 1996.

[20] S. K. Mondal, M. R. Uddin, S. Majumder and J. Pokhrel, “HYSYS Simulation of Chemical Process Equipments,” SUST, Sylhet, 2015.

[21] A. T. Inc., “Aspentech.com/HYSYS,” Aspen Technology Inc., 2020. [Online]. Available: https://www.aspentech.com/en/products/engineering/aspen-hysys. [Accessed 6 February 2020].

[22] B. Faissat and M. C. Duzan, “Fluid Modelling Consistency in Reservoir and Process Simulations,” *SPE 36932,* pp. 1-7, 1996.

[23] Z. E. Heinemann and G. Mittermeir, “Introduction to Reservoir Simulation,” in *PHDG Textbook Series*, Tehran, PHDG, 2013, pp. 1-98.

[24] Z. E. Heinemann and G. Mittermeir, “Systematic of Reservoir Flow Equations,” in *PHDG Textbook Series*, Tehran, PHDG, 2013, pp. 1-23.

[25] K. Aziz and A. Settari, Petroleum Reservoir Simulation, Essex: Applied Science Publishers Ltd., 1979.

[26] Z. E. Heinemann and B. E. Weinhardt, *Reservoir Fluids Textbook Series Volume 2,* Leoben: Montanuniversität Leoben, 2005.

[27] C. H. Whitson and M. L. Michelsen, “The negative Flash,” *Fluid Phase Equilibria,* vol. 53, pp. 51-71, 1989.

[28] H. H. Rachford and J. D. Rice, “Procedure for Use of Electrical Digital Computers in Calculating Flash Vaporization Hydrocrabon Equilibrium,” *Journal Petroleum Technologies,* vol. Trans. AIME, no. 195, p. 19, 1952.

[29] C. H. Whitson and M. R. Brulé, “Phase Behaviour,” in *SPE Monograph Series Volume 20*, Texas, Society of Petroleum Engineers Inc., 2000, pp. 1-240.

[30] J. M. Smith, H. C. Van Ness, M. M. Abbott and M. T. Swihart, Introduction to Chemical Engineering Thermodynamics, New York: McGraw-Hill Education, 2005.

[31] F. Montel and P. L. Gouel, “A New Lumping Scheme of Analytical Data for Compositional Studies,” *SPE 13119,* pp. 1-12, 1984.

[32] K. S. Pedersen, P. Thomassen and A. Fredenslund, “Thermodynamics of petroleum mixtures containing heavy hydrocarbons. 1. Phase envelope calculations by use of the Soave-Redlich-Kwong equation of state,” *Ind. Eng. Chem. Process Des. Dev.,* no. 23, pp. 163-170, 1984.

[33] Y. K. Li, L. X. Nhgiem and A. Siu, “Phase Behaviour Computations for Reservoir Fluids: Effect of Pseudo-Components on Phase Diagrams and Simulation Results,” *Journal Canadian Petroleum Technology,* vol. 24, no. 06, pp. 29-36, 1985.

[34] R. Rastegar and K. Jessen, “A Flow Based Lumping Approach for Compositional Reservoir Simulation,” in *SPE Reservoir Simulation Symposium*, Texas, 2009.

[35] R. Rastegar and K. Jessen, “Lumping and Delumping for Integrated Compositional Modeling,” *SPE 125017,* 2009.

[36] E. H. Stenby, J. R. Christensen, K. Knudsen and C. Leibovici, “Application of a Delumping Procedure to Compositional Reservoir Simulations,” *SPE 36744,* 1996.

[37] E. Vignatti, A. Cominelli, R. Rossi and P. Roscini, “Innovative Implementation of Compositional Delumping in Integrated Asset Modeling,” *SPE 113769,* 2009.

[38] D. V. Nichita and C. Leibovici, “An analytical consistent pseudo-component delumping procedure for equations of state with non-zero binary interaction parameters,” *Fluid Phase Equilibria,* vol. 245, pp. 71-82, 2006.

[39] D. V. Nichita and A. Graciaa, “A new reduction method for phase equilibrium calculations,” *Fluid Phase Equilibria,* vol. 302, no. 1-2, pp. 226-233, 2011.

[40] D. V. Nichita, D. Broseta and C. Leibovici, “Reservoir fluid applications of a pseudo-component delumping new analytical procedure,” *Journal of Petroleum Science & Engineering,* vol. 59, pp. 59-72, 2007.

[41] M. Assareh, C. Ghotbi, M. R. Pishvaie and G. M. Mittermeir, “An analytical delumping methodology for PC-SAFT with application to reservoir fluids,” *Fluid Phase Equilibria,* vol. 339, pp. 40-51, 2013.

[42] Schlumberger, *ECLIPSE V2018.1 Technical Description,* 2018.

[43] Schlumberger, *ECLIPSE v 2018.1 Reference Manual,* 2018.

[44] J. M. Smith, H. C. Van Ness, M. M. Abbott and B. I. Bhatt, Introduction to Chemical Engineering Thermodynamics 6th Edition, New York: McGraw-Hill Education, 2001.

[45] P. Shapley, “Real Gases,” University of Illinois, 2011. [Online]. Available: http://butane.chem.uiuc.edu/pshapley/GenChem1/L14/2.html. [Accessed 6 February 2020].

[46] T. Y. Kwak and G. A. Mansoori, “Van der Waals Mixing rules for cubic equations of state, applications for supercritical fluid extraction modelling,” in *Chemical Engineering Science vol. 41*, Chicago, Pergamon Press Ltd., 1985, pp. 1303-1309.

[47] T. O. Allen and A. P. Roberts, Production Operations, Well Completion, Workover, and Stimulation Volume 2, Tulsa, Oklahoma: OGCI,Inc.,PetroSkills,LLC., 2008.

[48] A. Kuntadi, C. H. Whitson and M. F. Hoda, “Dynamic Delumping of Reservoir Simulation,” *SPE Annual Technical Conference and Exhibition,* pp. 1-22, 2012.

[49] H. Briesen and W. Marquardt, “New Approach to Refinery Process Simulation with Adaptive Composition Representation,” *American Institute of Chemical Engineers,* vol. 50, pp. 633-645, 2004.

[50] J. W. Barker and C. Leibovici, “Delumping Compositional Reservoir Simulation Results: Theory and Applications,” *SPE 51896,* 1999.

[51] K. Ghorayeb, J. Holmes, R. Torrens and B. Grewal, “A General Purpose Controller for Coupling Multiple Reservoir Simulations and Surface Facility Networks,” *SPE 79702,* 2003.

[52] D. Peng and D. B. Robinson, “A New Two-Constant Equation of State,” *Industrial & Engineering Chemistry Fundamentals,* vol. 15, no. 1, pp. 59-64, 1976.

[53] A. T. Inc., *Aspen HYSYS V10 Help,* Bedford: Aspen Technology Inc., 2017.

List of Tables

List of Figures

Abbreviations

API°	American Petroleum Institute gravity
ASTM	American Society for Testing and Material
BHP	Bottom-hole pressure
BIC	Binary interaction coefficients
bp	Bubble point
BWRS	Benedict-Webb-Rubin-Starling
CPU	Central processing unit
CVD	Constant volume depletion
De-C2	De-Ethanizer fractionation column
De-C4	De-Butanizer fractionation column
DLE	Differential Liberation Experiment
dp	Dew point
E300	Schlumberger ECLIPSE® 2018.1 Compositional Reservoir Simulator
EoS	Equation of State
ESYS	PML proprietary developed software
fcm	Fuzzy Clustering Method
FTPC	Field Tracer Production Concentration
GasC	Gas Condensate
GIGO	Garbage in-Garbage out
GOR	Gas-oil-ratio
GTPC	Group Tracer Production Concentration
GTU	Gas treatment unit
hypos	Hypothetical components
HYSYS	Aspentech HYSYS® V10
K-value	Equilibrium ratio
LPG	Liquefied petroleum gas
LSK	Leibovici-Stenby-Knudsen
mD	Millidarcy
NGL	Natural gas liquids
PCS	Pseudocomponents
Pen	Peneloux
pg.	Page
PML	PM Lucas
PR-EoS	Peng-Robinson Equation of State
PVT	Pressure volume temperature
RD%	Relative deviation in percent
RK-EoS	Redlich-Kwong Equation of State
RVP	Reid Vapor Pressure
SAFT	Statistical associated fluid theory
SBM	Shoebox reservoir simulation model
SRK-EoS	Soave-Redlich-Kwong Equations of State

SWM	Single well reservoir simulation model
TBH	Tubing head
THP	Tubing head pressure
VdW	Van der Waals
VFP	Vertical Flow Performance
VLE	Vapor-liquid equilibrium
vOil	Volatile Oil
Vol	Volume
WTPC	Well Tracer Production Concentration

Nomenclature

g	Acceleration	[m/s²]
m	Acentric Factor Function	
k_{ij}	BIC	[-]
c_1, c_2	Coefficients	
Z	Compressibility Factor	[-]
p_c	Critical Pressure	[bar]
T_c	Critical Temperature	[K]
V_c	Critical Volume	[m³/mol]
Z_i	Detailed Component Fraction	[-]
X_i	Detailed Vapor Fraction	[-]
Y_i	Detailed Vapor Fraction	[-]
dx	Differential of Length	[m]
D	Diffusion Constant	[m²/s]
H	Enthalpy	[J]
S	Entropy	[J/K]
a	Eos Parameter, Attraction	
b	Eos Parameter, Repulsion	
K_i	Equilibrium Ratio of Component i	[-]
z_i	Feed Fraction of Component i	[-]
f	Fugacity	[bar]
$f(\ \ )$	Function of …	[-]
$\emptyset_{geo}(\ \ )$	Geometric Average of …	[-]
G	Gibbs Energy	[J]
FPR	Hydrocarbon Weighted Field Pressure	[bar]
R	Ideal Gas Constant	[J/mol. K]
U	Inner Energy	[J]
L	Length or Liquid Flux or Liquid Fraction	[m] or [m³/s] or [-]
x_i	Liquid Fraction of Component i	[-]
X	Liquid Mole Fraction of System	[-]
$\mathcal{R}$	Lumping Ratio	[-]
c	Molarity or Volume Shift	[mol/m³] or [-]
n	Mole	[mol]
MW	Molecular Weight	[g/mol]

$\bar{G}_i$	Partial Molar Gibbs Energy	[J/mol]
k	Permeability	[mD]
p	Pressure	[bar]
S	Saturation	[-]
T	Temperature	[°C] / [K]
$\Gamma(T)$	Temperature Dependent Integration Constant	
t	Time	[s]
F_V	Vapor Fraction / Vapor Split	[-]
y_i	Vapor Fraction of Component i	[-]
Y	Vapor Mole Fraction of System	[-]
I	VLE Parameter	
q	VLE Parameter	
V	Volume or Vapor Flux or Vapor Fraction	[m³] or [m³/s] or [-]
q	Well Flow or VLE Parameter	[m³/s] or [-]
Q	Well Flux	[m³/s]

Greek Symbols

ω	Acentric Factor	[-]
θ	Arbitrary Property character	
μ_i	Chemical Potential of Component i	[J]
ρ	Density	[kg/m³]
$\Omega_{a,b}$	EoS Coefficient	
η	EoS Parameter	
ϵ	Error	[-]
λ	Mobility	[m²/bar. s]
ϕ	Porosity or Fugacity Coefficient	[-]
Φ	Potential	[bar]
$\alpha(T)$	Temperature Dependent EoS Parameter	
τ	Transmissibility	[m³]
β	VLE Variable	

Superscripts

k	Detailed Number
ig	Ideal Gas
l	Liquid
res	Reservoir Conditions

R	Residual Property
$surf$	Surface Conditions
m	Timestep
v	Vapor

Subscripts

$\overline{\ }$	Average or Partial Molar Property
i	Component Count Variable
wc	Connate Water
I_0	Current Block
k	Eos Parameter Count Variable
g	Gas (Vapor)
HC	Hydrocarbon
L	Liquid
m	Molar
I_1	Neighbour Block
n	Number of Components
o	Oil (Liquid)
π	Phase
$\widehat{\ }$	Property in Mixture
j	Second Component Count Variable
$=$	Tensor
T	Total
V	Vapor

Components

Ben	Benzene
CO2	Carbon Dioxide
C*	Carbon Number / Alkanes
cC6	Cyclo-Hexane
C2Ben	Ethylbenzene
EGlycol	Ethylene Glycol
H2S	Hydrogen Sulphide
iC4, iC5	Iso Butane / Pentane
Hg	Mercury
mpXyl	Meta Para Xylene

CH4=C1	Methane
mcC5	Methyl-Cyclo-Pentane
MDEA	Methyl Diethanolamine
mC6	Methyl Hexane
N2	Nitrogen
nC4, nC5	Normal Butane / Pentane
oXyl	Ortho Xylene
PC* / PS*	Pseudocomponent Name
C*+	Plus Fraction
Tol	Toluene
TEG	Triethylene Glycol

Appendices

Appendix A VLE Theory

Since the delumping methods and algorithms are based on VLE calculation, necessary theory was outsourced into the appendices in order to keep the fundamental chapter concise.

For the derivation and explanation of Appendix A.1, chapter 4 from *"Phase Behaviour of Petroleum Reservoir Fluids"* by *Pederson et al.* [7], was used. The derivation of phase equilibria calculations in Appendix A.2 till Appendix A.6, are taken from *"Introduction to Chemical Engineering Thermodynamics"* by *Smith J. M. et al.* [44], and its hereby mentioned that all not explicitly otherwise cited references are coming from the above mentioned ones.

Appendix A.1 Equation of State

For modelling fluid phase behaviour, a mathematical model is needed. One of such models is called EoS.

The ideal gas law can be seen in **eq.** (39).

$$p = \frac{nRT}{V} \tag{39}$$

The equation can be described as the molar volume of an ideal gas is approaching asymptotically zero if its pressure is going to infinity. This led to the assumption that an ideal gas can be thought of infinitesimal small point like gas molecules which are in constant motion, having neglectable interactions with each other and the systems boundary as well as the particle collisions can be seen as ideal elastic [45].

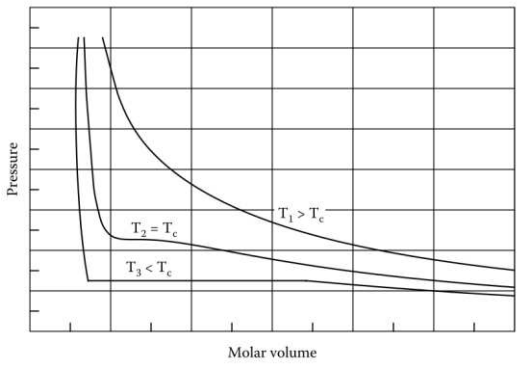

Figure 61 - p versus molar V of a gas, also called isotherms [7, p. 84]

As this is approximately true for gases at low pressure and high temperatures. It is not true for real gases, as one can see that in reality when the molar volume approaches a limiting value (see Figure 61, left). Johannes Diderik van der Waals (VdW), which derived the first cubic EoS, suggested therefore extending the ideal gas law by a parameter b which is referring to a volume of a gas particle, also known as co-volume:

$$V = \frac{RT}{p} + b \tag{40}$$

Deriving the VdW EoS further we can see that at temperatures below T_c (see Figure 61, T_3), the decrease of V_m (at constant temperature) will result in an increase in pressure and during the phase transition (by lowering V_m further) the pressure stays constant. When all vapour has been transformed to liquid (and hereby liquid is almost incompressible) the isotherm will take a steep increase, going towards infinity. This investigation lead to the fact that for a vapour, where the particles are far a part, towards a liquid, where the distance is small, attractive forces are acting between the particles. VdW found out that the attractive forces are inversely proportional to the square of volume. Thus **eq.** (39) becomes:

$$p = \frac{RT}{V - b} - \frac{a}{V^2} \tag{41}$$

Which is the popular form of the VdW EoS, where a and b are constants and EoS parameters.

Rearranging **eq.** (41), one can see why the VdW EoS is called cubic EoS

$$V^3 - \left(b + \frac{RT}{p}\right)V^2 + \frac{a}{p}V - \frac{ab}{p} = 0 \tag{42}$$

As it can be seen in Figure 61, $T_2 = T_c$, the critical isotherm is having an inflection point. Thus a and b are found by evaluating **eq.** (41) at the inflection point where:

$$\left(\frac{\partial p}{\partial V}\right)_{T\ at\ T=T_c\ ,p=p_c} = \left(\frac{\partial^2 p}{\partial V^2}\right)_{T\ at\ T=T_c,p=p_c} = 0 \tag{43}$$

And therefore a and b can be found analytically

$$a = \Omega_a \frac{R^2 T_c^2}{p_c} \tag{44}$$

$$b = \Omega_b \frac{RT_c}{p_c} \tag{45}$$

Where $\Omega_{a,b}$ are EoS coefficients varying with the EoS used.

Figure 62, is showing three VdW-isotherms for methane. One can see the oscillations of the T_3 curve. Comparing these curves with Figure 61, the similarity is clear for $T \geq T_c$, but for T_3 the curve is having two extremes which are unphysical, but comparing it with experimental data, one can find that the V_m at point C equals the V_m of the liquid phase and point A is referring to V_m of the vapour phase, therefore the VdW EoS can be used to qualitatively describe single component systems over all T.

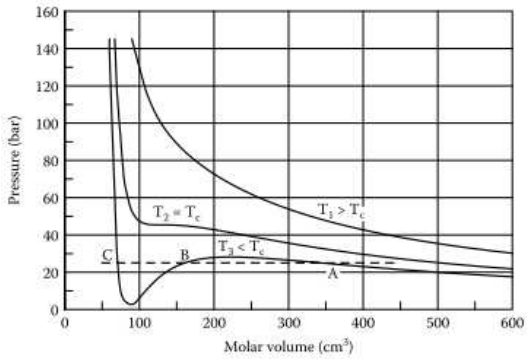

Figure 62 – isotherms calculated with VdW EoS & dashed line experimental vapour pressure [7, p. 86]

Since EoS problems are usually about multi-component mixtures, the EoS parameters needs to be approximated for the mixture. Since it is not possible to do an experiment on every mixture, a mathematical relation to combine single component properties was needed. Therefore, VdW proposed mixing rules [46]:

$$a = \sum_{i}^{N_c}\sum_{j}^{N_c} x_i x_j a_{ij} \qquad with \qquad a_{ij} = \left(1 - k_{ij}\right)\sqrt{a_i a_j} \tag{46}$$

$$b = \sum_{i}^{N_c} x_i b_i \tag{47}$$

Other mixing rules were developed e.g. for the Redlich-Kwong EoS, which is using the same a and b formulation but for a_{ij} they proposed: [7]

$$a_{ij} = 0.42748\frac{R^2 T_{cij}^{2.5}}{p_{cij}} \tag{48}$$

With $T_{cij} = \sqrt{T_{ci}T_{cj}}\left(1 - k_{ij}\right)$; $p_{cij} = Z_{cij}RT_{cij}/V_{cij}$ and $V_{cij} = \left(\frac{\sqrt[3]{V_{ci}} + \sqrt[3]{V_{cj}}}{2}\right)^3$

After VdW EoS was established many developments have been come up with, namely some popular EoS are hereby listed:

- Redlich-Kwong EoS (RK-EoS)
  First modern EoS. Introduced that $a = f(T)$, improves vapour pressure predictions, also formulated for mixtures
- Soave-Redlich-Kwong EoS (SRK-EoS)
  Introduced $a(T) = a_c(T_c, p_c) * \alpha(T_r, \omega)$, generalised temperature dependency – more accurate (especially on vapour pressure calculations), different mixture formulation
- Peng-Robinson EoS (PR-EoS)
  Revision of SRK EoS regarding underestimated pure component critical compressibility factors. The related equations are following:

$$p = \frac{RT}{V-b} - \frac{a(T)}{V(V+b)+b(V-b)} \quad (49)$$

Where the temperature dependent attractive forces term is:

$$a(T) = 0{,}45724\frac{R^2T_c^2}{p_c}\alpha(T) \quad (50)$$

And the temperature dependent function:

$$\alpha(T) = \left(1 + m\left(1 - \sqrt{\frac{T}{T_c}}\right)\right)^2 \quad (51)$$

and included for acentric factors 2 formulations which are commonly referred to PR-EoS corrected:

$$\begin{cases} m = 0.37464 + 1.54226\omega - 0.26992\omega^2, if\ \omega < 0.49 \\ m = 0.379643 + 1.48503\omega - 0.164423\omega^2 + 0.016666\omega^3, if\ \omega > 0.49 \end{cases} \quad (52)$$

And for the co-volume b:

$$b = \frac{0.0778RT_c}{p_c} \quad (53)$$

- Peneloux volume correction (SRK-Pen-EoS or PR-Pen-EoS)
  Extended SRK-EoS by introducing third EoS parameter (volume translation c) but can be also applied to PR-EoS.
  SRK EoS showed poor liquid density calculation results.
  Volume-shift parameter or volume translation will alter molar volume as well as phase densities and fugacities but without interfering with phase equilibrium.

  PR-Pen-EoS:

$$P = \frac{RT}{V-b} - \frac{a(T)}{(V+c)(V+2c+b)+(b+c)(V-b)} \quad (54)$$

Whereas for C1-C6

$$c = \frac{0.40768RT_c(0.00385 - 0.08775\omega)}{p_c} \quad (55)$$

For non-hydrocarbons lighter than C7

$$c = \frac{0.50033RT_c(-0.03087 - 0.08775\omega)}{p_c} \tag{56}$$

Independency of c on the phase equilibrium can be shown as

$$\ln \phi_{i,SRK} = \ln \phi_{i,Pen} + \frac{c_i p}{RT} \tag{57}$$

We can conclude that by the definition in **eq.** (3) on can say:

$$K_i = \frac{y_i}{x_i} = \frac{\phi_{i,SRK}^l}{\phi_{i,SRK}^v} = \frac{\phi_{i,Pen}^l \exp\left(\frac{c_i p}{RT}\right)}{\phi_{i,Pen}^v \exp\left(\frac{c_i p}{RT}\right)} = \frac{\phi_{i,Pen}^l}{\phi_{i,Pen}^v} \tag{58}$$

Many other corrections where performed also with different approaches (Virial series, other cubic EoS like BWRS-EoS and statistical associating fluid theory (SAFT)…) but are not expounded here further. Most of them are relating to enhancements of empirical formulations and every EoS has its different field of applications, whereby SRK- and PR-EoS are the most common used in the petroleum industry.

Appendix A.2 Phase Equilibria for Pure Substance

The criteria for phase equilibrium can be explained using the first and second laws of thermodynamics.

$$dU < TdS - pdV \tag{59}$$

For an irreversible, real process approaching any state of equilibrium, the inner energy dU will be decreased. The Gibbs energy G is defined as:

$$G \equiv H - TS \tag{60}$$

Where H, is the systems enthalpy:

$$H \equiv U + pV \tag{61}$$

And substituting the above Equations, we get:

$$G \equiv U + pV - TS \tag{62}$$

Taking the derivative, we obtain:

$$dG = dU + pdV + Vdp - TdS - SdT \tag{63}$$

$$dG = TdS - pdV + pdV + Vdp - TdS - SdT \tag{64}$$

$$dG = Vdp - SdT \tag{65}$$

Appendix A.2.1 Two Phases in a Closed System

In order to come up with a formulation for phase equilibria of a two-phase system of a pure substance, we will look on **eq.** (65) during a phase transition, see Figure 63, where the temperature as well as the pressure are constant during a phase transition.

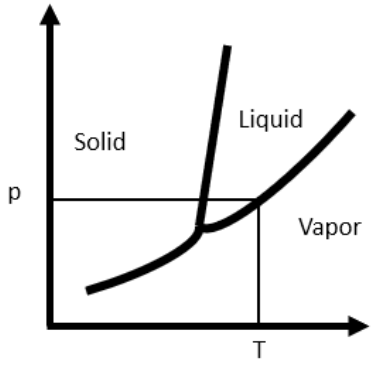

Figure 63 - phase transition for a pure substance

This means that for a closed system of a pure substance with n moles during a phase transition it is stated:

$$d(nG) = (nV)dp - (nS)dT \tag{66}$$

For constant temperature, pressure and moles

$$dG = 0 \tag{67}$$

Which results in the relation for a pure substance which phases are coexisting at equilibrium

$$G^v - G^l = 0 \quad \rightarrow \quad G^v = G^l \tag{68}$$

This is now the fundamental relationship for constant composition fluids in equilibrium. However, for the purpose of this thesis, systems where the composition is the primary variable are important. Thus, for a single-phase fluid in an open system, which can exchange material with its surroundings it follows:

$$nG = f(p, T, n_1, n_2, \dots n_i, \dots) \tag{69}$$

The total differential of nG is:

$$d(nG) = \left(\frac{\partial(nG)}{\partial p}\right)_{T,n} dp + \left(\frac{\partial(nG)}{\partial T}\right)_{p,n} dT + \sum_i \left(\frac{\partial(nG)}{\partial n_i}\right)_{p,T,n_j} dn_i \tag{70}$$

Where n_j denotes that all number of moles, except n_i, are kept constant.

Hereby, we define the chemical potential:

$$\mu_i \equiv \left(\frac{\partial(nG)}{\partial n_i}\right)_{p,T,n_j} \tag{71}$$

And now **eq.** (70) becomes the fundamental property relation for a single-phase fluid of variable composition.

Appendix A.2.2 Two Phases with Different Composition in a Closed System

Considering now a closed system of two phases in equilibrium. This can be seen as two open systems with mass transfer with each other. The fundamental property relation for variable composition written for each phase (each open system), as seen similar in **eq.** (70), is for vapour:

$$d(nG)^v = (nV)^v dp - (nS)^v dT + \sum_i \mu_i^v dn_i^v \tag{72}$$

And for liquid:

$$d(nG)^l = (nV)^l dp - (nS)^l dT + \sum_i \mu_i^l dn_i^l \tag{73}$$

Since both phases in a closed system are in equilibrium at constant pressure and temperature conditions, where $d(nG) = 0$, it follows:

$$\sum_i \mu_i^v dn_i^v + \sum_i \mu_i^l dn_i^l = 0 \tag{74}$$

Cause mass transfer occurs only between the two phases, mass conservation implies:

$$dn_i^v = -dn_i^l \qquad \rightarrow \qquad \sum_i \left(\mu_i^v - \mu_i^l\right) dn_i^v = 0 \tag{75}$$

It can be concluded that for multiple phases in equilibrium, at constant temperature and pressure, the chemical potential of all phases is equal.

$$\mu_i^v = \mu_i^l \tag{76}$$

Appendix A.3 Partial Molar Properties for use in VLE calculations

Introducing the partial molar property, by using the fundamental relation **eq.** (66) and differentiating by n_i at constant composition, temperature and pressure

$$d\left(\frac{\partial(nG)}{\partial n_i}\right)_{p,T,n_j} = \left(\frac{\partial(nV)}{\partial n_i}\right)_{T,n_j} dp - \left(\frac{\partial(nS)}{\partial n_i}\right)_{p,n_j} dT \tag{77}$$

By definition, the partial molar Gibbs energy can be written like:

$$d\bar{G}_i = d\left(\frac{\partial(nG)}{\partial n_i}\right)_{p,T,n_j} \tag{78}$$

This is now a response function for a change of the total Gibbs energy nG at constant temperature and pressure of a variable amount of species in a finite amount of solution.

For a finite amount (= constant composition) of a solution, it is valid that $\bar{G}_i = f(p,T)$. Thus,

$$d\bar{G}_i = \left(\frac{\partial\bar{G}_i}{\partial p}\right)_{T,n_j} dp + \left(\frac{\partial\bar{G}_i}{\partial T}\right)_{p,n_j} dT \tag{79}$$

It follows from **eq.** (77):

$$\left(\frac{\partial\bar{G}_i}{\partial p}\right)_{T,n_j} = \bar{V}_i \qquad and \qquad \left(\frac{\partial\bar{G}_i}{\partial T}\right)_{p,n_j} = -\bar{S}_i \tag{80}$$

Thus **eq.** (79) can be written as

$$d\bar{G}_i = \bar{V}_i dp - \bar{S}_i dT \tag{81}$$

This shows the similarity for a molar property in constant composition solution and the partial molar property of a species in solution, if **eq.** (81) is compared with **eq.** (65).

To stay within reasonable bounds for this thesis, the following equations for enthalpy and entropy for ideal gas mixtures, will be taken directly, without additional derivation, from [44].

It is shown, that as a result of the partial pressure, $p_i = y_i p$, - systems pressure, p, dependency, of a partial molar entropy of a species in an ideal gas mixture, and the molar entropy of the species as pure ideal gas, the partial molar entropy can be written as:

$$\bar{S}^{ig} = S^{ig} - R\ln y_i \tag{82}$$

And because of the pressure-independency of the partial molar enthalpy of a species in an ideal gas mixture, and the molar enthalpy of this species as pure ideal gas, the partial molar enthalpy in an ideal gas mixture can be expressed as their molar enthalpy for pure ideal gas.

$$\bar{H}^{ig} = H^{ig} \tag{83}$$

Now we can combine the Gibbs energy of an ideal gas mixture $G_i^{ig} = H_i^{ig} - TS_i^{ig}$, with the partial molar Gibbs energy of a species $\bar{G}_i^{ig} = \bar{H}_i^{ig} - T\bar{S}_i^{ig}$, by use of **eq.** (82) and (83).

$$\bar{G}_i^{ig} \equiv \mu_i^{ig} = G_i^{ig} + RT \ln y_i \tag{84}$$

If G_i^{ig} is expressed in **eq.** (65) for constant temperature:

$$dG_i^{ig} = V_i^{ig} dp = \frac{RT}{p} dp \tag{85}$$

And then integrated

$$G_i^{ig} = \Gamma_i(T) + RT \ln p \tag{86}$$

Where $\Gamma_i(T)$ is a species dependent temperature integration constant and therefore will be cancelled if we think in Gibbs energy differentials (absolute measure of Gibbs energy is not feasible). Now **eq.** (86) substituted into (84), will result in the chemical potential for ideal gas mixtures:

$$\bar{G}_i^{ig} \equiv \mu_i^{ig} = \Gamma_i(T) + RT \ln y_i p \tag{87}$$

For real fluids, the assumption of partial pressure is incorrect, thus the fugacity f_i for a pure species will be introduced. By definition, let the pressure approach zero, the fugacity will become $f_i^{ig} = p$, this means that the ideal gas related **eq.** (86) gets transformed to the actual Gibbs energy of a pure species.

$$G_i \equiv \Gamma_i(T) + RT \ln f_i \tag{88}$$

The fundamental residual property relation $G^R = G - G^{ig}$, which is further investigated in Appendix A.4, we can subtract **eq.** (88) with **eq.** (86) to formulate the residual Gibbs energy

$$G_i^R = RT \ln \frac{f_i}{p} = RT \ln \phi_i \tag{89}$$

The newly introduced variable, ϕ_i, is called the fugacity coefficient. Note that the equations here apply only to pure species in any condition.

The relation of the residual Gibbs energy with the fugacity coefficient provides the basis for solutions to VLE problems.

Appendix A.4 Residual Properties for use in VLE Calculations

Consider a homogeneous phase of a pure species with 1 mole in a closed system.

$$dG = Vdp - SdT \tag{90}$$

Where G is a function of pressure and temperature:

$$G = f(p,T) \tag{91}$$

The fundamental property relation follows from the mathematical identity:

$$d\left(\frac{G}{RT}\right) \equiv \frac{1}{RT}dG - \frac{G}{RT^2}dT \tag{92}$$

Substitution of **eq.** (90) and (62) into **eq.** (92) gives the generating function[3] **eq.** (93).

$$d\left(\frac{G}{RT}\right) = \frac{V}{RT}dp - \frac{H}{RT^2}dT \tag{93}$$

Which has a dimensionless form and can be applied in its restricted form:

$$\frac{V}{RT} = \left(\frac{\partial(G/RT)}{\partial p}\right)_T \qquad \frac{H}{RT} = -T\left(\frac{\partial(G/RT)}{\partial T}\right)_p \tag{94}$$

The concept of residual property is defined by the deviation of a (real) property by its respective ideal gas state value.

$$G^R \equiv G - G^{ig} \tag{95}$$

Where G^R stands for the value of residual Gibbs energy, G the actual (real) and G^{ig} the ideal gas state.

Analogously, the residual volume has the form with $V = \frac{ZRT}{p}$ and $V^{ig} = \frac{RT}{p}$:

$$V^R = V - V^{ig} = \frac{RTZ}{p} - \frac{RT}{p} = \frac{RT}{p}(Z-1) \tag{96}$$

Eq. (93) at constant temperature shrinks to:

$$d\left(\frac{G^R}{RT}\right)_T = \frac{V^R}{RT}dp \tag{97}$$

[3] Represents implicitly complete property information

Integration leads to:

$$\left(\frac{G^R}{RT}\right)_T = \left(\frac{G^R}{RT}\right)_{p=0} + \int_0^p \frac{V^R}{RT} dp \tag{98}$$

Whereas, if $p = 0$ the $\frac{G^R}{RT}$ term will become zero as it is then, by definition, an ideal gas state. Thus, substituting **eq.** (96) into **eq.** (98) leads to **eq.** (99).

$$\frac{G^R}{RT} = \int_0^p (Z-1)\frac{dp}{p} \tag{99}$$

This is now the residual Gibbs energy for a homogeneous closed system in a pressure explicit formulation. Because of the deviations of the residuals the equation needs to be dependent on volume and not on pressure. Thus, it follows from the real gas law:

$$p = Z\rho RT \tag{100}$$

And its derivative at constant temperature, using the product rule

$$dp = RT(Zd\rho + \rho dZ)|_T \tag{101}$$

Dividing **eq.** (101) by (100) we get

$$\frac{dp}{p} = \frac{d\rho}{\rho} + \frac{dZ}{Z} \tag{102}$$

This can now be substituted into (99), and for $p \to 0$ it equals $\rho \to 0$ and $Z \to 1$

$$\frac{G^R}{RT} = \int_0^\rho (Z-1)\frac{d\rho}{\rho} + Z - 1 - \ln Z \tag{103}$$

Since the pressure explicit thermodynamic formulation of the residual property was altered towards a volume explicit formulation, **eq.** (103) can be used for deriving a solution to VLE problems by use of a cubic EoS.

Because the PR-EoS is one of the most common used in the industry, it is used for deriving the residual property. Recalling the PR-EoS (**eq.** (49))

$$p = \frac{RT}{V-b} - \frac{a(T)}{V(V+b)+b(V-b)} \tag{49}$$

By dividing the PR-EoS with ρRT, including the definitions in **eq.** (104) we transform the PR-EoS towards a Z-expression. This volume-explicit formulation is needed because the deviations of the residuals are more emphasized for the volume-explicit as for the pressure-explicit formulation, as also mentioned above.

$$V = \frac{1}{\rho} \qquad Z = \frac{p}{RT\rho} \qquad q = \frac{a(T)}{RTb} \tag{104}$$

As a result, we obtain:

$$Z = \frac{1}{1-\rho b} - \frac{q\rho b}{(1+\rho b)(1-\rho b)} \tag{105}$$

But since **eq.** (103) demands for the form $Z-1$, rearrangement of **eq.** (105) leads to:

$$Z - 1 = \frac{\rho b}{1-\rho b} - \frac{q\rho b}{(1+\rho b)(1-\rho b)} \tag{106}$$

Eq. (106) can be used to derive the residual property from **eq.** (103). This is done by substitution of **eq.** (106) into the first term of **eq.** (103).

$$\int_0^\rho (Z-1)\frac{d\rho}{\rho} = \int_0^\rho \frac{\rho b}{1-\rho b}\frac{d(\rho b)}{\rho b} - q\int_0^\rho \frac{\rho b}{(1+\rho b)(1-\rho b)}\frac{d(\rho b)}{\rho b} \tag{107}$$

After integration it can be re-substituted into **eq.** (103) which results in the fundamental residual property relation based on the PR-EoS.

$$\frac{G^R}{RT} = Z - 1 - \ln(Z - Z\rho b) - \frac{q}{2}\ln\left(\frac{1+\rho b}{1-\rho b}\right) \tag{108}$$

For later convenience we define I

$$I = \frac{1}{2}\ln\left(\frac{1+\rho b}{1-\rho b}\right) \tag{109}$$

Since the EoS for multicomponent systems behave the same as for a pure substance we can use the residual property developed through the EoS unconditionally. However, it is mentioned that different EoS will have different I terms.

$$\frac{G^R}{RT} = Z - 1 - \ln(Z - Z\rho b) - qI \tag{110}$$

Appendix A.5 Phase Equilibria for Species in Solution or Mixtures

We can develop this further and define now the residual Gibbs energy for species i in solution of liquids or in a mixture of real gases. For this we use **eq.** (87) from the ideal gas mixture, but we have to introduce the fugacity of species i in solution, which accounts for the partial pressure $y_i p$, but makes the fugacity of a species $\hat{f}_i$ not a partial property.

$$\mu_i \equiv \Gamma_i(T) + RT \ln \hat{f}_i \tag{111}$$

Since multiple phases are in equilibrium if temperature and pressure are constant by $\mu_i^v - \mu_i^l = 0$ we can determine:

$$\mu_i^v - \mu_i^l = 0 = RT \ln \frac{\hat{f}_i^v}{\hat{f}_i^l} \tag{112}$$

In order to fulfil this equation, the fugacities need to form unity, this means $\hat{f}_i^v = \hat{f}_i^l$, which is the equilibrium criteria of species in solution for VLE problems.

Recalling now the use of residual property, we can define the partial residual Gibbs energy:

$$\bar{G}_i^R = \bar{G}_i - \bar{G}_i^{ig} = \mu_i - \mu_i^{ig} = RT \ln \hat{f}_i - RT \ln y_i p \tag{113}$$

Introducing here the fugacity coefficient of species i in solution, $\hat{\phi}_i^v = \frac{\hat{f}_i^v}{y_i p}$:

$$\bar{G}_i^{\,R} = RT \ln \hat{\phi}_i \tag{114}$$

This fugacity coefficient of a species in solution can also be applied to liquids if the liquid mole fraction is used, $\hat{\phi}_i^l = \frac{\hat{f}_i^l}{x_i p}$.

$$\ln \hat{\phi}_i = \frac{\bar{G}_i^{\,R}}{RT} = \left(\frac{\partial (nG^R/RT)}{\partial n_i} \right)_{p,T,n_j} \tag{115}$$

The extended relation between the fugacity coefficient of species i in solution with its partial molar residual Gibbs energy is the key for solving VLE problems.

Appendix A.6 Mixture VLE from EOS

Because the iso-fugacity criterion from **eq.** (112) is an VLE requirement,

$$\hat{f}_i^v = \hat{f}_i^l \tag{112}$$

Which can be expressed by use of the, above mentioned definitions for $\hat{\phi}_i^v$and $\hat{\phi}_i^l$:

$$\frac{y_i}{x_i} = \frac{\hat{\phi}_i^l}{\hat{\phi}_i^v} = K_i \tag{116}$$

Therefore,

$$\hat{\phi}_i^v = f(p, T, y_i) \qquad \hat{\phi}_i^l = f(p, T, x_i) \tag{117}$$

Where the fugacity coefficient is implicitly given within an EoS, we can make use of this by doing the same approach as we have done in **eq.** (70), but now for a phase of a mixture in an open system, which is a little bit more complex to derive.

Considering the residual Gibbs energy with $G^R = f(p, T, n_i)$ and divide the total derivative by RT:

$$d\left(\frac{nG^R}{RT}\right) = \left(\frac{\partial(nG^R/RT)}{\partial p}\right)_{T,n} dp - \left(\frac{\partial(nG^R/RT)}{\partial T}\right)_{p,n} dT + \sum_i \left(\frac{\partial(nG^R/RT)}{\partial n_i}\right)_{p.T.n_j} dn_i \tag{118}$$

Now considering the system for constant temperature and substituting the residual Volume from **eq.** (96) with **eq.** (97), and the partial molar fugacity coefficient (**eq.** (115)):

$$d\left(\frac{nG^R}{RT}\right) = n(Z-1)\frac{dp}{p} + \sum_i \ln \hat{\phi}_i \, dn_i \tag{119}$$

Division by dn_i:

$$\left(\frac{\partial(nG^R/RT)}{\partial n_i}\right)_{T,nV,n_j} = \frac{n(Z-1)}{p}\left(\frac{\partial p}{\partial n_i}\right)_{T,nV,n_j} + \ln \hat{\phi}_i \tag{120}$$

Again, we have a pressure explicit equation but express it as volume-explicit equation with $p = nZRT\rho/n$ leads to:

$$\frac{\partial p}{\partial n_i} = \frac{RT\rho}{n}\frac{\partial(nZ)}{\partial n_i} = \frac{p}{nZ}\frac{\partial(nZ)}{\partial n_i} \tag{121}$$

Substitute and rearrange:

$$\ln \hat{\phi}_i = \left(\frac{\partial(nG^R/RT)}{\partial n_i}\right)_{T,n/\rho,n_j} - \frac{(Z-1)}{Z}\left(\frac{\partial(nZ)}{\partial n_i}\right)_{T,n/\rho,n_j} \tag{122}$$

Rearrangement for further derivation steps

$$\ln \hat{\phi}_i = \left(\frac{\partial(nG^R/RT)}{\partial n_i}\right)_{T,n/\rho,n_j} - \frac{\partial(nZ)}{\partial n_i} + \frac{1}{Z}\left(Z + n\frac{\partial Z}{\partial n_i}\right)_{T,\frac{n}{\rho},n_j} \tag{123}$$

Substitute now for the residual Gibbs energy term, the derived residual property relation from the PR-EoS, **eq.** (110) and multiply it with n number of moles:

$$\frac{nG^R}{RT} = nZ - n - n\ln(Z - Z\rho b) - nqI \tag{124}$$

Eq. (124) can be differentiated by n_i

$$\left(\frac{\partial(nG^R/RT)}{\partial n_i}\right)_{T,\frac{n}{\rho},n_j} \tag{125}$$
$$= \frac{\partial(nZ)}{\partial n_i} - 1 - \ln(Z - Z\rho b)$$
$$- n\left(\frac{\partial \ln(1-\rho b)}{\partial n_i} + \frac{\partial \ln Z}{\partial n_i}\right)_{T,\frac{n}{\rho},n_j} - nq\frac{\partial I}{\partial n_i} - I\bar{q}_i$$

Since $\bar{q}_i$ is related to a and b but not linearly, we define:

$$\bar{q}_i \equiv q\left(1 + \frac{\bar{a}_i}{a} - \frac{b_i}{b}\right) \tag{126}$$

Substitute **eq.** (125) into **eq.** (123), leads after reduction to

$$\ln \hat{\phi}_i = \frac{n}{1-\rho b}\frac{\partial(\rho b)}{\partial n_i} - nq\frac{\partial I}{\partial n_i} - \ln(Z - Z\rho b) - \bar{q}_i\, I \tag{127}$$

Where the two derivatives are

$$\frac{\partial(\rho b)}{\partial n_i} = \frac{\rho}{n}b_i \qquad \& \qquad \frac{\partial I}{\partial n_i} = \frac{\rho b_i}{n(1+\rho b)(1-\rho b)} \tag{128}$$

And **eq.** (127) becomes:

$$\ln \hat{\phi}_i = \frac{\rho b_i}{1-\rho b} - \frac{q\rho b_i}{(1+\rho b)(1-\rho b)} - \ln(Z - Z\rho b) - \bar{q}_i\, I \tag{129}$$

Recalling **eq.** (106) we can see the similarities for the first two terms.

$$Z - 1 = \frac{\rho b}{1 - \rho b} - \frac{q\rho b}{(1 + \rho b)(1 - \rho b)} \tag{106}$$

Thus, **eq.** (106) substituted into **eq.** (129), results in:

$$\ln \hat{\phi}_i = \frac{b_i}{b}(Z - 1) - \ln(Z - Z\rho b) - \bar{q}_i \, I \tag{130}$$

Because **eq.** (130) is used for VLE calculations by combining it with **eq.** (116), it needs to be calculated for both phases. A dimensionless parameter gets hereby introduced.

$$\beta \equiv \frac{bp}{RT} \tag{131}$$

The resulting basis for VLE calculations expressed for vapour is:

$$\ln \hat{\phi}_i^v = \frac{b_i}{b}(Z^v - 1) - \ln(Z^v - \beta^v) - \bar{q}_i^v \, I^v \tag{132}$$

And for the liquid phase analogously

$$\ln \hat{\phi}_i^l = \frac{b_i}{b}(Z^l - 1) - \ln\left(Z^l - \beta^l\right) - \bar{q}_i^l \, I^l \tag{133}$$

Also, **eq.** (105) needs to be expressed for both phases. However, it should be mentioned, as already discussed in Figure 62, that in a PV-plot the EoS will produce isotherms, see Figure 64. These isotherms evolve because of the cubic character of the EoS. Whereas the middle root is unphysical the outer two roots are respectively saturated liquid (bp for bubble point) and saturated vapour (dp for dewpoint). Because one curve is representing a mixture with same composition, bp and dp are not located on the same line because they have not the same composition. This means that the mixture is in a two-phase equilibrium but with different composition for each phase.

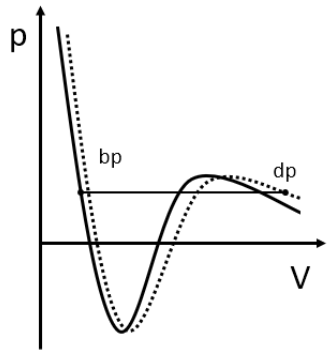

Figure 64 - isotherms for mixtures of two different compositions

The two (outer) real roots formulations are arranged in order to calculate iteratively these above-mentioned liquids (**eq.** (135)) and vapour (**eq.** (134)) roots in a faster converging manner.

$$Z^v = 1 + \beta^v - q^v\beta^v \frac{Z_i^v - \beta^v}{\left(Z^{2v} + 2Z^v\beta^v - \beta^v\right)} \tag{134}$$

$$Z^l = \beta^l + \left(Z^{2l} + 2Z^l\beta^l - \beta^l\right)\frac{\left(1 + \beta^l - Z^l\right)}{q^l\beta^l} \tag{135}$$

Appendix B MATLAB® Fuzzy Clustering

```
% Short code for generating Lumping Schemes from a Fuzzy Clustering
% Algorithm by using the MATLAB inbuilt fcm facility
%% ------------------------------------------------
% Define the number of clusters
clusterNr=18;
% data=xlsread('data_GasCond.xlsx','B2:H16');
% data=xlsread('data_vOil.xlsx','B2:H49');
% A is clustering to ai & bi and B is clustering pci,Tci,acc.Fi
mode=A
%% Fuzzy Clustering Mode A
if mode==A
fcmdata=[data(:,6),data(:,7)];[centers,U]=fcm(fcmdata,clusterNr);
maxU=max(U);   index=zeros(clusterNr,1);
for i=1:clusterNr
indexNr= find(U(i,:) == maxU);     iter=length(indexNr);
for j=1:iter
index(i,j)=indexNr(j);
end    end
plot(fcmdata(:,1),fcmdata(:,2),'-s','Color','b','MarkerSize',8)
grid on; hold on; title('FCM Clustering'); xlabel('a'); ylabel('b');
plot(centers(:,1),centers(:,2),'ok','MarkerSize',20)
%% Fuzzy Clustering Mode B
elseif mode==B
fcmdata=[data(:,1:3)]; [centers,U]=fcm(fcmdata,clusterNr);
 maxU=max(U);       index=zeros(clusterNr,1);
for i=1:clusterNr
indexNr= find(U(i,:) == maxU);      iter=length(indexNr);
for j=1:iter
index(i,j)=indexNr(j);
end    end
plot3(fcmdata(:,1),fcmdata(:,2),fcmdata(:,3))
grid on;    hold on; title('FCM Clustering'); xlabel('critPress');
ylabel('critTemp');   zlabel('acentric');
plot3(centers(:,1),centers(:,2),centers(:,3),'ok','MarkerSize',20)
end
```

Appendix C Gas Condensate

Appendix C.1 Lumping Schemes

Allocation determines which detailed component gets lumped to which PCS.

Table 11 - Lumping scheme Lump_ME (left panel) and Lump_2 (right panel)

Lump_ME		
Component	Allocation	PCS
N2	1	N2C1
CO2	2	CO2C
C1	1	N2C1
C2	2	CO2C
C3	3	C3
iC4	4	C4
nC4	4	C4
iC5	5	C5
nC5	5	C5
PC6	6	C6+
PC7	6	C6+
PC8	6	C6+
PC9	6	C6+
C10+	7	C10+
C18+	8	C18+

Lump_2		
Component	Allocation	PCS
N2	1	N2
CO2	2	CO2
C1	3	C1
C2	4	C2
C3	5	C3
iC4	6	C4
nC4	6	C4
iC5	7	C5
nC5	7	C5
PC6	8	C6+
PC7	8	C6+
PC8	8	C6+
PC9	8	C6+
C10+	8	C6+
C18+	8	C6+

Table 12 - Lumping schemes with Mode A

Lump_ML_10A		
Component	Allocation	PCS
N2	1	PC1
CO2	1	PC1
C1	1	PC1
C2	1	PC1
C3	2	C3
iC4	3	C4
nC4	3	C4
iC5	4	C5
nC5	4	C5
PC6	5	PC6
PC7	6	PC7
PC8	7	PC8
PC9	8	PC9
C10+	9	C10+
C18+	10	C18+

Lump_ML_5A		
Component	Allocation	PCS
N2	1	PC1
CO2	1	PC1
C1	1	PC1
C2	1	PC1
C3	1	PC1
iC4	2	C4+
nC4	2	C4+
iC5	2	C4+
nC5	2	C4+
PC6	2	C4+
PC7	3	C7+
PC8	3	C7+
PC9	3	C7+
C10+	4	C10+
C18+	5	C18+

Table 13 - Lumping schemes with Mode B

Lump_ML_10B		
Component	Allocation	PCS
N2	1	N2
CO2	2	CO2C
C1	3	C1
C2	2	CO2C
C3	4	C3
iC4	5	iC4
nC4	6	nC4
iC5	7	C5
nC5	7	C5
PC6	8	C6+
PC7	8	C6+
PC8	9	C8+
PC9	9	C8+
C10+	10	C10+
C18+	10	C10+

Lump_ML_5B		
Component	Allocation	PCS
N2	1	N2C1
CO2	2	CO2C
C1	1	N2C1
C2	2	CO2C
C3	2	CO2C
iC4	3	C4+
nC4	3	C4+
iC5	3	C4+
nC5	3	C4+
PC6	4	C6+
PC7	4	C6+
PC8	4	C6+
PC9	4	C6+
C10+	5	C10+
C18+	5	C10+

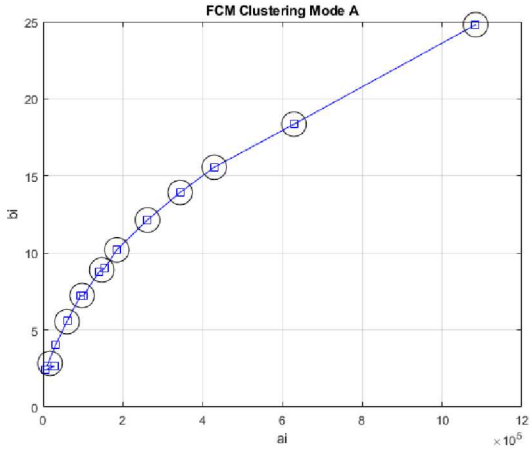

Figure 65 - Clustering Result for lumping scheme, mode A, example picture

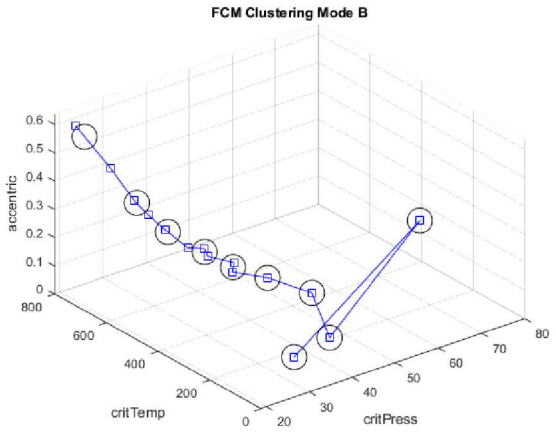

Figure 66 - Clustering Result for lumping scheme, mode B, example picture

Appendix C.2 Lumped Fluid Flash Analysis

In order to achieve a reasonable quality check, three flash stages at different pressures and temperatures where defined in order to cover a typical range of the conditions which will mimic a production path. The three flash stages are following:

1. Initial reservoir conditions: $p = 583\ bar$ and $T = 106\ °C$
2. Intermediate (~ sandface) conditions: $p = 292\ bar$ and $T = 106\ °C$
3. Standard (~ surface) conditions: $p = 1.0132\ bar$ and $T = 20\ °C$

Table 14 - Flash stages result for gas condensate fluid and its lumped descriptions.

	Stage	F_V	MW^v [g/mol]	MW^l [g/mol]	Z^v	Z^l	ρ^v [kg/m³]	ρ^l [kg/m³]
DET	1.	1.00	31.41		1.39		417.32	
	2.	0.85	26.52	58.62	0.93	1.00	264.99	543.57
	3.	0.93	22.77	141.73	1.00	0.01	0.95	779.02
ME	1.	1.00	31.41		1.39		417.01	
	2.	0.85	26.66	58.66	0.93	1.00	266.47	543.27
	3.	0.93	22.89	140.34	1.00	0.01	0.96	776.96
10A	1.	1.00	31.41		1.40		416.10	
	2.	0.87	26.70	62.09	0.93	1.03	265.97	560.04
	3.	0.93	22.77	142.03	1.00	0.01	0.95	779.34
5A	1.	1.00	31.41		1.40		414.55	
	2.	0.88	26.98	64.99	0.93	1.05	267.60	572.95
	3.	0.93	22.88	142.53	1.00	0.01	0.96	779.58
10B	1.	1.00	31.41		1.39		417.18	
	2.	0.84	26.63	57.46	0.93	0.99	266.07	536.54
	3.	0.93	22.79	141.61	1.00	0.01	0.95	778.27
5B	1.	1.00	31.41		1.39		416.69	
	2.	0.85	26.85	57.69	0.93	0.99	268.25	537.33
	3.	0.93	22.92	140.78	1.00	0.01	0.96	777.18

For interpreting these results the relative deviations were calculated with **eq.** (136):

$$RD\% = \left(1 - \frac{\theta^{Lump}}{\theta^{Detailed}}\right) * 100\ \% \tag{136}$$

For an easier interpretability and quantification of the deviations the geometric weighted mean was calculated for all variables (all three stages were averaged, see Table 16) and all errors

(all variables were averaged, see Table 15) in order to obtain a single measure which is describing the inaccuracy of a lumped fluid to the reference fluid.

$$\emptyset_{geo}(\epsilon) = \frac{\sum \theta_i \epsilon_i}{\sum \theta_i} \quad (137)$$

Table 15 - Relative error (RD%) and its average of the lumped to detailed description of the gas condensate

	Stage	$RD\%(\,)$ [%]							$\emptyset_{geo}(RD\%())$ [%]
		F_V	MW^v	MW^l	Z^v	Z^l	ρ^v	ρ^l	
ME	1.		-0.1		0.1		0.0	0.0	0.10
	2.	-0.1	0.0	-0.1	-0.6	0.1	-0.5	-0.5	
	3.	1.0	0.0	1.3	-0.6	0.3	0.0	-0.5	
10A	1.		-0.3		0.3		0.0	0.0	-0.92
	2.	-5.9	-0.3	-2.8	-0.4	-3.0	-2.3	-0.7	
	3.	-0.2	0.0	0.0	0.0	0.0	0.0	0.0	
5A	1.		-0.7		0.7		0.0	0.0	-1.71
	2.	-10.9	-0.7	-5.2	-1.0	-5.4	-4.2	-1.7	
	3.	-0.6	0.0	0.0	-0.5	-0.1	-0.1	-0.5	
10B	1.		0.0		0.0		0.0	0.0	0.34
	2.	2.0	0.0	0.7	-0.4	1.3	0.3	-0.4	
	3.	0.1	0.0	0.0	-0.1	0.1	0.0	-0.1	
5B	1.		-0.2		0.2		0.0	0.0	0.29
	2.	1.6	0.0	0.5	-1.2	1.1	-0.5	-1.2	
	3.	0.7	0.0	1.3	-0.7	0.2	-0.1	-0.7	

Table 16 - Deviations of the three flash stages summarized as geometric average

	$\emptyset_{geo}(RD\%(Stage))$ [%]						
	F_V	MW^v	MW^l	Z^v	Z^l	ρ^v	ρ^l
ME	-0.15	-0.33	0.67	-0.02	-0.10	-0.17	0.18
10A	-0.71	-0.23	-1.95	-0.21	-2.78	0.03	-1.29
5A	-1.37	-0.72	-3.79	-0.49	-5.14	0.02	-2.33
10B	0.09	-0.17	0.63	-0.01	0.70	-0.14	0.59
5B	-0.18	-0.60	0.94	-0.07	0.46	-0.39	0.61

Appendix C.3 Reservoir Simulation Results

Table 17 - Component concentration for the last timestep in the gas condensate simulation

[%]	Detailed	ME	ML_10A	ML_5A	ML_10B	ML_5B
N2	2.15	2.16	2.16	2.14	2.16	2.17
CO2	0.87	0.87	0.87	0.88	0.86	0.86
C1	72.99	72.92	72.82	72.61	72.98	72.84
C2	11.63	11.64	11.76	11.82	11.64	11.70
C3	4.65	4.66	4.67	4.72	4.65	4.63
IC4	0.79	0.79	0.80	0.81	0.79	0.80
NC4	1.36	1.36	1.37	1.40	1.36	1.37
IC5	0.55	0.55	0.56	0.56	0.55	0.55
NC5	0.53	0.53	0.53	0.54	0.53	0.53
PC6	0.75	0.78	0.76	0.76	0.76	0.77
PC7	0.68	0.70	0.69	0.73	0.68	0.70
PC8	0.56	0.56	0.57	0.58	0.56	0.57
PC9	0.26	0.26	0.27	0.26	0.26	0.26
C10+	2.13	2.15	2.10	2.11	2.14	2.16
C18+	0.09	0.09	0.08	0.08	0.09	0.10

Table 18 - Component relative error of delumped cases for gas condensate

At Last Time Step	$RD\%\ (\ )$ [%]				
	ME	ML_10A	ML_5A	ML_10B	ML_5B
N2	-0.45	-0.25	0.51	-0.03	-0.84
CO2	0.08	-0.52	-1.33	0.30	0.36
C1	0.10	0.22	0.51	0.01	0.20
C2	-0.06	-1.06	-1.58	-0.03	-0.54
C3	-0.07	-0.34	-1.47	0.08	0.55
IC4	0.03	-0.59	-2.14	0.08	-1.16
NC4	-0.29	-0.71	-2.85	0.07	-0.71
IC5	-0.33	-1.05	-2.02	0.00	-0.04
NC5	-0.21	-0.87	-2.11	0.13	0.32
PC6	-4.29	-1.08	-2.03	-0.92	-2.75
PC7	-1.73	-1.24	-6.14	0.64	-2.00
PC8	0.96	-1.30	-2.94	-0.62	-0.84
PC9	3.59	-1.25	0.60	0.98	0.42
C10+	-0.73	1.45	0.85	-0.30	-1.40
C18+	-0.34	6.49	10.25	-5.92	-9.45

Table 19 - Initialization RD% for lumped gas condensate reservoir simulation cases

	$RD\%\ (FPR_{HC})$ [%]	$RD\%\ (V_g^{res})$ [%]	$RD\%\ (V_g^{surf})$ [%]	$RD\%\ (V_o^{surf})$ [%]	$RD\%\ (n_T)$ [%]	$\emptyset_{geo}^{case}(RD\%)$ [%]
ME	0.00	0.00	0.20	-0.92	-0.18	0.16
ML_10A	0.00	0.00	0.34	-0.06	0.04	0.29
ML_5A	0.00	0.00	0.50	1.81	0.41	0.45
ML_10B	0.00	0.00	0.06	-0.22	-0.22	0.05
ML_5B	0.00	0.00	0.09	0.35	-0.10	0.07

Appendix D Volatile Oil

Appendix D.1 Lumping Schemes

Lumping scheme overview was changed due to space restrictions for a single page.

Table 20 - Lumping scheme Lump_ME

PCS	Count	Components
N2	1	N2
CO2	1	CO2
C1	1	C1
C2	1	C2
C3	1	C3
iC4	1	iC4
nC4	1	nC4
iC5	1	iC5
nC5	1	nC5
PS1	8	Ben, C6, mcC5, cC6, mC6, Tol, C7, C8
PS2	5	C2Ben, mpXyl, oXyl, C9, C10
PS3	5	C11 – C15
PS4	6	C16-C21
PS5	6	C22- C27
PS6	6	C28-C35
C36+	1	C36+

Table 21 - Lumping scheme Lump_ML_10A

PCS	Count	Components
N2C1	2	N2, C1
CO2C	2	CO2, C2
C3	1	C3
C4	2	iC4, nC4
C5	2	iC5, nC5
PS1	17	Ben, C6, mcC5, cC6, mC6, Tol, C7, C2Ben, mpXyl, oXyl, C8 – C14
PS2	8	C15 – C22
PS3	8	C23 – C30
PS4	3	C31 – C35
C36+	1	C36+

Table 22 - Lumping scheme Lump_ML_18A

PCS	Count	Components
N2C1	2	N2, C1
CO2C	2	CO2, C2
C3+	3	C3, iC4, nC4
PS1	8	iC5, nC5, Ben, C6, mcC5, cC6, mC6, Tol
PS2	6	C7, C2Ben, mpXyl, oXyl, C8, C9
PS3	3	C10, C11, C12
PS4	2	C13, C14
PS5	2	C15, C16
PS6	2	C17, C18
C19	1	C19
PC7	2	C20, C21
PS8	2	C22, C23
PS9	2	C24, C25
PS10	2	C26, C27
PS11	2	C28, C29
PS12	2	C30, C31
PS13	4	C32, C33, C34, C35
C36+	1	C36+

Table 23 - Lumping scheme Lump_ML_10B

PCS	Count	Components
N2C1	2	N2, C1
CO2C	2	CO2, C2
C3	1	C3
C4	2	iC4, nC4
C5	2	iC5, nC5
PS1	8	Ben, C6, mcC5, cC6, mC6, Tol, C7, C8
PS2	8	C2Ben, mpXyl, oXyl, C9, C10, C11, C12, C13
PS3	10	C14 – C23
PS4	12	C24 – C35
C36+	1	C36+

Table 24 - Lumping scheme Lump_ML_18B

PCS	Count	Components
N2C1	2	N2, C1
CO2C	2	CO2, C2
C3+	3	C3, iC4, nC4
C5	2	iC5, nC5
C6+	2	C6, mcC5
PS1	5	Ben, cC6, mC6, C7, C8
PS2	2	Tol, C9
PS3	4	C2Ben, mpXyl, oXyl, C10
PS4	2	C11, C12
C13	1	C13
PS5	3	C14, C15, C16
PS6	2	C17, C18
PS7	3	C19, C20, C21
PS8	3	C22, C23, C24
PS9	3	C25, C26, C27
PS10	4	C28, C29, C30, C31
PS11	4	C32, C33, C34, C35
C36+	1	C36+

Appendix D.2 Lumped Fluid Flash Analysis

Again, three flash stages were selected in order to check the quality of the lumping.

1. Initial reservoir conditions: $p = 533\ bar$ and $T = 107.9\ °C$
2. Intermediate conditions: $p = 150\ bar$ and $T = 107.9\ °C$
3. Standard conditions: $p = 1.0132\ bar$ and $T = 20\ °C$

Table 25 - Flash stages result for volatile oil and its lumped descriptions

	Stage	F_V	MW^v [g/mol]	MW^l [g/mol]	Z^v	Z^l	ρ^v [kg/m³]	ρ^l [kg/m³]
DET	1.	0.00		51.00		1.55		552.21
	2.	0.46	25.18	73.31	0.81	0.61	147.82	570.40
	3.	0.81	26.87	157.06	0.99	0.01	1.12	793.73
ME	1.	0.00		51.00		1.55		552.21
	2.	0.46	25.18	73.31	0.81	0.61	147.82	570.40
	3.	0.81	26.87	157.06	0.99	0.01	1.12	793.73
18A	1.	0.00		51.00		1.56		551.22
	2.	0.46	25.18	72.87	0.81	0.61	147.78	566.79
	3.	0.81	26.82	155.98	0.99	0.01	1.12	789.42
10A	1.	0.00		51.00		1.56		551.71
	2.	0.46	25.30	72.88	0.80	0.61	148.97	567.63
	3.	0.82	27.01	156.88	0.99	0.01	1.13	792.41
18B	1.	0.00		51.00		1.57		545.51
	2.	0.43	25.27	70.37	0.81	0.61	148.22	545.82
	3.	0.80	26.04	151.49	0.99	0.01	1.09	768.48
10B	1.	1.00		51.00		1.56		551.25
	2.	0.46	25.34	73.19	0.80	0.61	149.25	568.54
	3.	0.82	26.94	157.35	0.99	0.01	1.13	791.68

Using the same procedure as for the gas condensate, we calculate the relative deviation and geometric average by use of **eq.** (136) and (137).

Table 26 - Relative error (RD%) and its average of the lumped to detailed description of the volatile oil

	Stage	$RD\%(\,)$ [%]							$\emptyset_{geo}(RD\%)$ [%]
		F_V	MW^v	MW^l	Z^v	Z^l	ρ^v	ρ^l	
ME	1.			0.0		-0.2		0.2	0.44
	2.	1.0	0.0	0.6	0.0	0.0	0.0	0.6	
	3.	0.2	0.2	0.7	0.0	0.0	0.2	0.5	
10A	1.			0.0		-0.1		0.1	0.16
	2.	0.8	-0.5	0.6	0.3	0.1	-0.8	0.5	
	3.	-0.1	-0.5	0.1	0.0	0.0	-0.5	0.2	
5A	1.			0.0		-1.2		1.2	2.70
	2.	7.3	-0.4	4.0	-0.1	-0.3	-0.3	4.3	
	3.	1.7	3.1	3.5	0.0	0.0	3.1	3.2	
10B	1.			0.0		-0.2		0.2	0.12
	2.	-0.1	-0.6	0.2	0.3	-0.2	-1.0	0.3	
	3.	-0.1	-0.2	-0.2	0.0	-1.2	-0.2	0.3	
5B	1.			0.0		-0.3		0.3	0.69
	2.	1.7	0.0	1.0	0.0	-0.1	0.0	1.1	
	3.	0.3	0.3	0.7	0.0	0.0	0.3	0.8	

Table 27 - Deviations of the three flash stages summarized as geometric average

	$\emptyset_{geo}(RD\%)$ [%]						
	F_V	MW^v	MW^l	Z^v	Z^l	ρ^v	ρ^l
ME	0.53	0.09	0.54	-0.03	-0.14	0.03	0.46
18A	0.23	-0.51	0.21	0.12	-0.04	-0.78	0.24
10A	3.65	1.38	3.00	-0.07	-0.97	-0.25	2.94
18B	-0.05	-0.44	-0.06	0.14	-0.18	-0.96	0.25
10B	0.80	0.17	0.66	-0.01	-0.27	0.01	0.77

Appendix D.3 Reservoir Simulation Results

Table 28 - Mole percent of last time step of volatile oil

	Detailed	ME [%]	ML_18A	ML_10A	ML_18B	ML_10B
N2	0.59	0.58	0.57	0.56	0.57	0.57
CO2	0.86	0.86	0.83	0.82	0.83	0.83
C1	65.67	65.53	65.49	64.29	65.54	65.42
C2	15.57	15.55	15.62	15.48	15.63	15.59
C3	7.28	7.28	7.27	7.33	7.28	7.29
IC4	0.99	0.99	1.00	1.00	1.00	0.98
NC4	2.26	2.26	2.31	2.34	2.30	2.28
IC5	0.74	0.74	0.72	0.78	0.74	0.74
NC5	0.79	0.80	0.78	0.84	0.80	0.80
BEN	0.02	0.03	0.03	0.03	0.03	0.03
C6	0.86	0.85	0.86	0.92	0.86	0.85
MCC5	0.12	0.12	0.12	0.13	0.12	0.12
CC6	0.12	0.12	0.12	0.13	0.12	0.13
MC6	0.26	0.27	0.27	0.30	0.27	0.27
TOL	0.08	0.09	0.09	0.10	0.09	0.09
C7	0.63	0.63	0.63	0.71	0.63	0.64
C2BE	0.03	0.03	0.03	0.04	0.03	0.04
MPXY	0.13	0.14	0.14	0.16	0.14	0.15
OXYL	0.03	0.03	0.03	0.04	0.03	0.04
C8	0.62	0.62	0.63	0.73	0.62	0.64
C9	0.42	0.43	0.42	0.51	0.42	0.44
C10	0.46	0.47	0.48	0.59	0.46	0.48
C11	0.30	0.32	0.31	0.40	0.31	0.32
C12	0.22	0.23	0.23	0.30	0.22	0.23
C13	0.19	0.19	0.20	0.26	0.19	0.19
C14	0.13	0.14	0.14	0.19	0.13	0.14
C15	0.11	0.12	0.12	0.17	0.11	0.12
C16	0.08	0.09	0.09	0.13	0.08	0.09
C17	0.07	0.07	0.07	0.11	0.07	0.07
C18	0.06	0.06	0.06	0.09	0.06	0.06
C19	0.05	0.05	0.05	0.08	0.05	0.05
C20	0.04	0.04	0.04	0.06	0.04	0.04
C21	0.03	0.03	0.03	0.05	0.03	0.04
C22	0.03	0.03	0.03	0.04	0.03	0.03
C23	0.02	0.02	0.02	0.04	0.02	0.03
C24	0.02	0.02	0.02	0.03	0.02	0.02
C25	0.02	0.02	0.02	0.03	0.02	0.02
C26	0.02	0.02	0.02	0.02	0.02	0.02
C27	0.01	0.01	0.01	0.02	0.01	0.02
C28	0.01	0.01	0.01	0.02	0.01	0.01
C29	0.01	0.01	0.01	0.02	0.01	0.01
C30	0.01	0.01	0.01	0.01	0.01	0.01
C31	0.01	0.01	0.01	0.01	0.01	0.01
C32	0.01	0.01	0.01	0.01	0.01	0.01
C33+	0.02	0.02	0.02	0.03	0.02	0.02
C36+	0.03	0.03	0.03	0.04	0.03	0.03

Table 29 - RD% of molar fractions for last timestep

[%]	ME	ML_18A	ML_10A	ML_18B	ML_10B
N2	0.15	2.22	3.62	1.93	2.80
CO2	0.15	4.30	5.49	4.26	3.92
C1	0.20	0.26	2.10	0.20	0.38
C2	0.13	-0.32	0.55	-0.40	-0.12
C3	0.00	0.22	-0.57	0.12	-0.01
IC4	-0.16	-1.01	-1.69	-0.89	0.85
NC4	-0.29	-2.37	-3.56	-2.02	-1.05
IC5	-0.54	2.19	-5.54	-0.46	-0.73
NC5	-0.65	1.73	-6.68	-0.78	-1.45
BEN	-8.20	-8.20	-16.39	-6.56	-11.07
C6	1.58	0.50	-7.41	-0.35	1.45
MCC5	-3.96	-4.57	-12.66	-4.91	-5.60
CC6	-5.99	-6.42	-15.40	-4.96	-8.38
MC6	-4.36	-5.02	-17.64	-3.27	-6.81
TOL	-9.56	-9.81	-23.12	-8.35	-13.68
C7	-0.16	-0.78	-13.37	0.06	-1.38
C2BE	-9.74	-7.79	-27.27	-6.82	-14.61
MPXY	-9.90	-7.84	-28.05	-6.97	-14.90
OXYL	-11.22	-9.29	-30.13	-8.01	-16.99
C8	-1.32	-1.82	-18.01	-0.57	-3.32
C9	-2.45	-1.27	-22.65	-0.38	-5.36
C10	-1.71	-4.22	-26.78	0.24	-4.94
C11	-4.23	-3.25	-30.68	-1.44	-4.36
C12	-3.78	-2.56	-34.47	-0.49	-4.18
C13	-3.54	-4.55	-37.98	-1.12	-4.18
C14	-3.91	-4.66	-41.88	-0.98	-8.72
C15	-4.15	-5.39	-51.33	-0.71	-9.10
C16	-5.88	-5.14	-53.73	-0.37	-9.18
C17	-6.19	-5.60	-55.82	-0.88	-9.57
C18	-6.31	-5.46	-57.17	-0.68	-9.73
C19	-6.58	-5.76	-58.44	-0.62	-10.08
C20	-6.81	-5.76	-59.69	-0.79	-10.47
C21	-7.06	-5.83	-60.74	-0.92	-10.74
C22	-7.22	-5.78	-61.37	-0.36	-10.83
C23	-7.33	-6.03	-62.93	-0.43	-11.21
C24	-7.04	-5.53	-62.81	-0.50	-12.06
C25	-7.47	-6.32	-63.79	-0.57	-12.64
C26	-8.00	-6.00	-64.00	-0.67	-13.33
C27	-7.46	-5.97	-64.18	-0.75	-12.69
C28	-7.63	-5.93	-64.41	-0.85	-12.71
C29	-7.84	-5.88	-63.73	0.00	-12.75
C30	-7.78	-6.06	-64.76	-0.57	-13.04
C31	-7.59	-5.82	-64.56	-0.38	-12.66
C32	-7.54	-5.97	-65.01	-0.57	-12.66
C33+	-7.27	-6.06	-64.24	-0.61	-12.73
C36+	-7.91	-5.93	-65.22	-0.79	-13.04

Table 30 - Initialization RD% for lumped volatile oil reservoir simulation cases

	$RD\%\ (FPR_{HC})$ [%]	$RD\%\ (V_o^{res})$ [%]	$RD\%\ (V_o^{surf})$ [%]	$RD\%\ (V_g^{surf})$ [%]	$RD\%\ (n_T)$ [%]	$\emptyset_{geo}^{case}(RD\%)$ [%]
ME	0.00	0.00	-0.35	0.29	0.19	0.28
ML_18A	0.00	0.00	0.76	-0.24	0.10	-0.22
ML_10A	-0.01	0.00	-1.83	1.64	1.27	1.61
ML_18B	0.00	0.00	1.33	-0.52	0.18	-0.48
ML_10B	0.00	0.00	-0.48	0.45	0.34	0.44

Appendix E Comparative Analysis HYSYS – PVTi

To ensure the consistency between the different software fluid models the same three-stage flash analysis was conducted. Compared were the detailed fluid description from PVTi with the equivalent fluid description of HYSYS. Since the two fluids need two different fluid models, it is also necessary to set up two HYSYS fluid packages and hence, two HYSYS simulation models. In Table 31 the different flash stages are elucidated, the comparative analysis in for both fluids in Table 32 and Table 33 and the results respectively in Table 34 and Table 35. Since the starting fluid description was completed with PVTi the RD% errors are referred to the detailed description from PVTi.

Table 31 - Multi Flash Stages for HYSYS PVTi comparison

	Gas Condensate	Volatile Oil
1.) Reservoir Conditions:	$p = 583\ bar$ and $T = 106\ °C$	$p = 533\ bar$ and $T = 107.9\ °C$
2.) Intermediate:	$p = 292\ bar$ and $T = 106\ °C$	$p = 150\ bar$ and $T = 107.9\ °C$
3.) Standard Conditions:	$p = 1.0132\ bar$ and $T = 20\ °C$	$p = 1.0132\ bar$ and $T = 20\ °C$

Table 32 - Comparative analysis of PVTi and HYSYS for gas condensate

Stage	Software	F_V	MW^v [g/mol]	MW^l [g/mol]	Z^v	Z^l	ρ^v [kg/m³]	ρ^l [kg/m³]
1.	PVTi	1.000	31.410		1.392		417.320	
	HYSYS	1.000	31.410		1.389		418.308	
2.	PVTi	0.848	26.521	58.624	0.927	0.999	264.987	543.568
	HYSYS	0.847	26.537	58.374	0.925	0.996	265.741	542.776
3.	PVTi	0.927	22.766	141.728	0.996	0.008	0.950	779.021
	HYSYS	0.927	22.765	141.720	0.996	0.008	0.950	778.948

Table 33 - Comparative analysis of PVTi and HYSYS for volatile oil

Stage	Software	F_V	MW^v [g/mol]	MW^l [g/mol]	Z^v	Z^l	ρ^v [kg/m³]	ρ^l [kg/m³]
1.	PVTi	0.000		51.004		1.554		552.210
	HYSYS	1.000		51.053		1.552		553.412
2.	PVTi	0.463	25.177	73.309	0.806	0.609	147.818	570.400
	HYSYS	0.462	25.177	73.246	0.806	0.608	147.920	570.700
3.	PVTi	0.815	26.872	157.058	0.994	0.008	1.124	793.727
	HYSYS	0.815	26.878	157.227	0.994	0.008	1.124	794.570

Table 34 – RD% of gas condensate, Table 32

Stage	Software	$RD\%(\,)$ [%]							$\emptyset_{geo}^{stage}(RD\%)$ [%]	$\emptyset_{geo}^{all}(RD\%)$ [%]
		F_V	MW^v	MW^l	Z^v	Z^l	ρ^v	ρ^l		
1.	PVTi	0.00	0.00	-0.11	0.24		-0.24		0.22	-0.03
	HYSYS									
2.	PVTi	0.09	-0.06	0.43	0.23	0.28	-0.28	0.15	0.03	
	HYSYS									
3.	PVTi	0.00	0.00	0.01	0.00	0.49	0.00	0.01	0.01	
	HYSYS									

Table 35 – RD% of volatile oil, Table 33

Stage	Software	$RD\%(\,)$ [%]							$\emptyset_{geo}^{stage}(RD\%)$ [%]	$\emptyset_{geo}^{all}(RD\%)$ [%]
		F_V	MW^v	MW^l	Z^v	Z^l	ρ^v	ρ^l		
1.	PVTi	0.00		-0.10		0.12		-0.22	-0.21	-0.11
	HYSYS									
2.	PVTi	0.37	0.00	0.09	0.07	0.14	-0.07	-0.05	-0.04	
	HYSYS									
3.	PVTi	0.02	-0.02	-0.11	0.00	-0.31	-0.02	-0.11	-0.10	
	HYSYS									

Appendix F Simulation Keyword Structure

Appendix F.1 E300 *.DATA File – Gas Condensate

```
--*                          LUMPING DELUMPING                          *
--*Directory:  GasCondensate-W1                                         *
--*Created by: MF                                                       *
--*Date:       NOV-19                                                   *
--*Purpose:  testing SWM GC 15 component PVT                            *
--*           for comparison with delumping facility                    *
--*Sim: DETAILED  monthly rate                                          *
--*Fluid: Gas Condensate                                                *
--*Features: Single well model with 15 component PVT                   *
--*************************************************************************
--* VERS|AUTHOR/CONTR|   DATE   |      COMMENT                          *
--* 1.0 |MF          |22-AUG-19 |                                       *
--* 1.0 |MF          |05-SEP-19 |   New Structure  (from GM)            *
--* 1.0 |MF          |06-NOV-19 |   New Run after New grouping         *
--* 1.1 |MF          |26-NOV-19 |   Final Check + Run for HYSYS         *
--*************************************************************************

RUNSPEC

VFPPDIMS
  20 20 20 20 1* 30 /
COMPS
  15 /
TITLE
  GC_W1_DET_Nc_15_monthly
WELLDIMS
  1 50 1* 1 /
START
  1 JUL 2010 /
WATER    NOMIX   METRIC
DIMENS
  20 16 24 /
TABDIMS
  3 1* 1* 1* 4 5* 1* 1* 3 /

GRID
INCLUDE
'./include/1_HEADER_COORD.GRDECL' /
INCLUDE
'./include/1A_ZCORN.GRDECL' /
INCLUDE
'./include/2_PORO_SWM_W1.grdecl' /
'./include/3_PERMX_SWM_W1.grdecl' /
'./include/4_PERMY_SWM_W1.grdecl' /
'./include/5_PERMZ_SWM_W1.grdecl' /
'./include/6_NTG_SWM_W1.grdecl' /

EDIT
```

```
PROPS
INCLUDE
'./include/7_ROCK_REL_PERM-HYSYS6.INC' /
'./include/GC_DET_Nc_15.PVO' /
STCOND
20 1.01325 /
PVTW
           583       1.0446     8.7E-007       0.3751            0 /
DENSITY
   600.        1175.  1. /

REGIONS
INCLUDE
'./include/9_SATNUM_SWM_W1.grdecl' /
'./include/12_FIPNUM_SW_W1.grdecl' /
'./include/14_ROCKNUM_SWM_W1.grdecl' /

SOLUTION
FIELDSEP
  1 38 39.2 /
  2 20 1.01325 /    /

EQUIL
     5067
     583
     5067
     0
     5067
     0
     0
     0
     0
     1 /

SUMMARY
INCLUDE
'./include/16_SUMMARY.INC' /

SCHEDULE
INCLUDE
'./include/17_VFP_W1.INC' /
'./include/18_SCH_W1_monthly_rate.SCH' /
```

Appendix F.2 E300 Delumping Keywords – Gas Condensate

```
--*                        DELUMP SECTION                                *
--* Because of the Lumping Scheme following ordering is important:      *
--* N2....._1                                                           *
--* C1....._3                                                           *
--* CO2...._2                                                           *
--* C2....._4                This ordering is used                      *
--* C3....._5                for all detailed parameters                *
--* iC4...._6                used by the e300                           *
--* nC4...._7                delumping facility                         *
--* iC5...._8                                                           *
--* nC5...._9                _*Nr* is referring to detailed             *
--* PC6...._10               fluid descriptions order                   *
--* PC7...._11               used in HYSYS Coupling Algorithm           *
--* PC8...._12                                                          *
--* PC9...._13                                                          *
--* C10+..._14                                                          *
--* C18+..._15                                                          *
--* Ordering is conditioned by Keyword LUMPING                          *
--*********************************************************************

--tracer names are also in SUMMARY section needed

-- lumping scheme
LUMPING
N2C1  2  _1 _3 /
CO2C  2  _2 _4 /
C3    1  _5 /
C4    2  _6 _7 /
C5    2  _8 _9 /
C6+   4  _10 _11 _12 _13 /
C10+  1  _14 /
C18+  1  _15 /
/
-- detailed mole fraction; determines composition variation over depth
DETAILMF                      -- e.g.
1.0    0.019971               -- N2....._1
       0.68671                -- C1....._3
       0.0084903              -- CO2...._2
       0.11581                -- C2....._4
       0.048182               -- C3....._5
       0.0086203              -- iC4...._6
       0.015101               -- nC4...._7
       0.0064003              -- iC5...._8
       0.0062703              -- nC5...._9
       0.0093404              -- PC6...._10
       0.0091304              -- PC7...._11
       0.0081503              -- PC8...._12
       0.0042102              -- PC9...._13
       0.050403               -- C10+..._14
       0.0032091              -- C18+..._15
```

```
1000.0 0.019971              -- N2....._1
       0.68671               -- C1....._3
       0.0084903             -- CO2...._2
       0.11581               -- C2....._4
       0.048182              -- C3....._5
       0.0086203             -- iC4...._6
       0.015101              -- nC4...._7
       0.0064003             -- iC5...._8
       0.0062703             -- nC5...._9
       0.0093404             -- PC6...._10
       0.0091304             -- PC7...._11
       0.0081503             -- PC8...._12
       0.0042102             -- PC9...._13
       0.050403              -- C10+..._14
       0.0032091             -- C18+..._15
/
-- acentric factor for the detailed components
ACFDET
   0.04  0.013   0.225   0.0986  0.1524  0.1848  0.201   0.227   0.251   0.24963
0.31548 0.36553 0.41058 0.49599 0.63647 /
-- molecular weight for the detailed components
MWDETAIL
   28.013  16.043 44.01  30.07  44.097 58.124 58.124 72.151 72.151 86.2   100.2
114.2  127    153.6  196.98 /
-- critical temperature for the detailed components
TCRITDET
   126.2  190.6  304.7  305.43 369.8  408.1  425.2  460.4  469.6  498.71 528.32
559.03 586.09 653    717.12 /
-- critical pressure for the detailed components
PCRITDET
    33.944 46.042 73.866 48.839 42.455 36.477 37.966 33.893 33.701 31.605 28.146
25.961 24.359 23.012 18.696 /
-- detailed EOS parameter for the detailed components
OMEGAADE
    0.457235529 0.457235529 0.457235529 0.457235529 0.457235529 0.457235529
0.457235529 0.457235529 0.457235529 0.457235529 0.457235529 0.457235529 0.457235529
0.457235529 0.457235529 /
OMEGABDE
    0.077796074 0.077796074 0.077796074 0.077796074 0.077796074 0.077796074
0.077796074 0.077796074 0.077796074 0.077796074 0.077796074 0.077796074 0.077796074
0.077796074 0.077796074 /
```

Appendix G GTU Validity Analysis

The empty cells in Table 36 were set to 0 because the concentration of respective component was below the 10^{-5}, and the calculated results are determined as numerical artefacts.

Table 36 - INIT_GTU detailed modification deviation analysis

	$RD\%$ ( ) [%]				
	Dried gas	De-C2 Top	Total Sales Gas	Total LPG	Total Condensate
N2	0.24	-3.05	-0.05		
CO2	-79.01	-77.11	-78.30	-82.58	
C1	0.58	0.06	0.48		
C2	-0.77	2.00	0.56	-6.31	
C3	-2.90	12.22	-3.13	-6.41	-0.04
iC4	2.44		2.21	0.68	-0.04
nC4	10.79		10.58	9.85	-0.04
iC5	16.97		16.78	46.10	-4.47
nC5	24.45		24.27	76.78	5.38
PC6	-38.12		-38.44	60.44	-0.19
PC7	-45.49		-45.82		-0.22
PC8	-59.81		-60.19		-0.20
PC9					-0.15
C10+					-0.08
C18+					-0.04
H2O	10.41	9.61	10.35	9.05	-0.04
F_V	0.00	0.00	0.00	1.23	0.00
T	47.77	0.00	45.42	7.13	0.01
p	-1.93	0.00	0.00	0.00	0.00

Table 37 - MF_GTU detailed comparative deviation analysis

	$RD\%\ (\ )$ [%]								
	TBH	Stabilized Gas	Dried Gas	De-C2 Feed	De-C2 Top	De-C4 Feed	Total Sales Gas	Total LPG	Total Condensate
N2	0.00	0.07	-0.25	1.92	1.73		-0.02		
CO2	0.00	-0.01	-0.04	-0.58	-0.77		-0.35		
C1	0.00	0.06	-0.14	0.65	0.46		-0.03		
C2	0.00	-0.12	0.65	-0.67	-0.86	-0.48	-0.20	-0.39	
C3	0.00	-0.68	1.86	-1.00	-6.35	-0.43	2.06	-0.33	4.92
iC4	0.00	0.08	4.18	0.29		0.85	4.39	0.95	-1.24
nC4	0.00	-0.06	4.67	0.37		0.93	4.87	1.02	-0.73
iC5	0.00	-0.99	5.27	-0.10		0.47	5.47	-0.07	-0.12
nC5	0.00	-1.38	5.42	-0.35		0.22	5.62	-0.68	-0.22
PC6	0.00	0.86	8.25	2.06		2.61	8.45		-0.16
PC7	0.00	-2.27		-0.71		-0.15			0.02
PC8	0.00	-5.31		-3.26		-2.68			0.09
PC9	0.00	-7.85		-4.82		-4.23			0.12
C10+	0.00	-11.93		6.19		6.72			0.14
C18+	0.00								0.13
H2O	0.00	-0.61							
F_V	-0.02	0.00	0.00	0.65	0.00	0.05	0.00	2.29	0.00
T	0.00	3.65	0.00	4.61	0.00	0.32	-1.65	-1.01	-0.02
p	0.00	0.57	1.88	-2.04	0.00	0.00	0.00	-1.12	0.00